Redox-Dependent Signalling Via Protein Kinase A Type I Within Distinct Subcellular Compartments

A thesis submitted for the degree of
Doctor of Philosophy
in the
University of Oxford

Trinity Term 2016

Dr Oliver Christopher Lomas
BA, BM BCh, MRCP

Department of Cardiovascular Medicine
University of Oxford

Merton College,
Oxford

ABSTRACT

Redox-Dependent Signalling Via Protein Kinase A Type I Within Distinct Subcellular Compartments

Oliver Christopher Lomas, Merton College

Doctor of Philosophy, University of Oxford, Trinity Term 2016

Background and Aims : Numerous proteins, important for cell signalling, are modified by the balance of oxidative or reducing stimuli within the cell – the redox state. The regulatory subunit Iα (RIα) of Protein Kinase A (PKA) contains conserved cysteine residues that are readily oxidised to form a disulphide bond via the thiol group of other cysteines. It has been suggested that the formation of the disulphide bond between RIα subunits of the PKA holoenzyme increases the activity of the enzyme. The aims of the project were to examine whether the intrinsic activity of the enzyme or its functional localisation were increased by redox modification.

Methods : Live-cell fluorescent imaging of Fluoresence Resonance Energy Transfer (FRET) has been used to investigate real-time changes in PKA activity and Fluorescence Resonance After Photo-Bleaching (FRAP) has been used to investigate changes in sub-ceullar localisation of PKA regulatory subunits.

Results : The addition of the oxidant, hydrogen peroxide, to cells expressing FRET-based reporters of PKA activity was not associated with an increase in PKA activity compared to cells that expressed PKA-RIα that were incapable of undergoing disulphide bond formation. Mutation of the cysteine residue in PKA-RIα was, however, associated with subtle differences in sub-cellular diffusibility of the protein, which supports the hypthesiss that such redox modification appears to influence the mobility and hence anchoring of the protein within the cell.

Conclusions : In summary, the data presented in this thesis do not support the notion that PKA can be activated directly through oxidation the RIα subunit. However, modulation of classical cAMP-PKA signalling by the redox state of the cell may be brought about by subtle changes in the anchoring and hence localisation of PKA-RIα as implied by changes in diffusibility within the cytoplasm.

Table of Contents

List of Figures and Tables 7
Abbreviations 11
Chapter 1 - Introduction 14
1.1 Redox protein modification – an evolutionary necessity 15
1.1.1 Redox-sensitive cysteine residues and protein function 15
1.1.2 Sources of Reactive Oxygen Species 18
1.1.3 Reactive Oxygen Species scavenging 20
1.2 Protein Kinase A signalling 21
1.2.1 Protein Kinase A activation and its regulation 21
1.2.2 Activators of cAMP-PKA signalling via G-protein coupled receptor activation 24
1.2.3 Compartmentalisation of downstream targets of Protein Kinase A signalling 25
1.2.4 The Type I Regulatory subunit of PKA and its redox sensitivity 29
1.2.5 cAMP-independent change in PKA activity 30
1.2.6 Redox signalling and molecular switches 31
1.3 Detection of PKA activity by fluorescence microscopy 34
1.3.1 FRET sensors for cAMP-PKA signalling 34
1.4 Aim of the thesis 37
Chapter 2 - Methods 39
2.1 Experimental Models 40
2.1.1 Adult mouse cardiomyocytes 40
2.1.1.1 Isolation procedure 40
2.1.1.1.1 Redox Dead Mouse and its Genotyping 47
2.1.2 Measurement of contractility in adult mouse cardiomyocytes 51
2.1.3 Culture of primary adult mouse cardiomyocytes 53
2.2 Continuous cell culture 55
2.2.1 HeLa cells 55
2.2.2 HEK-293 cells 56
2.3 Plasmid construction and site-directed mutagenesis 57
2.4 Gene transfer 61
2.4.1 Transfection 61
2.4.2 Adenoviral preparation and gene transfer 63

2.5 Detection of protein expression 63
2.5.1 Sample preparation 63
2.5.2 Protein quantification, Western gel electrophoresis and immunodetection 64
2.5.3 Fractionation 71
2.5.4. List of primary and secondary antibodies 75
2.5.5 Comparison of PKA RI vs RIα antibodies 76
2.6 Immunoprecipitation and 'pull-down' 79
2.7 Fluorescence Microscopy 81
2.7.1 Fluorescence Resonance Energy Transfer Microscopy (FRET) 81
2.7.1.1 FRET Microscopy Equipment 81
2.7.1.2 Pharmacological agents used to assess cAMP-PKA signalling dynamically in FRET imaging experiments 85
2.7.1.3 FRET biosensors 88
2.7.2 Fluorescence Recovery After Photo-Bleaching (FRAP) 90
2.7.2.1 Principles of FRAP 90
2.7.2.2 FRAP Microscopy equipment 91
Chapter 3 - *Ex vivo* culture and adenoviral gene transduction of FRET reporters in adult mouse cardiomyocytes 92
3.1 Background 93
3.2 Methods 95
3.2.1 Cardiomyocyte Isolation, Infection and Culture 95
3.2.2 Measurement of viability and contractility of cardiomyocytes 97
3.2.3 Statistical analysis 98
3.3 Results 99
3.3.1 Adenoviral gene transfer 99
3.3.2 Effects of cell culture and viral infection on viability of cardiomyocytes 103
3.3.3 Effects of viral infection and Cytochalasin D on contractile properties of primary adult mouse cardiomyocytes 104
3.4 Discussion 107
Chapter 4 - Effects of disulphide bond formation between RIα subunits on PKA activity 110
4.1 Background 111
4.2 Methods 112
4.2.1 Adult mouse cardiomyocyte FRET reporter analysis 112

4.2.2 *In vitro* assessment of the effects of H_2O_2 on PKA activity in the cytosolic compartment of HEK-293 cells 114

4.2.3 Statistical analysis 114

4.3 Results 115

4.3.1 Effects of exogenously applied 250µM H_2O_2 on PKA activity in adult mouse cardiomyocytes expressing AKAR3ev FRET biosensor 115

4.3.2 Effects of 250µM H_2O_2 on cAMP concentration in adult mouse cardiomyocytes expressing the H187 FRET biosensor 119

4.3.3 Effects of 30µM H89 on adult mouse cardiomyocytes expressing AKAR3ev FRET biosensor 120

4.3.4 *In vitro* measurement of PKA activity in a cytosolic fraction of HEK cells expressing the AKAR3ev sensor 122

4.4 Discussion 125

Chapter 5 - Effects of disulphide bond formation in RIα subunits on PKA holoenzyme localisation 130

5.1 Introduction 131

5.2 Methods 139

5.2.1 Cell culture, plasmid generation and transfection 139

5.2.2 Fluorescence recovery after photo-bleaching (FRAP) 141

5.2.3 Protein preparation from whole cell lysates and subcellular fractions 143

5.2.4 Immunoblotting and immunoprecipitation 143

5.2.5 Isolation of adult mouse myocytes and preparation for assessment of effects of endogenous growth hormones 145

5.2.6 Growth hormones as potential drivers of endogenous H_2O_2 production 146

5.3 Results 148

5.3.1 Effects of mutations in the PKA RIα D/D and exogenous H_2O_2 on the ability to form disulphide bonds between PKA RIα subunits 148

5.3.2 Diffusibility of GFP-tagged RI subunits in HeLa cells as measured by Fluorescence Recovery After Photo-bleaching (FRAP) 150

5.3.3 Anchored GFP-tagged RI subunits as determined by measurement of immobile fraction of RI-GFP after Fluorescence Recovery After Photo-bleaching 155

5.3.4 The effects of R-subunit mutation on co-immunoprecipitation of GFP-tagged RI subunits with AKAP10 160

5.3.5 Localisation of AKAP10 by subcellular fractionation 162

5.3.6 Effects of Insulin, VEGF and Gkt137831 on PKA RI disulphide bond formation in adult cardiomyocytes from wild-type mice 163

5.4 Discussion 168

5.4.1 Mobility of GFP-tagged PKA RIα compared to mutants in the RI domain 168
5.4.2 Relative immunoprecipitation of AKAP10 by PKA RI-GFP compared to mutations in the dimerization and docking domain of the R subunit 172
5.4.3 PKA RIα dimerization driven by an endogenous source of hydrogen peroxide .172
5.4.5 Summary 175
Chapter 6 177
Appendices 180
Timing and Venue of Research 181
Research Funding 181
Publications arising out of this work 182
Presentation of Work at Scientific Meetings 182
References 183

List of Figures and Tables

Chapter 1

Figure 1.1 Cysteine and cystine structure

Figure 1.2 Reversible and irreversible cysteine modifications

Figure 1.3 Cartoon to depict the heterotetrameric structure of PKA Types I and I

Figure 1.4 Domain organisation of the Type I Regulatory (RI) subunit of PKA

Table 1.1 A Kinase Anchoring Proteins (AKAPs) that bind Type I PKA

Figure 1.5 Cartoon to describe the mechanism of Fluorescence Resonance Energy Transfer (FRET) that takes place in response to phosphorylation of the A-Kinase Activity Reporter (AKAR) class of sensor

Figure 1.6 Cartoon to describe the mechanism of Fluorescence Resonance Energy Transfer (FRET) that takes place in response to the binding of cAMP to Epac-H187 to detect changes in cAMP concentration in response to cAMP-binding.

Chapter 2

Figure 2.1 Key stages in the isolation of primary cardiomyocytes from adult mice

Table 2.1 Equipment and Pre-procedure preparation for Langendorff perfusion and isolation of adult mouse cardiomyocytes

Figure 2.2 Freshly isolated adult mouse cardiomyocytes

Table 2.2 PCR Reaction constituents for genotyping

Figure 2.3 Details of the PCR reaction program used for genotyping

Figure 2.4 Sample DNA electrophoresis for genotyping

Table 2.3 Constituents of Modified Eagle's Medium (MEM) for culture of primary adult mouse cardiomyocytes

Table 2.4 Constituents of Dulbecco's Modified Eagle's Medium (DMEM) for continuous cell culture

Figure 2.5 Base sequence of murine pCDNA3-mouse PKA-RIα-mEGFP

Figure 2.6 Site-directed mutagenesis reaction conditions

Figure 2.7 Base sequence of the dimerization and docking (D/D) of murine PKA RIα and associated mutations.

Table 2.5 Transfection conditions for HeLa and HEK cell lines

Table 2.6 Constituents of RIPA lysis buffer

Figure 2.8 Sample curve of a serially diluted protein standard plotted against optical density

Figure 2.9 Two immunoblots performed simultaneously to show the effect of the type of gel on the relative abundance of oxidised cysteine

Figure 2.10 Schematic representation of the transfer of protein from gel to PVDF membrane

Figure 2.11 Immunoblot to show cytosolic and mitochondrial subcellular fractions derived from two repeats from cultured HEK-293 cells

Table 2.7 Primary and secondary antibodies - dilution, species and suppliers

Figure 2.12 Immunoblot of serially diluted purified PKA RI α or β isoforms probed with PKA RI antibody.

Figure 2.13 Immunoblot of serially diluted purified PKA RI α or β isoforms probed with PKA RIα antibody.

Figure 2.14 Cartoon to summarise the process of immunoprecipitation using cAMP-coated agarose beads

Figure 2.15 Photograph of RC-21 (Warner Instruments, UK) chamber setup showing aspiration ducts to allow removal of bath applied stimuli during FRET microscopy experiments.

Figure 2.16 Fluorescence of primary adult mouse cardiomyocytes

Figure 2.17 Graph to show an experiment involving cytosolic EPAC-based FRET biosensor to show the effects of an increase in cAMP

Chapter 3

Figure 3.1 Sample raw trace from Ionoptix® software of the contraction of an adult mouse cardiomyocyte.

Figure 3.2 Primary adult mouse cardiomyocyte expressing a FRET biosensor for PKA activity with a characteristic experiment.

Figure 3.3 Primary adult mouse cardiomyocyte expressing an EPAC H187 FRET biosensor for cAMP concentration with a characteristic experiment.

Figure 3.4 Graph to show viability of primary adult mouse cardiomyocytes with and without adenoviral infection.

Figure 3.5 Graph to show the effects of adenoviral infection and 0.5μM cytochalasin D on Fractional Shortening (FS) in primary adult mouse cardiomyocytes.

Figure 3.6 Graph to show the effects of adenoviral infection and 0.5μM cytochalasin D on *Tau* in primary adult mouse cardiomyocytes.

Chapter 4

Figure 4.1 Dose-response curve showing FRET changes for AKAR3ev expressed in adult mouse cardiomyocytes in response to forskolin

Figure 4.2 Immunoblot of PKA RI in whole cell lysates from adult mouse cardiomyocytes to show the presence of disulphide bonds between RIα-subunits (dimers) compared to reduced monomeric subunits

Figure 4.3 Graph to show the FRET ratio in response to the incubation of adult mouse cardiomyocytes from wild-type and 'redox-dead' animals with 250μM H_2O_2

Figure 4.4 Graph to show the FRET ratio in response to the incubation with 250μM H_2O_2 on adult mouse cardiomyocytes from wild-type and redox-dead animals expressing the H187 FRET biosensor.

Figure 4.5 Immunoblot and semi-quantitative analysis of the proportion of oxidised cysteine residues in PKA RIα associated with cell culture conditions at 4 and 24 hours.

Figure 4.6 Graph to show the effects of the PKA inhibitor H89 on adult mouse cardiomyocytes from 'wild-type' or 'redox dead' animals expressing the AKAR3ev FRET biosensor for PKA activity.

Figure 4.7 Immunoblot to show cytosolic and membranous subcellular fractions derived from two repeats from cultured Human Embryonic Kidney (HEK-293) cell lines.

Figure 4.8 Immunoblot run in reducing conditions for PKA RI in cytosolic and membranous samples from HEK-293 cells

Figure 4.9 Bar graph to show steady-state *in vitro* PKA activity in a variety of conditions

Chapter 5

Table 5.1 Summary of plasmid sequences of human wild-type PKA RIα and mutations that give rise to C17S; H24A and C17S:H24A mutants. Mutated bases shown in bold and capitalised.

Figure 5.1 Schematic representation of a FRAP experiment showing bleaching and derivations of the mobile and immobile fractions.

Figure 5.2 Experimental design of effects of VEGF, Insulin with and without the Nox inhibitor GKT137831

Table 5.2 Summary of reaction conditions for effects Nox4 modulation on PKARIα oxidation.

Figure 5.3 Primary antibody directed against GFP against protein from whole cell lysates from HeLa cells expressing PKA RIα-GFP constructs : wild-type, C17S, H24A and C17S-H24A.

Figure 5.4 Scatter dot-plot to show rate constants for diffusibility of PKA RIα-GFP constructs : wild-type, C17S, H24A and C17S-H24A.

Figure 5.5 Rate-constants from HeLa cells expressing wild-type or C17S PKA RIα-GFP that were exposed to 250μM H_2O_2 or vehicle control.

Figure 5.6 Rate-constants from HeLa cells expressing wild-type PKA RIα-GFP or C17S PKA RI-GFP with or without AKAP10 co-expression

Figure 5.7 FRAP rate-constants from HeLa cells co-expressing AKAP10 with either wild-type PKA RI-GFP or C17S PKA RI-GFP. The cells are then subjected to either treatment with 250μM H_2O_2 or vehicle control.

Figure 5.8 Bar chart to represent the immobile fraction found in FRAP experiments involving PKA RIα-GFP and mutants expressed in HeLa cells.

Figure 5.9 Bar chart to represent the immobile fraction found in FRAP experiments involving wild-type and C17s variants of PKA RIα-GFP expressed in HeLa cells

Figure 5.10 Bar chart to represent immobile fraction found in FRAP experiments involving PKA RIα-GFP and mutants with and without co-expression with AKAP10 in HeLa cells

Figure 5.11 Bar chart to represent immobile fraction found in FRAP experiments involving PKA RIα-GFP and mutants co-expressed with AKAP10 and treated with H_2O_2 or control.

Figure 5.12 Co-immunoprecipitation of GFP-tagged PKA RIα (WT, C17S, H24A, C17S-H24A) with RI-binding AKAPS – AKAP10 and AKAP149

Figure 5.13 Immunoblot for AKAP10 in subcellular fractions of HeLa cells

Figure 5.14 Experimental design with example immunoblot of conditions tested to investigate the effects of VEGF and insulin and Nox4 inhibition on endogenous oxidation of PKA RIα

Figure 5.15 Effects of VEGF, Insulin and Gkt137831 on the formation of PKA RI disulphide bonds compared to total.

Figure 5.16 Effects of VEGF with and without Gkt137831 on PKA RIα disulphide bond formation

Figure 5.17 Effects of Insulin with and without Gkt137831 on PKA RI disulphide bond formation.

Abbreviations

AC	Adenylyl cyclase
AKAP	A-Kinase Anchoring Protein
AKAR	A-Kinase Activity Reporter
α-KGDH	α-ketoglutarate dehydrogenase
ATP	Adenosine Triphosphate
BME	β-mercapto-ethanol
cAMP	Cyclic adenosine monophosphate
CAR	Coxsackie Adenovirus Receptor (CAR)
CFP	Cyan Fluorescent Protein
CHO	Chinese Hamster Ovary cell line
CMV	Cytomegalovirus
CNB	Cyclic Nucleotide Binding domain
DNA	Deoxyribonucleic Acid
DMSO	Dimethyl Sulphoxide
D/D	Docking Domain
EDTA	Ethylene-diamine-tetra-acetic acid
EPAC	Exchange protein directly activated by cAMP
ER	Endoplasmic Reticulum
ETC	Electron Transport Chain
FRAP	Fluorescence Recovery After Photo-bleaching
FRET	Fluorescence Resonance Energy Transfer
FS	Fractional shortening
GAPDH	Glyceraldehyde 3-phosphate dehydrogenase
GFP	Green Fluorescent protein
GSH	Glutathione - reduced

GSSG	Glutathione - oxidised
HEK	Human Embryonic Kidney cell line
IBMX	3-Isobutyl-1-Methylxanthine
IMS	Inter-Membrane Space
LPS	Lipopolysaccharide
MAO	Monoamine Oxidase
MAPK	Mitogen Activated Protein Kinase
MISS	Mitochondrial IMS-sorting signal
MOI	Multiplicity of Infection
NADPH	Nicotinamide adenine dinucleotide phosphate
NOX	NADPH Oxidase
ORF	Open Reading Frame
PBS	Phosphate Buffered Saline
PCR	Polymerase Chain Reaction
PDE	Phosphodiesterase
PFU	Particle Forming Units
PKA	Protein Kinase A
PKC	Protein Kinase C
PKG	Protein Kinase G
PKI	Protein Kinase A Inhibitor
PMSF	Phenylmethylsulfonyl Fluoride
PP	Protein Phosphatase (1 or 2)
RI	Regulatory Subunit Type I of the PKA holoenzyme
RII	Regulatory Subunit Type II of the PKA holoenzyme
ROS	Reactive Oxygen Species
SD	Standard Deviation
SEM	Standard Error of the Mean
SOD	Superoxide Dismutase

SR	Sarcoplasmic Reticulum
TAE	Buffer containing Tris base, acetic acid and EDTA
TBST	TRIS-buffered saline (TBS, 10X) with 1% Tween 20
TGF-β	Transforming Growth Factor-β
Trx	Thioredoxin
VEGF	Vascular Endothelial Growth Factor
YFP	Yellow Fluorescent Protein

Chapter 1

Introduction

1.1 Redox protein modification – an evolutionary necessity

Most organisms on Earth, apart from anaerobic bacteria and yeast, require molecular oxygen (O_2) to drive the production of energy at a greater efficiency than is possible under anaerobic conditions. Such energy-producing reactions are redox in nature; in that they involve the oxidation of one reactant coupled with the reduction of another. Despite the necessity for O_2 by aerobic organisms, oxygen possesses many toxic and mutagenic properties. Through comparison with ionising radiation, the toxicity of O_2 was first attributed to chemical derivatives of oxygen radicals (oxygen with unpaired electrons) that inactivate particular cellular enzymes[1]. Sequential chemical reduction of O_2 leads to the formation of a group of reactive oxygen species (ROS) that include the superoxide (O_2^-) and hydroxyl (OH^-) radicals as well as (non-radical but still reactive) hydrogen peroxide (H_2O_2). The term 'oxidative stress' was first coined in 1985 and was used to describe how an imbalance in redox state in favour of oxidation can lead to cellular damage[2]. Oxidative stress has since been implicated in numerous human pathologies such as diabetes mellitus[3], heart failure[4] and cancer[5] as well as the ageing process itself[6]. However, recent evidence suggests that ROS are not simply a group of inherently toxic molecules that inevitably cause oxidative stress but act physiologically by being produced transiently in a compartmentalised manner to modulate redox-sensitive proteins in other signalling pathways – especially those concerned with growth, development and differentiation[7].

1.1.1 Redox-sensitive cysteine residues and protein function

Cysteine is a biogenic (non-essential), amino acid that is encoded by two possible codons UGU and UGC. Cysteine is a sulphur amino acid due to the presence of the element in its side chain (Figure 1.1). Cysteine can be readily oxidised to form a dimer

containing a disulphide bond between the sulphur of each cysteine residue - the dimer may be referred to as cystine. The formation of disulphide bonds between cysteine residues that are separate in the amino acid sequence therefore contribute to the secondary and tertiary structure of proteins.

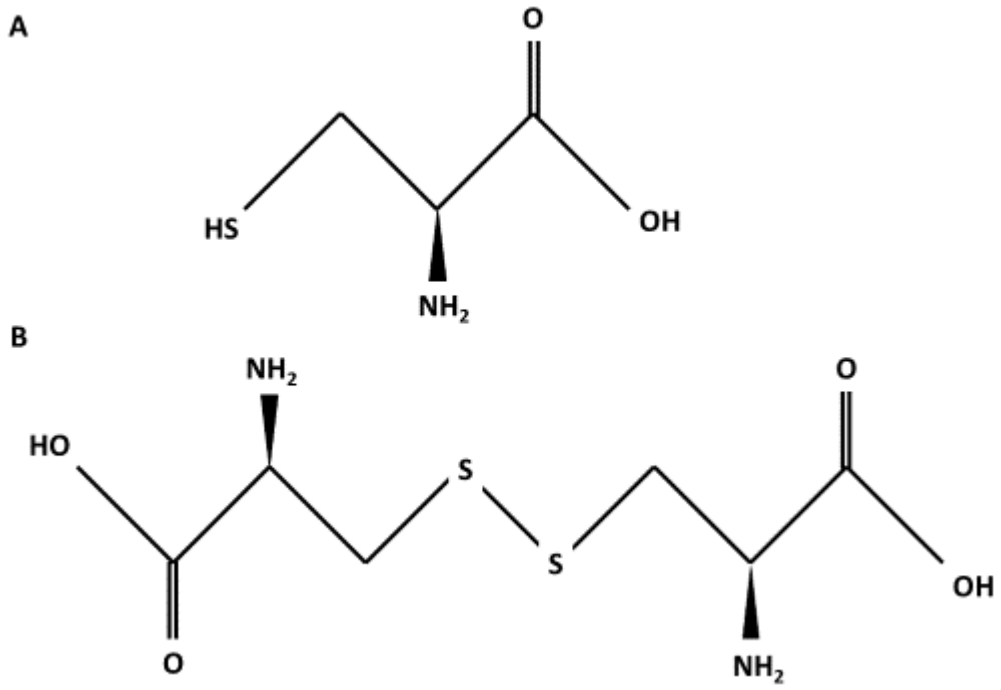


Figure 1.1 Cysteine (A) and cystine (B) of two cysteine residues linked by a disulphide bond. The thiol group -SH is visible in A; Oxidised to R-S-S-H in B.

Cysteine residues, especially those that occur in clusters, are often highly conserved and hence likely to be functionally important[8-10]. The reversible modifications of cysteine thiol groups were first identified in proteins that are involved in defence against oxidative stress including transcription factors and enzymes involved in cell survival signalling. Cysteine residues contain a polarisable sulphur atom that can be readily oxidised or reduced (Figure 1.1). When cysteine thiols encounter reactive oxygen species (as well as nitrogen and chlorine derivatives), sulphenic acid (R-SOH) forms.

This is an inherently unstable molecule that most commonly reacts rapidly with nearby cysteines to form disulphide bonds (R-S-S-R) within or between peptides. Another fate of R-SOH is to react with the small tripeptide GSH, which leads to S-glutathionylation. Specialised reductases such as thioredoxin and glutaredoxin, are responsible for the reduction of oxidised cysteine residues[11]. Disulphide bond formation has the ability to mediate extensive and reversible structural and hence functional changes of proteins in response to the prevailing redox status of the cell. Not all cysteine residues are necessarily conserved for their role as redox sensors. Oxidant-mediated disulphide bond formation, which typically occurs within the reducing environment of the cytosol, is distinct from the formation of structural disulphide bonds, which takes place in the oxidising milieu of the endoplasmic reticulum and is catalysed by enzymes with redox-catalytic cysteines[12].

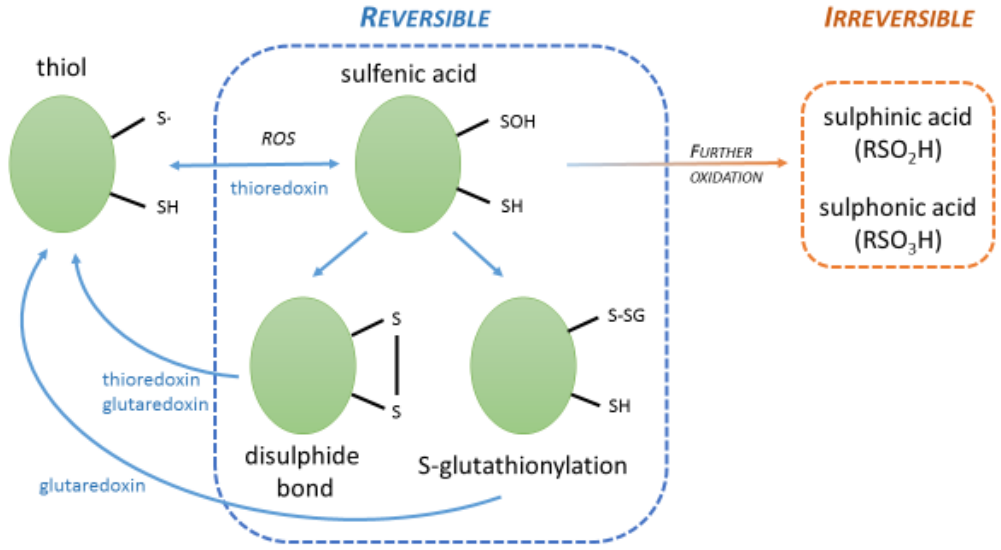


Figure 1.2 Reversible and irreversible cysteine modifications

Redox signalling depends on the particular reactive species involved and its localised concentration within the cell. For example, a rapid rise in intracellular superoxide production from an enzyme such as NADPH oxidase or an exogenous drug such as an anthracyclin chemotherapeutic agent causes indiscriminate, irreversible oxidation with widespread protein, lipid and nucleotide modifications that lead to irreversible cell death by necrosis. Milder oxidation with reactive species such as hydrogen peroxide (H_2O_2), which can be produced in distinct subcellular compartments, have been found to cause reversible oxidations that can modulate physiological signalling events[13].

1.1.2 Sources of Reactive Oxygen Species

In eukaryotes, there are numerous potential sources of ROS including the reduction of oxygen by the catalysis of enzymes such as xanthine oxidase, NADPH Oxidases (NOX), cyclo-oxygenase, lipoxygenase as well as Complexes I and III of the mitochondrial electron transport chain (ETC). Mitochondria are considered to be the most redox-active compartment in the cell accounting for more than 90% of oxygen utilisation[14]. These organelles play an important role in energy metabolism and may act as nutrient and oxygen sensors. Although the majority of oxygen undergoes complete reduction to water at the level of cytochrome oxidase, partial reduction accompanied by ROS generation can occur as well[15]. The mitochondrial ETC is the main endogenous source of ROS during physiological cellular respiration, whereby electrons from Complex I or III react with oxygen to form superoxide (O_2^-) anions. Uncoupling of the mitochondrial respiratory chain, i.e. the dissociation of electron transport from phosphorylation to form ATP, has been proposed as a significant source of these ROS[16]. In addition to leak from the ETC, there are several enzymatic sources of

mitochondrial ROS production such as monoamine oxidases (MAOs)[17] and α-ketoglutarate dehydrogenase (α-KGDH)[18].

NADPH oxidases (Nox) are a family of membrane-bound enzymes whose main function appears to be the controlled generation of ROS. The family of enzymes comprises seven catalytic subunits termed Nox1-5 and Duox1 and 2, regulatory subunits p22phox, p46phox, Noxa1, p40phox and the binding partner Rac. Originally identified in phagocytes as the driver of the respiratory burst of ROS that kills pathogens as part of the innate immune response, non-phagocytic Nox, such as Nox4, appear to play a role in physiological cell signalling. The Nox2 and Nox4 isoforms are expressed in cardiomyocytes[19, 20]. A number of factors can stimulate NADPH oxidases in the cardiovascular cells including agonists of G-protein coupled receptors like angiotensin II[21]; growth factors such as Vascular Endothelial Growth Factor (VEGF)[22]; cytokines such as Transforming Growth Factor-β (TGF-β)[23] and hormones such as insulin[24].

The Nox4 isoform was originally identified as ‘renox’ due to its abundance in renal cells[25] but has since been found to be expressed in a variety of cells, including cardiomyocytes[26], where the predominant subcellular localisation is in mitochondria and has been implicated in cardiac apoptosis in the context of hypertrophic stimuli[21]. Nox4 differs from other Nox isoforms in that its product is H_2O_2 rather than superoxide anion ($O_2^{\cdot}$)[27] and is constitutively active without recruitment of regulatory subunits from the cytosol. Nox4 and Nox2 appear to mediate signalling in distinct cellular

compartments in cell line models, with Nox2 at the plasma membrane and Nox4 associated with organelles such as the mitochondria and ER[28].

1.1.3 Reactive Oxygen Species scavenging

Reactive Oxygen Species (ROS) can be harmful to cells, especially at high concentrations[1]. Therefore, cells express enzymes that degrade ROS in order to maintain homeostasis. Antioxidants are compounds that delay or prevent oxidation of a particular substrate. There are a number of ways in which antioxidant effects can be achieved, either through the catalysis of reactions that remove ROS, such as superoxide dismutase (SOD), catalase and peroxidase; providing compounds that are preferentially oxidised by ROS to protect the biologically important compounds from oxidation; and compounds that diminish the formation of ROS at source.

Antioxidant enzymes remove the intermediates of oxygen reduction, in particular, SOD, catalase and glutathione peroxidase. Hydrogen peroxide (H_2O_2) can be removed by two types of enzyme: catalase causes the direct decomposition of H_2O_2 to O_2; whereas peroxidase enzymes remove H_2O_2 by using it to oxidise another substrate. Glutathione peroxidases remove H_2O_2 by coupling its reduction to H_2O with oxidation of reduced glutathione, GSH, a thiol-containing tri-peptide. Diamide oxidises GSH to form glutathione disulphide (G-S-S-G)[29] thereby limiting the efficacy of glutathione peroxidase. This makes diamide a potent inducer of oxidative stress within cells. Apart from enzymatic degradation of ROS, non-catalytic redox-active molecules exert anti-oxidant activity. These can be divided into two different classes: non-thiol compounds, essentially vitamins (e.g. ascorbate, tocopherols, β-carotene) and polyphenols, which

are able to block the radical chain reaction by delocalizing the positive charge formed upon the interception of radicals; sulphur-containing compounds, such as reduced glutathione (GSH) and thioredoxin (Trx), which act as donors of reducing equivalents either directly or in concert with specific enzymes.

1.2 Protein Kinase A signalling

1.2.1 Protein Kinase A activation and its regulation

In eukaryotic cells, phosphorylation of amino acid residues gives rise to an amplificatory mode of signalling, or cascade. Enzymes that catalyse the addition of phosphate groups, or kinases, phosphorylate either serine/threonine residues or tyrosine residues in order to alter protein conformation. As the protein conformation is key to its function, phosphorylation and hence removal of the group can greatly influence cellular function.

Protein Kinase A (PKA) is a ubiquitously expressed kinase that phosphorylates serine and threonine residues in proteins in response to activation by the binding of cyclic Adenosine Monophosphate (cAMP). This messenger cascade mediates many physiological functions, such as the force (inotropy) and frequency (chronotropy) of contraction of cardiomyocytes[30] photo-transduction in the retina[31] and glycogenolysis in the liver[32]. The PKA holoenzyme is a hetero-tetramer comprising a pair of regulatory (R) subunits and a pair of catalytic (C) subunits – R_2C_2 (Figure 1.3). In mammals, there are three isoforms of catalytic subunit (Cα, β, γ) which are functionally equivalent [33].

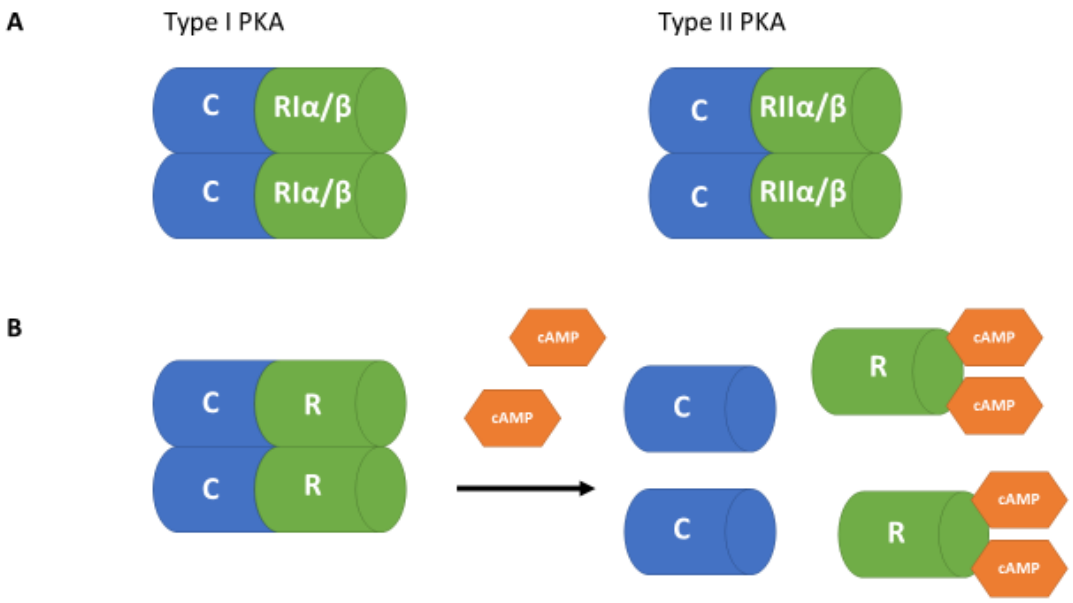


Figure 1.3 Cartoon to depict the heterotetrameric structure of PKA Types I and II (Panel A). Panel B depicts the activation of PKA by the binding of cAMP to the R subunits, which allows the catalytic subunits to be released to phosphorylate targets

The canonical cAMP-PKA signalling axis begins with the binding of a ligand to a G-protein coupled receptor, such as the β-adrenoceptor, that activates Adenylyl Cyclase (AC) to generate cyclic adenosine monophosphate (cAMP) and pyrophosphate from Adenosine Triphosphate (ATP). In the absence of cAMP, the dimer of regulatory (R) subunits binds the catalytic (C) subunits to keep them in an inactive state[34] (Figure 1.3). The R subunits may therefore be considered as constitutive inhibitors of phosphorylation by the C subunits. Only when the C subunits dissociate from the R subunits are they free to phosphorylate their targets by transferring the terminal phosphate group of ATP to the target serine or threonine amino acid. There are four isoforms of R subunit[35]; α and β variants of RI and RII. Each of the different R subunits is not functionally redundant and can form holoenzymes with any of the C subunit isoforms, display different binding affinities for cAMP and are distributed differently within cells and between tissues.

The PKA signalling cascade can be inhibited at three main points; upstream by removal of the cAMP through its breakdown by phosphodiesterases (PDEs); directly inactivated by Protein Kinase Inhibitor (PKI) that inhibits the free catalytic (C) subunit of PKA after dissociation from the regulatory (R) subunits[36, 37] or downstream by dephosphorylation of the targets of PKA through the action of protein phosphatases that dephosphorylate target proteins.

Upon inactivation of PKA by the removal of cAMP, new phosphorylation events are prevented but any phosphorylated substrate will persist until reversed by phosphatase activity. This reversibility of protein phosphorylation represents an important mechanism of cellular signalling. Protein phosphatases are classified into two categories PP1 and PP2, the latter class comprising three isoforms A, B and C[38].

The phosphodiesterase (PDE) family of enzymes catalyse the hydrolytic degradation of cAMP as well as the other second messenger cyclic guanosine monophosphate (cGMP). PDEs are encoded by 21 genes from which are derived eleven different families, designated PDE 1-11 according to their structure, kinetics, substrate specificity and regulatory mechanisms[39]. PDEs provide a key regulatory mechanism for controlling intracellular concentrations of cyclic nucleotides, a property that has been exploited by a number of pharmacological agents for therapeutic effect.

The domain organisation of the R subunits of PKA is conserved in all isoforms and comprises a dimerization and docking domain (D/D) located at the N terminus, followed by a flexible linker and two Cyclic Nucleotide Binding (CNB) domains (Figure 1.4). The linker contains an inhibitory site which mimics a peptide substrate and

docks to the active site cleft of the catalytic subunit in the holoenzyme. The D/D can function either as an independent docking motif or as an integral part of the holoenzyme by interacting with either the C subunit or the CNB domains. In the presence of cAMP, each R subunit binds two molecules of cAMP[40].

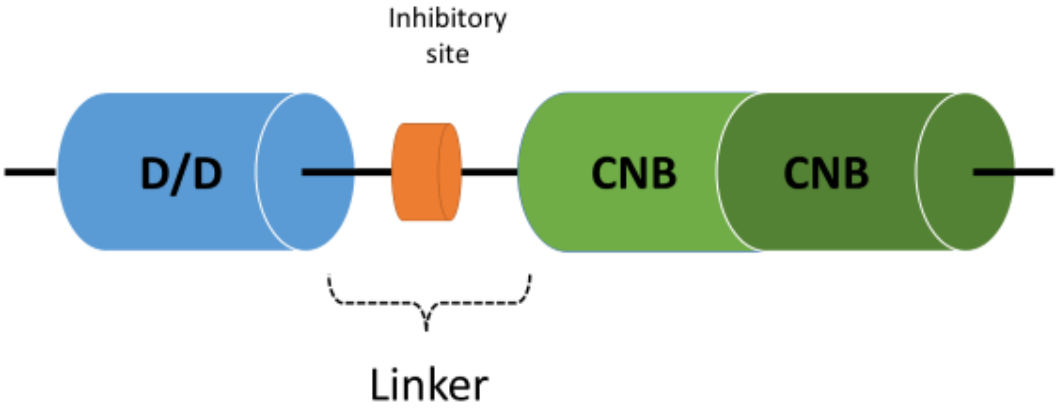


Figure 1.4 Domain organisation of the Type I Regulatory (RI) subunit of PKA.
D/D = Dimerisation / Docking domain. CNB = Cyclic nucleotide binding domain.

1.2.2 Activators of cAMP-PKA signalling via G-protein coupled receptor activation

The classical actions of PKA were first described in relation to what is now known as adrenergic signalling. These peptide hormones comprise noradrenaline and adrenaline that are able to bind adrenoceptors, which are coupled to cytosolic guanine nucleotide-binding proteins (G proteins). Therefore, the role of this membrane-bound, ligand-binding complex is to convery signals from outside the cell to the interior (Figure 1.5).

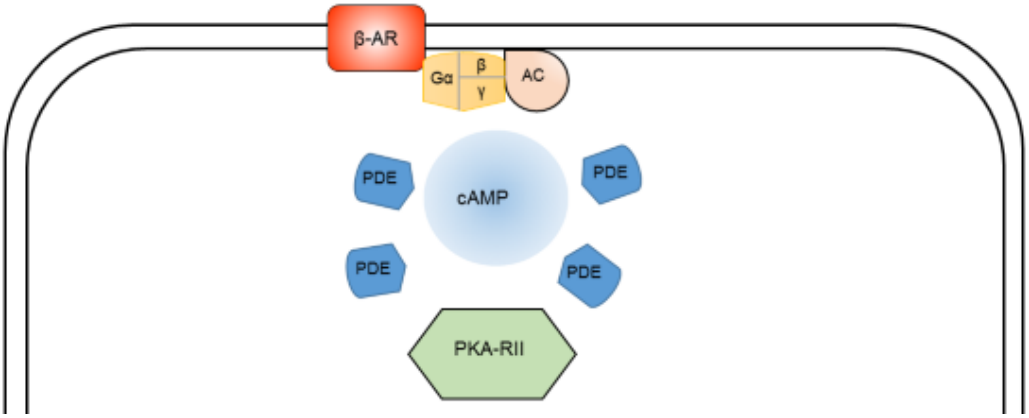


Figure 1.5 Cartoon to show the linking of an external hormonal stimulus at a β-adrenoceptor (β-AR) to the intracellular cAMP-signalling cascade. AC – adenylyl cyclase. PDE – phosphodiesterase.

Membrane-spanning G protein-coupled receptors (GPCRs), such as the adrenoceptors, undergo a conformational change in response to binding by a ligand such as adrenaline. This change in protein structure increases the affinity of the intracellular component of the GPCR for a G-protein. The trimeric G-proteins are anchored to the cytosolic surface of the plasma membrane and comprise α, β and γ subunits. The Gα subunit binds GDP or GTP interchangeably. In cAMP-dependent signalling, the Gα subunit is of a 'stimulatory' type ($G\alpha_s$) in that upon exchange of GDP for GTP by the $G\alpha_s$, the subunit dissociates from G β and γ to bind and activate adenylyl cyclase (AC). In turn, AC generates cyclic adenosine monophosphate (cAMP) and pyrophosphate from Adenosine Triphosphate (ATP) and thus triggers the intracellular cAMP-signalling cascade.

1.2.3 Compartmentalisation of downstream targets of Protein Kinase A signalling

The apparent lack of specificity of second messenger signalling was a concern from early in the development of the field. Indeed, Rall contemplated the "unsatisfying picture of the catalytic subunit of protein kinase swimming about, happily

phosphorylating a variety of cellular constituents whether they need it or not." From this, he presciently suggested the existence of "protein complexes" that "may become associated with other cellular components" to target the signal derived from second messenger cascades.

Functional and biochemical evidence of segregated cyclic nucleotide signalling pathways was presented by Brunton et al[41, 42] who described localised cAMP signalling in cardiomyocytes. When the non-selective β-adrenoceptor agonist, isoproterenol, was applied to cellular homogenates of rabbit myocardium, cAMP accumulation and PKA activation were recorded in both soluble and particulate subcellular sub-cellular fractions. However, the arachidonic acid-derived hormone Prostaglandin E_1 (PGE_1), when applied to similar cellular preparations, increased cAMP accumulation and PKA activity in the soluble fraction only. These observations were the first to suggest that different extracellular stimuli could exert distinct, localised cAMP-signalling.

Since these biochemical observations were made, live cell fluorescence imaging techniques have been developed that have allowed real-time observation of compartmentalised cAMP signalling. Using cAMP sensors that were targeted to PKA RI and PKA RII isoforms, spatially restricted compartments of cAMP have been observed in adult rat ventricular cardiomyocytes. Specifically, β-adrenoceptor-mediated signalling acted via PKA RII led to the phosphorylation of targets involved in myocardial contractility: Troponin I and Phospholamban. However, PGE_1 led to a small increase in cytosolic cAMP concentration in the RI but not the RII compartment. These observations were therefore consistent with Brunton's experiments showing segregated cAMP signalling. Specific targets of PKA-RI mediated signalling are not well defined.

PKA-RI has been localised to mitotic spindles[43], the neuro-muscular junction[44] and in the CD3 receptor complex of T lymphocytes[45].

Although the specific agonists and targets of localised PKA signalling remain unclear, there is growing understanding of how the RI and RII isoforms are localised within cells. Such targeting of PKA holoenzymes to subcellular regions of the cells is, at least in part, mediated by A-Kinase Anchoring Proteins (AKAPs), which are a group of structural proteins encoded by more than 50 human genes[46] that are classified by the ability to bind one or other of the R subunits of PKA. The physical constraint of PKA close to substrates and modulators such as phosphatases[47] and PDEs[48] allows localised signalling from such widely expressed proteins. Such a protein complex is often termed a signalosome. RII subunits are usually bound to membranous regions of the cell, whereas RI subunits are usually distributed diffusely in the cell but still have the ability to be recruited to specific subcellular locations[45]. RII subunits are normally considered to be defined by their ability to bind AKAPs, although AKAPs that are able to bind RI subunits as well have been described (Table 1). Structural differences in the Dimerisation/Docking domain (D/D) of the R subunits determines the predilection for RII subunits compared to RI subunits for AKAP-binding, thanks to RII forming a shallow two helical turn structure rather than the deeper four helical turn structure of RI subunits[49]. AKAPs that show dual-specificity for RI and RII, include AKAP149 (AKAP1 or D-AKAP1)[50], AKAP10 (D-AKAP2)[51] or AKAP220; RI-specific AKAPs include SKIP[52, 53] and smAKAP[54] .

Gene	Alternative Name	Location
AKAP1	D-AKAP1, AKAP149	Mitochondrial outer membrane, ER[50]
AKAP7	AKAP18 (α,β,δ,γ splice variants)	Cytoplasm (γ), plasma membrane (αβδ), nucleus (γ)[55]
AKAP10	D-AKAP2	Mitochondrial outer membrane[56]
AKAP11	AKAP220	Cytoplasm, Centrosome, Cytoskeleton, Peroxisome[57]
SKIP	SPHKAP	Mitochondria and cytoplasm[53]
smAKAP	-	Plasma membrane[54]
AKAP78	Ezrin	Plasma membrane, cytoskeleton[58]

Table 1.1 A Kinase Anchoring Proteins (AKAPs) that bind PKA RI

Despite their name, AKAPs do not merely restrict the diffusion of PKA Regulatory subunits to membranous regions of the cell but help to form macromolecular signalling complexes that integrate numerous signalling pathways. For example, AKAP79 has been found to bring PKA RII, PKC and the phosphatase calcineurin at specific subcellular sites in neurons[47].

1.2.4 The Type I Regulatory subunit of PKA and its redox sensitivity

Isoforms of the R subunit differ in their affinity for cAMP. The RI subunits have a higher affinity for cAMP than RII isoforms[59]. Therefore holoenzymes containing RI subunits become active at a lower threshold of cAMP concentration compared to RII-containing holoenzymes[35]. Germline deletion of RIα in mice results in embryonic lethality[60], and haploinsufficiency leads to tumour development[61] which suggests that the isoform is vital for normal development. Mutations in the gene encoding RIα in humans cause the Carney Complex of benign cardiac tumours (myxomata), skin pigmentation and endocrine dysfunction[62]. Aberrant over-expression of the RIα subunit has also been associated with the initiation and progression of several human cancers including adrenocortical tumours[63], breast cancer[64], colorectal cancer[65] and melanoma[66]. In a large number of human cancer cell lines, RI is the only identifiable R subunit of PKA. Over-expression of RIα in Chinese Hamster Ovary (CHO) cell line confers a growth advantage in monolayer and soft agar conditions whereas overexpression of the C subunit does not[67].

The RIα, but not the RIβ, subunit can serve as a redox sensor as the D/D domain contain cysteine residues that can be oxidised to form inter-chain disulphide bonds[68]. The RIα subunit contains a total of four cysteine residues[69]. Two of these sulfhydryl groups lie close to the NH_2-terminal end of the polypeptide chain and, in the purified protein, both of these cysteine residues are disulphide bonded to the adjacent subunit even in the presence of exogenous-reducing agents. The remaining sulfhydryl groups lie in the cAMP-binding domain and are fully reduced. Through peptide digestion assays, the RI subunit is aligned in an antiparallel manner by which C17 is bonded to C37 – therefore means that dimers are prevented with mutation of one cysteine as parallel

disulphide alignment cannot take place[68]. Disulphide bond formation between RI subunits at C17 and C37 is not required for dimerization between R subunits and hence the heterotetrameric structure of the PKA holoenzyme can be maintained[70] even in the absence of the C17 or C37.

1.2.5 cAMP-independent change in PKA activity

A number of protein kinases such as Protein Kinase C (PKC)[71] and Protein Kinase G (PKG)[72] have been described as being modulated in their activity directly by redox modification. Classical PKA activation in terms of its ability to phosphorylate targets requires the dissociation of R subunits from C subunits (Figure 1.3). Apart from the binding of cAMP to R subunits, there is accumulating evidence of PKA activation that may occur independently of changes in cAMP concentration. For example, the C subunit of PKA may be associated with, and inactivated by, IκB in an NF-κB-IκB(C-subunit) complex. Stimulation of cells with LPS, endothelin-1 or angiotensin II induces IκB degradation, resulting in the ensuing C subunit-catalysed phosphorylation of NF-κB p65[73, 74]. Another mechanism of c-AMP independent dissociation of C and R subunits is by proteolysis of the tetramer by the enzyme calpain[75]. Furthermore, an RI-specific mechanism of PKA activation has been reported that depends upon the redox-sensing capabilities of the RI subunit. The mechanism by which PKA activation occurs is attributed to the susceptibility of Type I PKA to disulphide bond formation between cysteine residues, which are not found in Regulatory Subunit Type II of PKA[76].

The RI subunit of PKA can undergo oxidation to form intermolecular disulphide bond formation between cysteine residues at positions 17 and 37 of RI. The oxidation of RI

monomers to form such dimers has been associated with an increase in PKA activity as measured by down-stream phosphorylation of putative targets in the absence of an increase in cAMP [77]. These downstream effects were also associated with an increase in contractility of rat ventricular myocytes[77].

Oxidation of PKA RII has been shown to inhibit target phosphorylation[78], which has been taken to mean decreased PKA activity. In this instance, H_2O_2 oxidises the type II holoenzyme to form a disulphide bond between Cys^{97} of regulatory IIα or IIβ subunit and Cys^{199} of the catalytic α subunits. The mechanism of inhibition is proposed to be via binding of the RII and C subunits, which prevents the C subunit from leaving the inhibitory RII subunit, even in the presence of cAMP[78]. PP2A, which dephosphorylates serine/threonine residues, that have been phosphorylated by PKA, exhibits increased activity on oxidation[79]. However, the effect of redox state on phosphatase activity is not uniform and may be related to the extent of the redox state. Indeed, mild oxidation enhances the duration of substrate phosphorylation via inhibition of phosphatase activity[80]. Indeed, Adenylyl Cyclase, which indirectly modifies PKA activity through its production of cAMP exhibits a biphasic effect in response to oxidation[81]. Therefore, the effects of oxidation may be multiple and potentially opposing within this signalling pathway.

1.2.6 Redox signalling and molecular switches

From the negative connotations of oxidative stress as an intrinsically pathological process, the concept has since been updated to include the role of redox modulation of cellular signalling under physiological circumstances[82]. The term oxidative stress implicitly conveys the notion of an organism responding to its environment. The

concept of molecular signalling switches was first developed in relation to the phosphorylation / dephosphorylation of proteins to form the basis of molecular signalling[83]. A bridge between phosphorylation / dephosphorylation and protein cysteine reduction / oxidation is given by the reversible redox sensitivity of critical cysteine residues in protein phosphatases, opening the molecular pathway for integration of signalling through phosphorylation and cellular redox state[84]. A change of redox state may therefore allow cross-talk between signalling cascades that make use of protein phosphorylation by kinases and dephosphorylation by phosphatases.

The reversible covalent modification of cysteine residues by oxidants is vital for their role in physiological cellular signalling[85]. Cysteine residues may be oxidised to produce a number of modifications including sulphenic (R-SOH), sulphinic ($R\text{-}SO_2H$) species, sulfonic ($R\text{-}SO_3H$), nitrosylation (R-SNO), glutathionylation (R-SSG) and the formation of inter/intra-molecular disulphide bonds (R-SS-R). It has been predicted that over five hundred proteins with redox-sensitive cysteine residues may exist[86].

The redox-environment differs by location within the cell, depending on the balance of sources of oxidation and antioxidant defences. The cytosol and nucleus are net reducing environments[87] whereas, in particular, the mitochondrion is an oxidising environment due to activity of oxidative respiration and the electron transport chain, which release ROS such as superoxide and H_2O_2[88]. Exposure of cells to ROS activates a range signalling pathways. Oxidation occurring in the cytoplasmic compartment is frequently exploited as a signal that then triggers the translocation of proteins to other compartments. There is growing evidence that ROS are not ‘second messengers’ but modifiers of a primary signalling cascade linking the redox state of the cell to pre-

existing signalling cascade – encoding physiological adaptation by the cell. For example, one view of mitochondrial H_2O_2 production is that it acts as a signal that advises the cytoplasm and nucleus what the mitochondria are doing - leading to changes in nuclear gene transcription via activation of Mitogen Activated Protein Kinases (MAPKs)[89]. An increase in intracellular ROS as a result of exposure to a number of different stimuli can lead to oxidation of cysteine residues in cytoplasmic proteins such as kinases and phosphatases, ultimately affecting signal transduction processes.

Although both redox modification of cysteine residues and protein phosphorylation represent reversible post-translational modifications of proteins that are necessary for signal transduction, there are a number of differences between these two signalling mechanisms. Protein phosphorylation is an energy-dependent process, which renders the modification permanent until dephosphorylation by phosphatases takes place. This allows the signal to propagate, contributing to the amplificatory nature of the mechanism. Redox modifications, however, are energy independent and proportional to the degree of oxidative stimulus encountered. In this way, redox signalling represents a linear process compared to the amplificatory cascade of protein phosphorylation. These features are informative about the roles such signalling mechanisms may play in the adaptive response by cells to their environment. Protein phosphorylation is the result of an agonist-induced activation of a signalling cascade with modulation of the response by the redox state of the cell. For H_2O_2 to act as a signalling molecule, its concentration must reach a certain threshold and remain elevated for a sufficient length of time for it to oxidise target molecules.

1.3 Detection of PKA activity by fluorescence microscopy

Early intracellular optical sensors included small molecules that bind to analytes, for example Fura-2 binds calcium to elicit a change in fluorescence[90]. Fluorescent proteins are a useful tool for measuring intracellular signalling because they are genetically encodable, bright and available in many colours, which enables the monitoring of more than one target simultaneously. The genetic encodability is particularly desirable as it takes advantage of the intrinsic capacity of the cell to synthesise protein, allowing fluorophores to be introduced with minimal disruption to the cell and target the probes to particular regions of interest with the addition of targeting sequences. A wide range of biosensors have been developed for monitoring different cellular events such as changes in pH[91], accumulation of second messengers like calcium[90] and cAMP[92] and activation of enzymes such as PKA[93].

1.3.1 FRET sensors for cAMP-PKA signalling

The first fluorescent biosensors for cAMP were developed in the early 1990s [94] but were superseded by genetically encoded biosensors, principally those that make use of the phenomenon of Fluorescence Resonance Energy Transfer (FRET) to measure dynamic, ratiometric changes in cyclic nucleotide signalling[95]. The development of fluorescent reporters of specific components of nucleotide signalling, such as those that make use of FRET, have permitted the direct visualization of the limited diffusion of cyclic nucleotides that characterizes subcellular regions. FRET describes the phenomenon of the non-radiative transfer of energy from one fluorophore to another, such that in response to the excitation of one fluorophore (donor) by light, there is a transfer of energy to the other fluorophore (recipient), provided that it is in sufficiently close proximity. The efficiency of energy transfer is highly dependent on the distance

between donor and acceptor, making the method highly sensitive to changes in protein conformation as occurs following post-translational protein modification, in this case phosphorylation. The change in structure alters the distance between the two fluorophores, affecting the efficiency of energy transfer between them. In this instance, the emission from the now excited recipient is measured thereby allowing a ratio of emissions from the two fluorophores to be detected and hence phosphorylation state to be inferred (Figures 1.5 and 1.6). Equally, it should be noted that any change in conformation of the FRET sensor that alters the distance between the fluorophores may induce a change in FRET ratio, whether secondary to phosphorylation or not. FRET reporters have been developed to measure dynamic, ratiometric changes in [cAMP][95] or PKA activity[96] within cells.

The genetically encoded FRET biosensors are divided into two classes : intra-molecular (unimolecular) biosensors and inter-molecular (or bimolecular) biosensors. The intramolecular sensors as in the case of H187 and AKAR3ev used in this thesis, contain both donor and acceptor fluorophores within a single biosensor. Inter-molecular sensors consist of a pair of distinct molecules conjugated with either a donor or an acceptor fluorophore. Intramolecular FRET biosensors have been widely used in cell biology due to the following advantages: high signal-to-noise ratio, easy loading of the biosensor into the cells, and simple ratiometric image analysis.

The A-Kinase Activity Reporter (AKAR) sensor was first developed in 2005[97] and comprised a fusion of cyan and yellow fluorescent proteins and a consensus substrate for PKA (Figure 1.5). Therefore, the AKAR FRET biosensors represent a method by which net PKA activity can be measured as the phosphorylation of the sensor is a

representation of the equilibrium of the activity of kinases and phosphatases. Through the choice of fluorophores and modification 'linker' amino acid sequences in the construction of the sensor, improvements in sensitivity have been achieved with the development of AKAR2[96], AKAR3[93], AKAR3ev[98] and AKAR4[99] sensors.

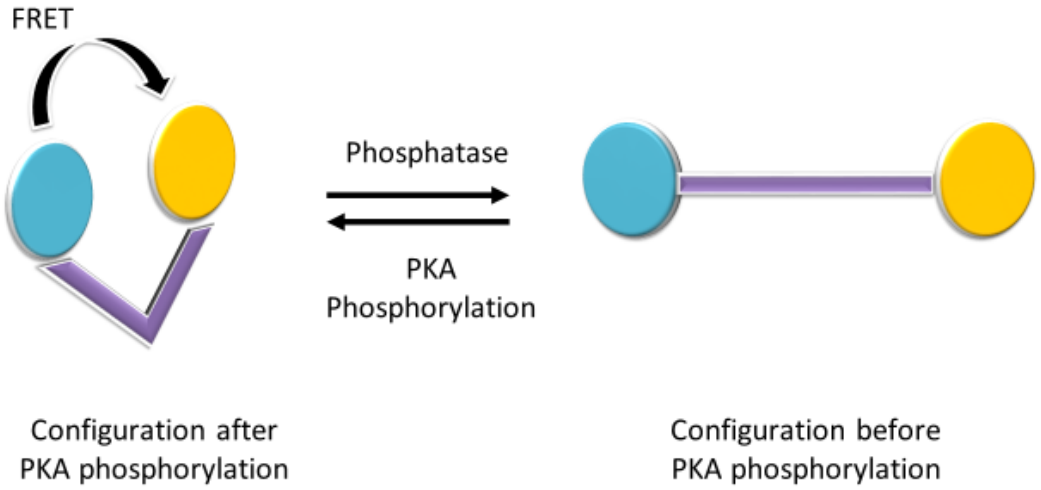


Figure 1.5 Cartoon to describe the mechanism of Fluorescence Resonance Energy Transfer (FRET) that takes place in response to phosphorylation of the A-Kinase Activity Reporter (AKAR) class of sensor, which detects PKA activity

In the case of cAMP, sensors have been developed whereby binding of the cyclic nucleotide to a molecule based on EPAC (exchange protein directly activated by cAMP)[100], an endogenous target of cAMP, leads to a change in protein conformation, which modulates the degree of FRET (Figure 1.6). From this conformational change, leading to a change in FRET efficiency, a change in cAMP concentration can be inferred. The latest generation of EPAC-based FRET sensor, EPAC-H187[101], comprises a truncated version of mTurquoise2[102] (an analogue of Cyan Fluorescent Protein (CFP))

as a donor fluorophore and a tandem of circular permutated Venus (Yellow Fluorescent Protein analogue) as an acceptor fluorophore. The sensor has an exceptionally high quantum-yield and brightness, with an excellent signal-to-noise ratio and is biochemically inert[101].

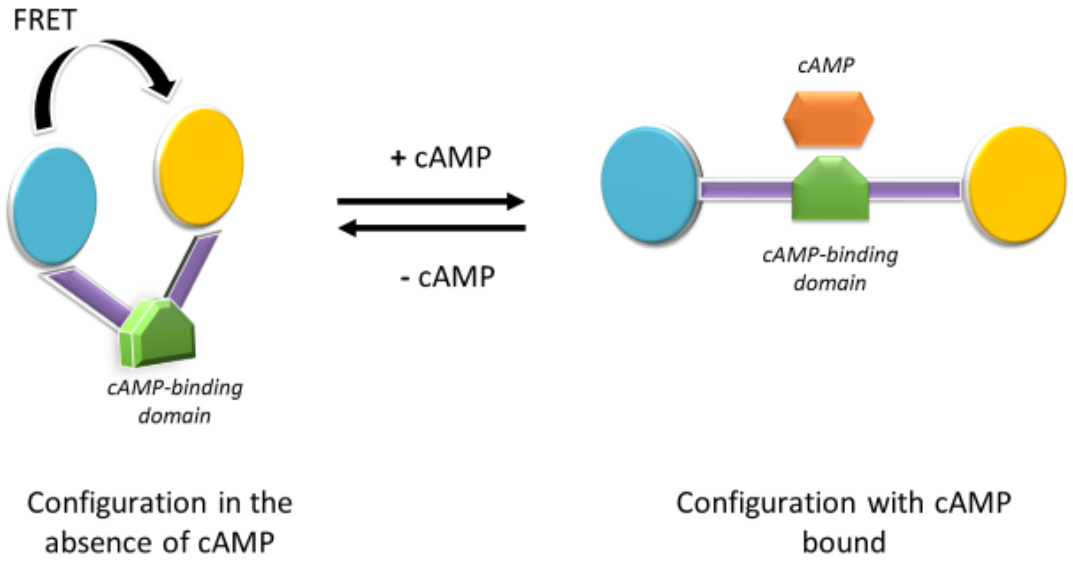


Figure 1.6 Cartoon to describe the mechanism of Fluorescence Resonance Energy Transfer (FRET) that takes place in response to the binding of cAMP to Epac-H187 to detect changes in cAMP concentration in response to cAMP-binding.

1.4 Aim of the thesis

Indirect evidence of cAMP-independent activation of Type I PKA has been proposed using a rat cardiomyocyte model, in which downstream target phosphorylation has been used as a marker of PKA activation[77]. Since this observation, a number of techniques and tools have become available that may help to provide direct evidence of cAMP-

independent PKA activation – a potentially important pathophysiological modulator of this important second messenger signalling cascade.

A transgenic mouse model that is insensitive to RIα subunit oxidation and FRET-based sensors can provide real-time, live-cell evidence of PKA activity. These techniques have allowed the proposed phenomenon of cAMP-independent PKA activation to be investigated more fully. The overall aim of this thesis has been to examine how the oxidation of PKA RIα may influence the activity of PKA signalling directly (Chapters 3 and 4). Subsequently, the effect of PKA RIα oxidation on its mobility within the cell has been examined to investigate how the redox state of the cell may indirectly modulate Type I PKA signalling (Chapter 5).

Chapter 2

Methods

2.1 Experimental Models

2.1.1 Adult mouse cardiomyocytes

With the advent of germline and tissue-specific transgenic technologies, the adult mouse represents a useful tool for the study of cardiovascular pathophysiology. The overall aim of the experiments described in this thesis were to elucidate the role played by the redox-sensitive cysteine residues at position 17 and 37 of the Type I Regulatory (R) subunit of PKA. A so-called 'redox-dead' transgenic mouse line has been developed by the group of Professor Philip Eaton (King's College, London), in which the cysteine 17 residue has been replaced by a serine (hence C17S nomenclature)[103]. This mutation prevents disulphide bond formation between RI subunits and hence acts as a robust negative control for investigations of the role of redox-dependent disulphide bond formation on the function of Type I PKA. Therefore, a protocol for the isolation of primary cardiomyocytes from adult mice was essential for many of the experiments described in subsequent chapters.

2.1.1.1 Isolation procedure

Although immortalised cardiac cell lines of mouse atrial origin exist (HL-1)[104], primary adult cardiomyocytes represent a more physiologically relevant model. The isolation of adult rodent cardiomyocytes makes use of the Langendorff method of retrograde perfusion, which utilises the coronary circulation to allow uniform deep penetration of the myocardium with a proteolytic solution[105]. It should be emphasised that a fastidious approach is required for successful isolation of adult mouse cardiomyocytes. The better the initial yield of cells, the greater the number and quality of cardiomyocytes obtained, ultimately improving the reliability of the subsequent experiments. In particular, any

glassware should be washed thoroughly in deionized, calcium-free water in order to prevent contamination. Fluctuations in calcium concentration during the isolation procedure can be disastrous for the cardiomyocyte survival[106].

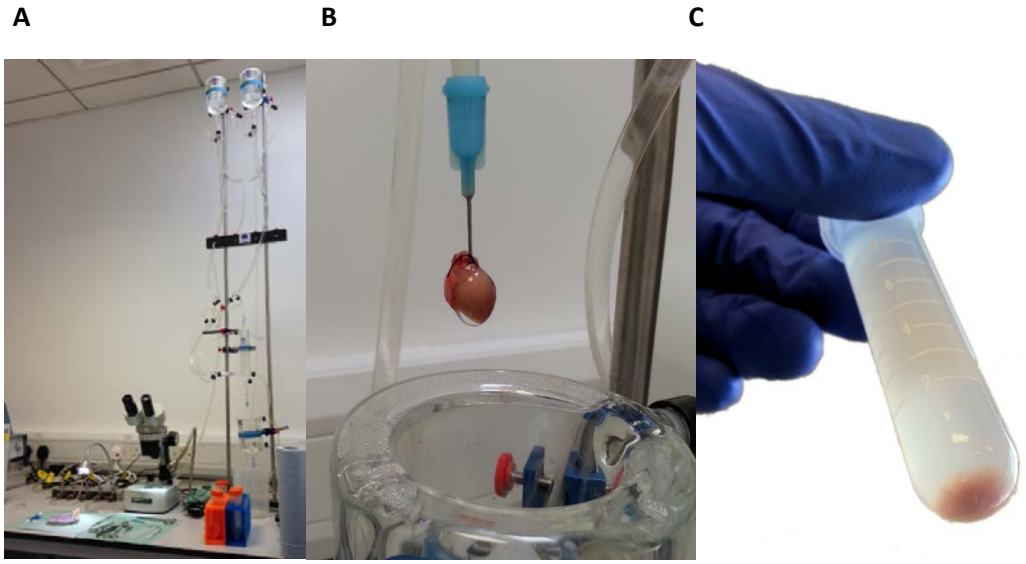


Figure 2.1

a) Example Langendorff perfusion apparatus with bench-top microscope and dissection equipment

b) Cannulate primary adult mouse heart undergoing Langendorff perfusion with digestive enzyme solution. Note the homogenous pale pink colour to the myocardium. In practice the warming jacket is positioned around the preparation but is lowered in this instance to allow the preparation to be seen clearly.

c) Example of pellet of cells achieved after first centrifugation of isolation suspension from a heart extracted from a 10 week old male C57/BL6 mouse

Coverslips – 15mm diameter borosilicate glass	**Solutions** *Tyrode buffer solution* : 130.0 mM NaCl, 5.6 mM KCl, 3.5 mM $MgCl_2$, 5.0 mM HEPES Buffer, 10.0 mM Glucose, 20.0 mM Taurine, 0.4 mM Na_2HPO_4. pH 7.4 and filter sterilized
Culture well plates to accommodate coverslips	
Laminin (100µg/ml)	
Langendorff apparatus – including heated water circulation and 100% oxygen supply (Figure 2.1A)	
2 x forceps, one small to allow tie to be placed around aorta and one large to aid gross dissection of skin and surround tissues	*1% Bovine Serum Albumin (BSA)* : three 10ml preparations using the Tyrode buffer described above with calcium-free, 600µM and 1200µM Ca^{2+} as three separate solutions
2 x scissors, one straight Vannas, one standard 11cm straight blade	
Cannula – 21 Gauge	
5/0 Gauge silk wax suture material – approximately 4cm in length	*Isolation solution* : Numerous tissue dissociation enzyme products are available. In our experience, we have found 50µg/ml Liberase® TH Research Grade (Roche, Switzerland) with 100 µM Ca^{2+} is highly effective, reliable and it is associated with good expression of fluorophore.
4 x 23 Gauge needles for limb transfixion – taping of limbs also possible	
Adult mouse usually >8 weeks of age for sufficiently large calibre of aorta to allow cannulation	
Bench-top microscope or other magnifying equipment	
Supply of calcium-free deionized water	
Water bath pre-heated to 37.5°C	
Bench-top centrifuge	
Plastic collection tubes – 15ml and 50ml	
Funnel to fit in 10-15ml collecting tube 3ml teat pipettes	

Table 2.1 Equipment and Pre-procedure preparation for Langendorff perfusion ond isolation of adult mouse cardiomyocytes

Isolation procedure

For FRET imaging experiments, where cells need to be adherent to coverslips, coat sterile borosilicate glass coverslips with laminin (e.g. 100µl of 100µg/ml on a 15mm coverslip) at least two hours prior to cardiomyocyte isolation.

1. After preparation of materials as described in Table 2.1, perform cervical dislocation of an adult mouse according to local rules and protocols.
2. Immediately place mouse supine on dissection pad with limbs held out laterally to leave the thorax clearly visible
3. Perform a midline skin incision using scissors and larger forceps to reveal the sternum
4. Perform two lateral thoracic / costal incisions
5. Reflect the xiphisternum to reveal underlying precordium
6. Excise the sternum and ribs via a manubrial incision
7. Switch to microscope or other magnification equipment such as magnifying spectacles (loops) to aid visualization of the aorta
8. Excise thymus to reveal great vessels
9. Place a suture deep to the aorta using small forceps
10. Make a single loose tie with suture material around the aorta
11. Perform a single incision into the aorta, just proximal to the first bifurcation of the aorta using straight Vannas scissors.
12. Insert a 21 Gauge cannula into the now open aorta, enough to allow the cannula to rest in place, but not too deep so as to pass into the left ventricle. If the cannula has entered the left ventricle, the principal of Langendorff retrograde perfusion via the coronary arteries is lost and the isolation fails. Equally, division of the aorta too

close to the first bifurcation can allow the vessel to collapse, which delays cannulation or makes it impossible.

13. Tighten knot around cannula and apply second tie

14. Lift knot by pulling the ends of the suture and use larger scissors to free the heart and cannula from the surrounding tissue

15. With the heart now attached to the cannula and free from the surrounding tissue, check that any air bubbles in the hub of the cannula are removed. Air bubbles prevent the flow of perfusate and hence can lead to loss of the preparation by infarction.

16. Open the tap at base of Langendorff apparatus and mount cannula and heart (Figure 2.1B)

17. Allow the Tyrode buffer to perfuse the heart to start with to ensure that perfusion takes place. The first few drops of perfusate should be heavily blood-stained, which will clear within approximately 1-2 minutes of perfusion.

18. When satisfactory perfusion is taking place, switch to a perfusate that contains a digestive enzyme solution

19. Digestion of myocardial interstitial tissue is complete when the drop rate from the perfused heart increases in speed rapidly to >1 drop per second from an initial drop rate of approximately 1 drop every 2-3 seconds. Collect digestive enzyme solution, as 2-4ml are required in the next step.

20. Place the heart in sterile dish with 1-2 ml of the collected enzyme solution and excise the atria and right ventricle with fine scissors and forceps – leaving only the left ventricular tissue.

21. Finely chop the remaining left ventricular tissue with scissors and place the suspension into a plastic centrifugation tube. Triturate the myocardial tissue using a 3ml teat pipette for 30 seconds

22. Filter through gauze into another centrifugation tube and add Tyrode + 1% BSA to terminate action of digestive enzymes (Table 2.1)

23. Centrifuge lysate ≈80 *g* for 3 minutes with slow acceleration / deceleration of the rotor. The centrifugation must be gentle. If the rotor speed or its rate of acceleration are too high, the cardiomyocytes become severely damaged. Gravity sedimentation may be used throughout the isolation procedure but it is slower compared to centrifugation.

24. A pellet of cells should be clearly visible after the first centrifugation (Figure 2.1C)

25. Remove and discard supernatant and re-suspend with Tyrode + 1% BSA supplemented with 600μM Ca^{2+}.

26. Leave to settle at room temperature and pressure for 7 minutes. During this time, a clearly visible pellet should form, similar but smaller than after step 21.

27. Carefully remove supernatant and replace with 1% BSA supplemented with 1.2mM Ca^{2+}. The aim of the serial washes is two-fold. Firstly, to allow gravitational separation of the heavier viable cardiomyocytes from the fibroblasts and lysed, dead cardiomyocytes which remain in suspension. Secondly, the rising concentration of calcium aims to prevent toxic calcium overload of the cells which occurs on placing the cells in the final MEM culture medium which has a Ca^{2+} concentration of 1.8mM. The procedure described above yields approximately ≈ 1 million viable cardiomyocytes from an excellent isolation, which represents about 80% of the total cellular population. (Figure 2.2). The remaining 20% of rounded, distorted cells are considered to be non-viable cardiomyocytes. Leave the suspension to settle under gravity at room temperature for 30 minutes

28. After this second wash, remove supernatant and re-suspend in MEM culture medium supplemented with 2.5% FBS and plate on coverslips that have been coated with laminin as described in the introduction.

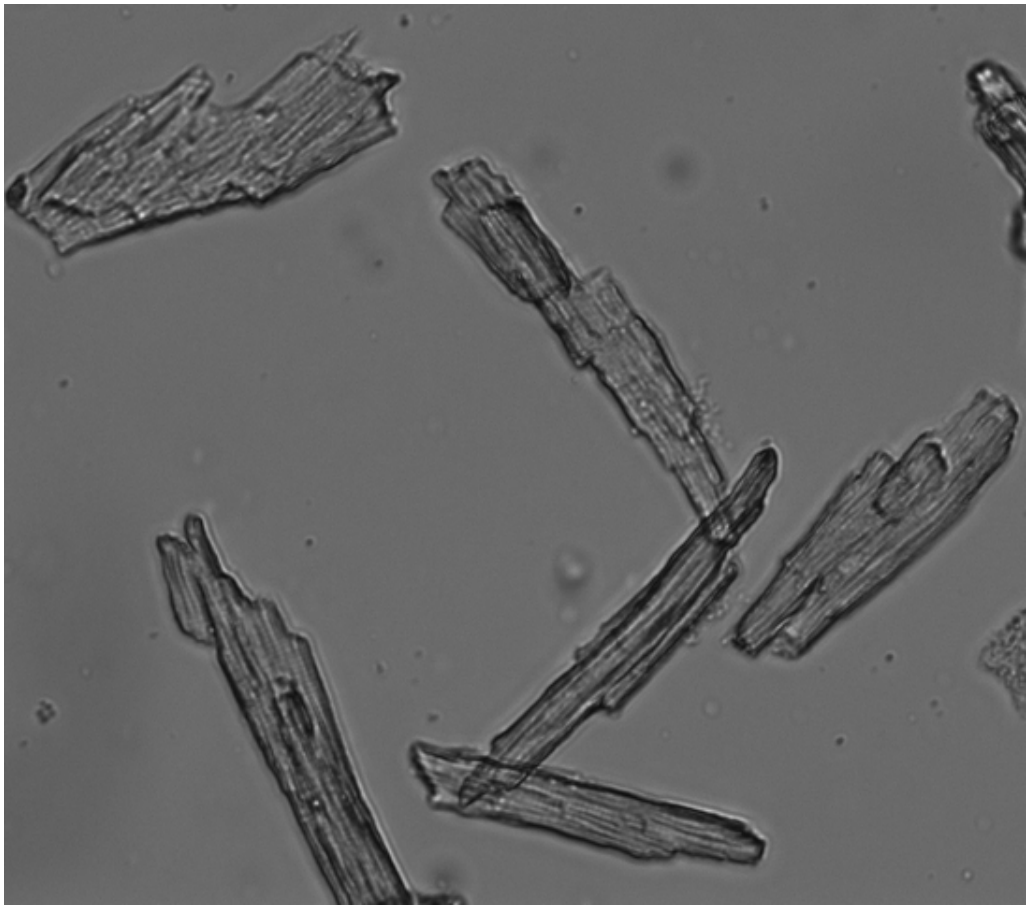


Figure 2.2 Freshly isolated adult mouse cardiomyocytes after serial washing in Tyrode solutions containing 1% bovine serum albumin (BSA) and a rising concentration of calcium from one wash to the next.

2.1.1.1.1 Redox Dead Mouse and its Genotyping

With the advent of transgenic mouse models that allow the germ-line or tissue-specific control of gene expression, primary adult mouse cardiomyocytes represent a readily available experimental tool that allow the laboratory investigation of mammalian cardiac pathophysiology at a cellular level.

The 'redox-dead' mouse model describes the substitution of a cysteine for serine at position 17 (C17S) of the RIα subunit of PKA holoenzyme. The transgenic mouse was developed by the group of Professor Phillip Eaton, King's College London[103] and was a kind gift to allow us to work on this project.

The genotype of each mouse was determined by obtaining an ear notch biopsy, extracting genomic DNA, using PCR primers to amplify the region of the desired mutation and finally DNA electrophoresis to detect different PCR products that correspond to different genotypes.

Ear notches

Punch biopsies from the ears of the mouse colony were obtained in accordance with the identification policy of the Biomedical Services Facility (Animal House) of the John Radcliffe Hospital, in accordance with the relevant requirements of the Home Office of the Her Majesty's Government. The ear notches were stored at -20°C until DNA isolation and PCR were carried out.

DNA isolation for genotyping

The Qiagen DNeasy kit (69504 – Qiagen, USA) is a commercially available system for the isolation of genomic DNA from tissue. The protocol using Qiagen's proprietary reagents can be summarised as follows :

1. Place the ear notch in 180µl Buffer ATL + 20µl proteinase K. Mix thoroughly by vortexing, and incubate with agitation at 56°C until the tissue is completely lysed (usually overnight). Take care to record ear notch source on micro-centrifuge tube.

2. After tissue lysis in Step 1, vortex for 15 seconds. Add 200µl Buffer AL to the sample, and mix thoroughly by vortexing. Then add 200µl ethanol (96–100%), and mix again thoroughly.

3. Pipette the mixture from step 2 into the DNeasy Mini spin column placed in a 2ml collection tube. Centrifuge at ≈6000 g for 1 min. Discard the flow-through and collection tube.

4. Place the DNeasy Mini spin column in a new 2 ml collection tube, add 500µl Buffer AW1, and centrifuge for 1 minute at ≈6000 g. Discard the flow-through and collection tube.

5. Place the DNeasy Mini spin column in a new 2 ml collection tube (provided), add 500µl Buffer AW2, and centrifuge for 3 minutes at ≈20 000 g to dry the DNeasy membrane. Discard the flow-through and collection tube.

6. Place the DNeasy Mini spin column in a clean 2ml microcentrifuge tube and pipette 200µl Buffer AE directly onto the DNeasy membrane. Incubate at room temperature for 1 minute, and then centrifuge for 1 minute at ≈6000 g to elute. At this stage, the sample is ready for gel electrophoresis.

Polymerase Chain Reaction (PCR) for genotyping

DNA primers were designed as follows :

Primer 1 : GCTTTCCTTTACCAAGCAGG

Primer 2 : GTCTGTGAGTCACACTGACC

The following reaction mixture was prepared for each sample (Table 2.2) and run according to the conditions in Figure 2.3.

5µl PCR Buffer 10x (Invitrogen)	2µl $MgCl_2$ (50Mm)
1µl dNTPs (10Mm)	0.4µl Taq polymerase (5U/µl, Invitrogen)
1µl Primer 1 (5uM)	37.6 µl H_2O
1µl Primer 2 (5µM)	2µl DNA (as purified by Qiagen DNAeasy kit)

Table 2.2 PCR Reaction constituents for genotyping

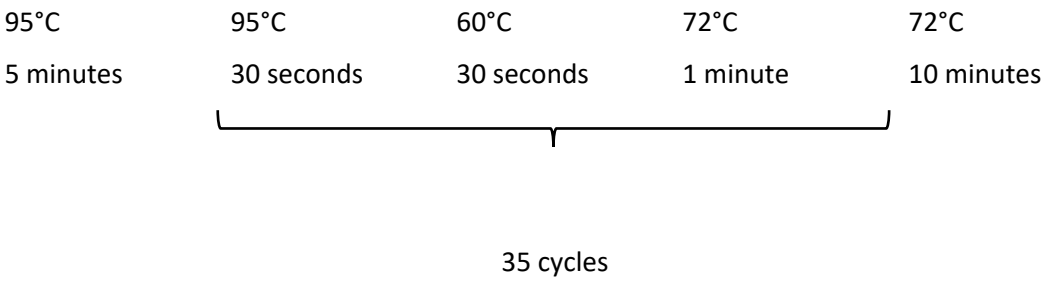


Figure 2.3 Details of the PCR reaction program used for genotyping

After completion of the reaction, the PCR product was run in a 2% TAE agarose gel until sufficient band separation had occurred to allow accurate identification of genotypes (Figure 2.4).

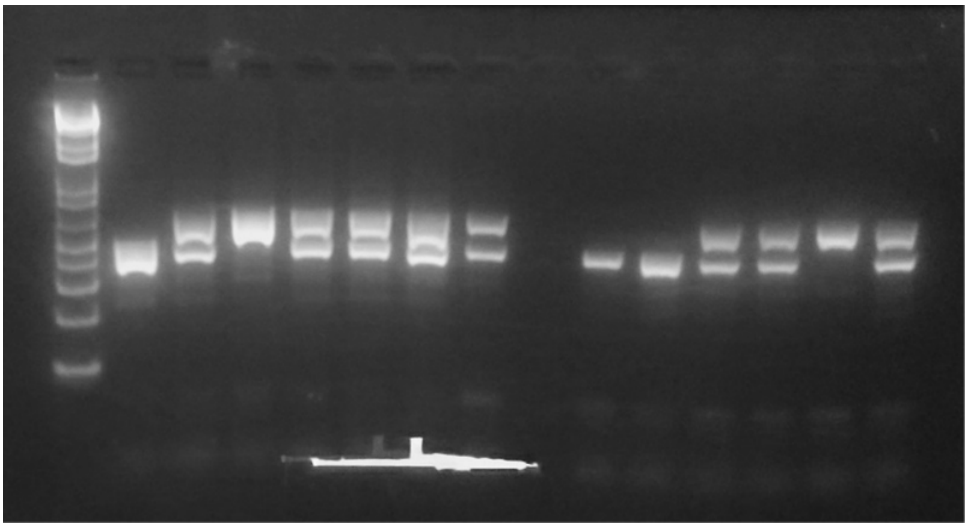


Figure 2.4 Sample DNA electrophoresis for genotyping. The marker column in the first, left lane is used to identify the fragments from particular genotypes based on their molecular mass.

Fragment size – Wild-type 385 kDa; Redox-Dead knock-in 548 kDa

2.1.2 Measurement of contractility in adult mouse cardiomyocytes

Contractility describes the ability of cardiomyocytes to develop contractile force in response to a stimulus, either electrical or chemical. At a single cell-level, systems have been developed that measure changes in cell length so as to allow calculation of cellular characteristics of contraction. A myocyte contractility recording system (Ionoptix, USA) was used to measure parameters of contractility in isolated primary adult mouse cardiomyocytes, through the serial acquisition of images of single cardiomyocytes, from which the edges of cells are detected (SoftEdge Software, Ionoptix, USA). From these data, changes in contractility may be derived. It should be borne in mind that this represents a measure of contractile properties in a single cardiomyocyte that is dissociated from the myocardium and hence the data are not directly translatable to whole organ function.

An important measure of cardiomyocyte integrity is its viability as determined by the ability of the cell to contract – a key function of cardiomyocytes that is known to be regulated by cAMP-PKA signalling[107]. After the isolation of adult mouse cardiomyocytes, cells were plated on laminin-coated glass coverslips as described in Chapter 2.1.1.1.1 and bathed in a Tyrode solution pH corrected to 7.4 and supplemented with 1.4mM Ca^{2+} (Table 2.1). The plating of cells in coated coverslips allowed the cells to become sufficiently adherent to allow recordings to take place but without fixing them to prevent contraction. The plating of the cells was performed consistently across all experiments to ensure consistency of approach, whether in functional or imaging experiments. As has been published elsewhere[108], viability was determined by simply counting the proportion of cells that contracted in response to 1Hz electrical field stimulation compared to non-contractile cells that had the characteristic morphology of

adult mouse ventricular cardiomyocytes of angular, striated often binucleate cells. All experiments were carried out at room temperature and pressure to ensure consistency with the experimental conditions encountered during FRET microscopy experiments.

A myocyte contractility recording system (Ionoptix, USA) was used to determine measures of cardiomyocyte contractility under 1Hz electrical field stimulation, from which changes in cell-length over time could be derived. Fractional shortening (FS) describes the relative change in myocyte length during a period of contraction, in this instance due to 1Hz electrical field stimulation. The measurement acts as a descriptor of the inotropic capacity of the cell. Conversely, 'Tau' (τ) is the exponential decay time constant that characterises the speed of recovery (relaxation or calcium reuptake) of the cardiomyocyte. A greater value of τ equates to a longer recovery or return to baseline and is considered to correspond to slower re-uptake of calcium by the Sarcoplasmic Reticulum (SR) during diastole of the cardiac cycle. Therefore, these two characteristics are frequently used to describe characteristics of contraction and relaxation of adult mouse cardiomyocytes.

2.1.3 Culture of primary adult mouse cardiomyocytes

Since the original observations that PKA activity could be enhanced through oxidation, not only has the transgenic 'redox-dead' mouse been developed[103], but there have been advances in live-cell fluorescence microscopy that permit real-time evaluation of PKA activity. The use of adult mouse cardiomyocytes with genetically encoded constructs, such as FRET biosensors, do present a number technical difficulties that needed to be overcome, namely their relative poor survival in culture[108] to allow gene expression to take place and their relative resistance to adenoviral infection[109].

After isolation of primary cardiomyocytes, the cells were plated on laminin-coated glass coverslips and needed to be maintained in culture over the period of 24 hours required to allow the expression of FRET biosensor to occur. The choice of Minimum Essential Medium Eagle (MEM) culture medium (Table 2.3) is an important factor that ultimately facilitates the expression of genes that have been transduced into murine cardiomyocytes by adenovirus[109].

Modified Eagle's Medium (MEM) with Hank's salts *(Sigma : M1018)*
9mM $NaHCO_3$
1% L- Glutamine
1% Penicillin & Streptomycin
2.5% solution by volume Fœtal Bovine Serum (FBS) – as required

Table 2.3 Constituents of Modified Eagle's Medium (MEM) for the culture of primary adult mouse cardiomyocytes after transient exposure to adenovirus

In mammals, cells are exposed to 4-5mM glucose under physiological conditions. Prolonged elevations in environmental glucose promotes the generation of reactive oxygen species by mitochondria in cardiomyocytes[110]. The medium used for the culture of primary adult mouse cardiomyocytes contains 5.5mM glucose in contrast to other available culture media, which may contain up to 50mM glucose, and hence be a source of potential artefact.

The following steps were required after isolation to maintain the cardiomyocytes in culture[109, 111].

1. After this second wash, remove supernatant and re-suspend in MEM culture medium supplemented with 2.5% (FBS Table2.x) and plate on coverslips that have been coated with laminin. The role of the FBS supplementation is to aid recovery of the myocytes after the isolation procedure. Later culture conditions do not contain FBS, in order to limit the growth of fibroblasts in culture.

2. After two hours of recovery and adherence to coverslips, gently remove medium and replace with fresh MEM medium (without FBS) and infect cells with adenovirus of choice using a Multiplicity of Infection (MOI) 1:100.

3. After three hours of incubation of cells with adenovirus, wash the cells carefully three times with fresh MEM medium, supplemented with 0.5µM cytochalasin D.

4. Incubate at 37°C in 5% CO_2 with expression within the next 24 hours. Conduct experiments in a Tyrode Buffer solution with 1.4mM [Ca^{2+}] The role played by cytochalasin D in maintaining cardiomyocyte function is described in Chapter 3.

2.2 Continuous cell culture

Although primary cells from model organisms, such as mice, provide an excellent physiological model for the investigation of cellular signalling, they can be limited by their relative lack of potential for *ad hoc* genetic manipulation. Gene transduction into adult mouse cardiomyocytes relies upon viral vectors and hence DNA plasmid constructs, with their opportunities for flexibility and rapid turnover are not useful in this form.

Mammalian cell lines derived from immortalised human cells are easily grown in laboratory conditions and are readily transfected by plasmid constructs without the need for the development of adenoviral vectors that are often required for primary cells and, in particular, cardiomyocytes. Although cell lines have lost many of their original *in vivo* characteristics, such cells maye allow specific questions to be answered in a mammalian cell where the ubiquitous PKA signalling cascade is found. However, specific to this thesis, cell lines do not have the negative control of a 'redox-dead' mutant as found in the mouse model available for the experiments described in Chapters 4 and 5.

2.2.1 HeLa cells

HeLa cells are an immortal cell line originally derived from a cervical carcinoma from a 31-year-old woman, Henrietta Lacks. This was the first cell line derived from human tissue to be maintained in continuous cell culture and has been used extensively for over 50 years[112]. The cells have a very flat morphology, making them a very good candidate for microscopy experiments as it allows for a clear focal plane to be obtained. The cells

are maintained easily in cell culture with DMEM-based medium (Table 2.4) with a rapid rate of division that requires frequent passage.

2.2.2 HEK-293 cells

HEK-293 cells are derived from human embryonic kidney cells that can be maintained indefinitely in culture. The cells are of epithelial origin and have been used extensively to produce recombinant protein owing to their easy transfection, simple maintenance and highly efficient protein production[113]. The cells have been used in the experiments in this thesis for biochemical assessment of recombinant protein from plasmids, for example in the production of positive control proteins for immunoblot analysis. The cells have an irregular morphology making them more cumbersome to use in microscopy experiments, a role better suited to HeLa cells. HEK293 cells are maintained easily in cell culture with DMEM-based medium (Table 2.4) with a rate of division a little slower than HeLa cells.

Dulbecco's Modified Eagle's Medium (MEM) *(Sigma : D5546)*
5.5 mM Glucose

1% L- Glutamine

1% Penicillin / Streptomycin

10% solution by volume Fœtal Bovine Serum – as required

Table 2.4 Constituents of Dulbecco's Modified Eagle's Medium (MEM) for continuous cell culture

2.3 Plasmid construction and site-directed mutagenesis

The plasmid pCDNA3-mouse PKA-RIalpha-mEGFP was a gift from Haining Zhong (Addgene plasmid # 45525)[114] and its truncated base sequence is shown in Figure 2.5.

gcg tct ggc agt atg gca acc agt gag gaa gag cgg agt ctc cgg gaa **tgc** gag ctc tat gtg cag aag **cac** aat atc cag gcc ctg aag gac tcc atc gtg cag ctg **tgc** act acg cgg ccc gag agg ccc atg gca ttc ctt cgg gaa tac ttt gag agg ttg gag aag gag gca aga cag att cag tgt cta cag aaa acc ggc atc cgt act gac tcg ag gga cga gat ctc tcc acc ccc caa tcc agt ggt gaa ggg ccg acg gcg ccg agg tgc tat cag tgc tga agt tta cac tga gga tgc ctc cta cgt tag aaa ggt tat tcc aaa aga tta taa gac aat ggc tgc ttt agc caa ggc cat cga aaa gaa tgt gct gtt ttc aca cct tga taa cga gag aag tga cat ttt tga tgc tat gtt tcc agt ctc ctt tat tgc tgg aga gac ggt tat tca gca agg tga agg gga taa ctt cta tgt gat tga tca agg aga aat gga tgt cta tgt caa taa tga atg ggc aac cag tgt tgg gga agg gag ctt tgg aga gct ggc ttt gat tta tgg aac acc cag agc cac tgt caa agc aaa gac aaa cgt gaa act gtg ggg cat cga ccg aga cag cta ccg aag aat cct cat ggg aag cac tct gcg aaa gag gaa gat gta tga aga att cct tag taa agt gtc tat ttt aga gtc tct gga caa gtg gga gcg tct cac agt agc cga tgc att gga gcc tgt cca gtt tga aga tgg aca gaa gat cgt ggt gca agg aga gcc ggg gga tga gtt ctt cat cat ttt aga ggg cac agc tgc tgt gct gca gcg tcg gtc aga aaa cga aga att tgt tga agt ggg acg act ggg gcc ttc tga tta ttt tgg tga aat tgc cct gct gat gaa tcg tcc tcg ggc tgc cac tgt ggt tgc ccg ggg ccc ttt gaa gtg cgt taa gtt gga ccg gcc tcg gtt tga acg cgt cct tgg ccc gtg ctc aga cat cct caa gcg gaa cat cca gca gta caa cag ctt cgt gtc cct gtc cgt cga tat cat ggt gag caa ggg cga gag ctg ttc acc ggg gtg gtg ccc atc ctg gtc gag ctg gac ggc gac gta aac ggc cac aag ttc agc gtg tcc ggc gag ggc gag ggc gat gcc acc tac ggc aag ctg acc ctg aag ttc atc tgc acc acc ggc aag ctg

Figure 2.5 Base sequence of murine PKA RIα-GFP. Red region represents Dimerisation / Docking Domain (D/D); Blue region represents cAMP-binding domain of the regulatory subunit; Green region represents GFP (truncated).

In a similar fashion to understanding the effects of a point mutation in a transgenic animal model on the function of a protein in systems physiology, the expression of a plasmid bearing a mutated base sequence provides a simple, flexible model of assessing the effects of particular amino acid sequences on protein function and hence cell

physiology. The expression of a protein derived from a plasmid leads to protein production in excess of, not in place, of endogenous, genomically-encoded, genes.

Template production – transformation of bacteria and DNA extraction

1. To one 5µl aliquot of competent cells – One Shot® TOP10 Chemically Competent E. coli (ThermoFisher Scientific, USA) kept on ice; add DNA to be transduced into the bacteria – 3µl of PCR product or 10µl of ligation mixture from a mutagenesis.
2. Mix by gently flicking base of tube – do not mix with pipetting action.
3. Leave on ice for 30 minutes
4. 30 seconds at 42°C in a water bath
5. On ice again for a further 2 minutes
6. 200µl Super Optimal broth with Catabolite repression (SOC) medium (ThermoFisher Scientific, USA) at room temperature dropped in gently to the mixture
7. Place tube (with loosened lid) in shaker for 45 minutes
8. After 45 mins – spread all contents onto a pre-warmed agar plate with antibiotic appropriate to resistance encoded in plasmid
9. Place the agar plate face down in incubator and leave overnight
10. The next day, carefully select a number of colonies for culture in Miller's LB Broth (L3522 - Sigma-Aldrich, USA) with appropriate antibiotic preparation. More than one colony is required to allow for random mutagenesis.
11. The amplified colonies of transformed E. coli are then collected, lysed and the replicated DNA is purified according to standard, commercially available kits such as the Qiagen DNA preparation kits (QIAprep Spin Miniprep Kit – 27104) and Maxiprep (QIAprep Spin Maxi – 12162). DNA eluted in TE buffer (Promega, USA) can be stored for many months at 4°C without sample degradation.

12. Determine the concentration of DNA and its purity using a spectrophotometer such as the NanoDrop 2000c (ThermoFisher Scientific, USA).

Mutagenesis reaction

The process of using a thermal cycler to allow the reversible separation (denaturing) and realignment (annealing) of double-stranded DNA, coupled with polymerase enzymes not only permits PCR but also allows the introduction of mutations into known plasmid sequences – site-directed mutagenesis (Figure 2.6). The purified, concentrated DNA may be used for many purposes in molecular biology including as a template for site-directed mutagenesis[115].

Constituents	**µl**	**Reaction conditions**
Template DNA – PKA RI-α 10ng		a) 95 – 1min *b-d) – 20 cycles*
Primer Forward 20 pmol	1	b) 95 – 30 sec
Primer Reverse 20 pmol	2	c) 60 – 1 minute
Buffer 10x	2	d) 68 – x minutes per x Kb of plasmid construct (e.g. 8 minutes for 7.5kb Construct)
dNTP	5	
DMSO (as sequence GC rich)	1	
PFU Turbo Enzyme	1	e) 68 – 10 min
	1	
H_2O	37	
Total = 50µl		

Figure 2.6 Steps involved in site-directed mutagenesis - based on a protocol derived from the Stratagene Quikchange kit (Agilent Genomics, USA). All constituents obtained from New England Biolabs, USA.

Mutations in the nucleotide base sequence are generated by using a pair of primers designed with mismatching bases at the centre of the oligonucleotide (Figure 2.7). The plasmid containing both mutations of C17S and H24A was prepared in two stages using the mutagenesis primers for the individual mutations i.e. by sequentially introducing the H24A mutation into a plasmid already containing the C17S mutation.

DNA constructs rich in the nucleotides Guanosine (G) and Cytosine (C) are so-called 'GC-rich' and are prone to secondary structure formation such as harpin-loops, which can interfere with the denaturing process involved in thermal cycling DNA reactions such as PCR. The addition of dimethyl sulphoxide (DMSO) inhibits such secondary structure formation, increasing the likelihood of successful DNA polymerisation[116]. The template DNA needs to be eliminated by enzymatic digestion with a restriction enzyme such as *DpnI* (20 U/µl, New England Biolabs), which is specific for methylated DNA is generated by *E. coli*. Therefore, treatment of the reaction mixture with *DpnI*, degrades the template plasmid but not the polymerisation product.

Once the mutagenesis reaction is complete, transformation and colony selection was performed. Note, that following mutagenesis, large quantities of plasmid reaction product (Step 1 of *Template production*) are required for successful transformation. Once the purified DNA is obtained, check that the desired mutation has taken place with Sanger nucleotide sequencing (SourceBioscience, UK).

A) Wild Type PKA RI-α

5’ **tgc** gag ctc tat gtg cag aag **cac** aat atc cag gcc ctg ctg aag gac tcc atc gtg cag ctg **tgc** 3’

B) PKA RI- α Cysteine → Serine mutation at position 17 (C17S)

5’ **A**gc gag ctc tat gtg cag aag cac aat atc cag gcc ctg ctg aag gac tcc atc gtg cag ctg tgc 3’

C) PKA RI- α Histidine → Alanine mutation at position 24 (H24A)

5’ tgc gag ctc tat gtg cag aag **GC**c aat atc cag gcc ctg ctg aag gac tcc atc gtg cag ctg tgc 3’

D) PKA RI-α C17S; H24A

5’ **a**gc gag ctc tat gtg cag aag **GC**c aat atc cag gcc ctg ctg aag gac tcc atc gtg cag ctg tgc 3’

Figure 2.7 Base sequence of the dimerization and docking (D/D) of murine PKA RIα and associated mutations.

A) In bold, tgc codes for C17; cac codes for H24; tgc codes for C37

B) In bold, agc replaced tgc to induce a cysteine to serine mutation.

C) In bold, gcc replaces cac to induce a histidine to alanine mutation.

D) The two mutations were introduced sequentially as a plasmid spanning the two sites was not a feasible approach due to its length.

2.4 Gene transfer

2.4.1 Transfection

Transfection describes the process by which genetic material, in the form of a plasmid construct, is delivered into cells, which then transcribe the encoded peptide sequences to express the desired proteins. Transfection can be achieved by a number of non-viral means, including liposomes, electroporation and calcium phosphate. The HeLa and HEK cell lines used in the experiments described in the thesis were subjected to liposomal transfection using FuGENE^{M} Lipid Reagent (Promega USA). Sample reaction conditions are shown in Table 2.9.

	DNA (µg)	Medium (µl)		FuGENE HD™ (µl)	Medium (µl)
Plasmid per cm^2 of growth area	0.6	15		1.8	15

Table 2.5 Transfection conditions for HeLa and HEK-293 cell lines

Protocol for transfection

1. Plate cultured cells at a density of approximately 250,000 cells per cm^2 into a relevant flask or plate of wells.

2. Calculate volume of plasmid preparation required as per Table 2.5 bearing mind mind the area of a well of a 6-well plate is 9.4cm^2; and as 12-well plate is 3.83cm^2. Suspend the DNA in 100µl DMEM medium (serum-free) (Chapter 2.2).
3. Separately, add FuGENE HD™ to DMEM medium (serum-free) in a ratio of 2µl to every 1µg of plasmid DNA used.
4. Allow separate preparations to incubate at room temperature for 2-5 minutes.
5. Combine the preparations made in steps 1 and 2 and allow to incubate for 20 minutes at room temperature.
6. Apply final volume of DNA-FuGENE HD mixture to each well of cells and allow to incubate at 35°C for approximately 12 hours

2.4.2 Adenoviral preparation and gene transfer

The EpacH187 and AKAR3ev FRET biosensors were sub-cloned separately into the pDual vector[117], which contains a mutagenised version of the promoter / enhancer of the human cytomegalovirus (CMV) immediate early gene (Gift from Dr K Lefkimmiatis, Oxford UK). The genes of interest were cloned and transferred into an adenovirus vector, amplified and concentrated by Vector Biolabs, USA. The viral samples were divided into 5µl aliquots and stored at -80°C until required. The use of small aliquots prevented repeated freeze-thaw cycles which are known to diminish viral activity. Both the viral constructs Ad-H187 and Ad-AKAR3ev had titres of Particle Forming Units (PFU) of the order of magnitude of 10^{11} PFU/ml.

2.5 Detection of protein expression

Protein expression was identified and semi-quantified, when necessary, using Western immunoblotting analysis. This technique relies on the principle of electrophoresis to separate protein on the basis of molecular mass in a gel with subsequent transfer, 'blotting', to a membrane. The membrane is then probed with primary antibodies (Chapter 2.5.4) raised against one or more epitopes of a target protein to identify the relative abundancy of a protein of interest.

2.5.1 Sample preparation

Protein was extracted from isolated primary adult mouse cardiomyocytes or from HEK-293 or HeLa cell line cultures. A pellet of isolated cells was suspended in a buffer based on the Radio-Immunoprecipitation Assay (RIPA) lysis buffer to disrupt cellular membranes and hence solubilise protein (Table 2.6).

RIPA (Radio-Immunoprecipitation Assay) buffer – 10ml (Sigma-Aldich, USA)

Protease Inhibitor (1 tablet in 10 ml lysis buffer, cOmplete Mini, Roche, Switzerland)

Phosphatase Inhibitor (1 tablet in 10 ml lysis buffer, PhoSTOP, Roche, Switzerland)

Maleimide 100mM (95mg) (Sigma-Aldrich, USA)

Table 2.6 Constituents of lysis buffer (10ml)

Protease inhibitor prevents degradation of the extracted proteins and phosphatase inhibitors are included to allow for examination in changes in phosphorylation state of proteins if desired. The alkylating agent, maleimide, is added to allow assessment of the redox status of the thiols (R-SH - as found in cysteine residues) in a protein of interest. Because maleimide specifically reacts with the reduced form of a thiol, it can be used to prevent further oxidation of the protein and hence allow partial states of oxidation to be examined if the subsequent gel electrophoresis is performed in non-reducing conditions.

2.5.2 Protein quantification, Western gel electrophoresis and immunodetection

In order to assess the relative abundance of a particular protein between different samples, equal masses of total protein need to be examined in order to allow comparisons to be made. A reliable method of protein quantification is via the Bradford protein assay. The assay is based on the formation of a complex between the dye Brilliant Blue G in Bradford solution (B6916 - Sigma-Aldrich, USA), and proteins in suspension. The protein-dye complex causes a shift in the spectrophotometric absorption maximum of the mixture from 465 to 595 nm. The degree of absorption is proportional to the concentration of protein present in solution. A commercially

available protein standard is serially diluted in Bradford solution to 5, 10, 15, 20 μg/μl and its optical density is measured by spectrophotometry. By plotting these values on a graph of concentration against optical density (Figure 2.8), the concentration of protein from each test sample can be deduced.

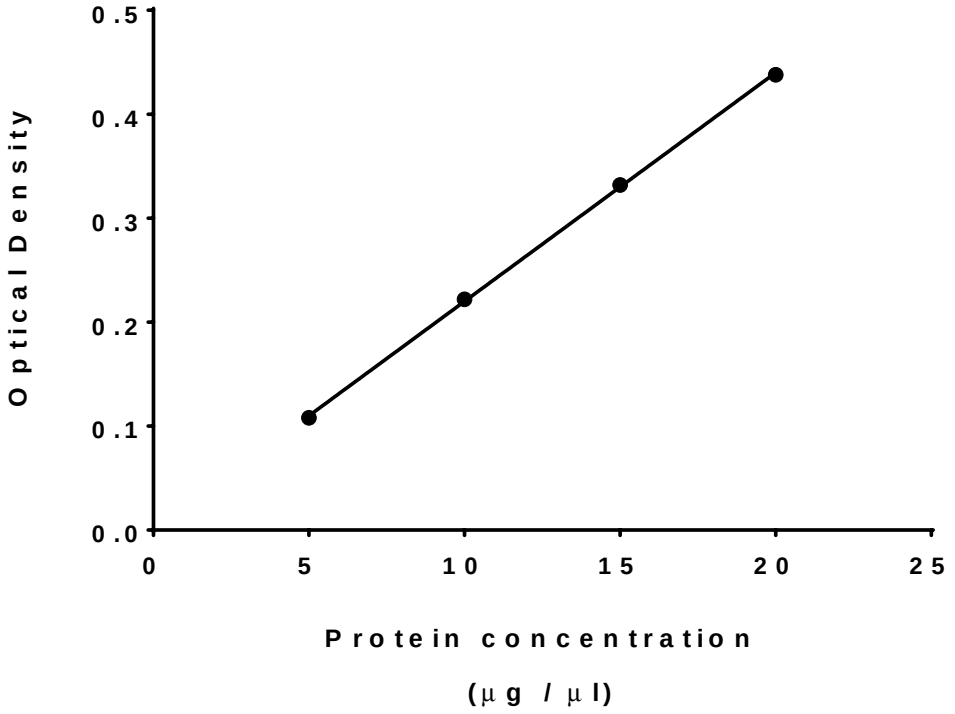


Figure 2.8 Example curve of a serially diluted protein standard diluted in Bradford reagent and the optical density measured by spectrophotometry

Gel Electrophoresis

The system used to separate proteins by sodium dodecyl sulphate (SDS) polyacrylamide gel electrophoresis (PAGE) was formulated by Laemmli in 1970[118]. Protein mixed in an SDS PAGE sample buffer is subjected to an electrical potential difference across a polyacrylamide gel that permits resolution of proteins by their mass. Most sample buffers contain SDS, bromophenol blue, glycerol, and Tris-glycine at pH

6.8. SDS is an anionic detergent that binds to and imparts a negative charge to the proteins in the sample, giving every protein the same charge-to-mass ratio. Mobility through the gel therefore becomes a function of molecular mass, vital for the process of electrophoresis. A reducing agent, such as β-mercapto-ethanol (BME), is added to disrupt disulphide bonds. However, if the protein sample is to be run in non-reducing conditions, in order to preserve cysteine oxidation, BME is omitted. As most primary antibodies are optimised for use with chemically reduced protein samples, non-reducing conditions may affect the quality of immunoblotting. Bromophenyl blue is a dye that that aids visualisation of the sample in the well of a gel and as the sample progresses during electrophoresis. Glycerol, being denser than the aqueous buffers used in gel electrophoresis, helps the sample to sink into well and hence prevent spillage of the sample.

In order for the proteins to be separated in an orderly manner, the gel is constructed in a discontinuous fashion i.e. a stacking gel on top of a running gel. Traditionally, each of these two gels is cast at a different pH – the stacking gel at pH 6.8 and the running gel at pH 8.8. The running buffer in which the gels run is Tris-based and its pH is adjusted using the weak acid glycine to a pH of 8.3. At low pH, the glycine is uncharged but at higher pH it becomes negatively charged. Therefore, when a potential difference is applied to the system, negatively charged glycine ions in the running buffer are repelled from the cathode and hence towards to sample in the stacking gel. The low pH of the stacking gel causes a loss of charge by the glycine, which means that their rate of migration in the electric field slows down. The chloride ions in the running buffer remain negatively charged and continue to migrate under the influence of the electric field. The net effect of this change in conductance generates a region of high electrical

resistance in the stacking gel. This region of high electrical potential difference makes the negatively charged proteins move together, away from the cathode in a narrow band behind a front of chloride ions.

When the front of cations meets the resolving gel, pH 8.8 from 6.8 in the stacking gel, the glycine molecules lose protons and become more negatively charged. The now negatively charged glycine moves more freely under the electrical field, allowing glycine to overtake the proteins as they become progressively slowed by the ever denser resolving gel. The electric field within the resolving gel becomes more uniform than was found in the stacking gel, allowing the proteins to move at different rates, therefore allowing the proteins to separate by weight in the resolving gel.

Choice of gel for the analysis of proteins in non-reducing conditions

The chemistry of the gel used for protein electrophoresis can influence cysteine oxidation in a non-reducing sample preparation[119, 120]. In-gel oxidation of cysteine is suppressed by casting and running gels under slightly acidic (≈pH 6.8) conditions, which favour cysteine protonation in the reduced state. Unlike traditional Tris-Glycine gels, Bolt® Bis-Tris Plus gels (Invitrogen, USA) have an operating pH of about 7.0. This neutral pH therefore can permit cysteine re-oxidation compared to traditional gel chemistries, for example as found in BioRad PROTEAN™ gels (BioRad, USA). Figure 2.9 demonstrates how the sample of protein prepared in a non-reducing sample buffer but run in gels of different chemistries can give different results when examining the relative oxidation of cysteine residues. Therefore, for all cases where the examination of the relative oxidation of cysteine residues is important, a BioRad Mini-PROTEAN™ gel system was used to allow comparison with earlier studies. For reasons of

practicality, all samples run in reducing conditions were performed using the Bolt ® (Invitrogen, USA) system of gels.

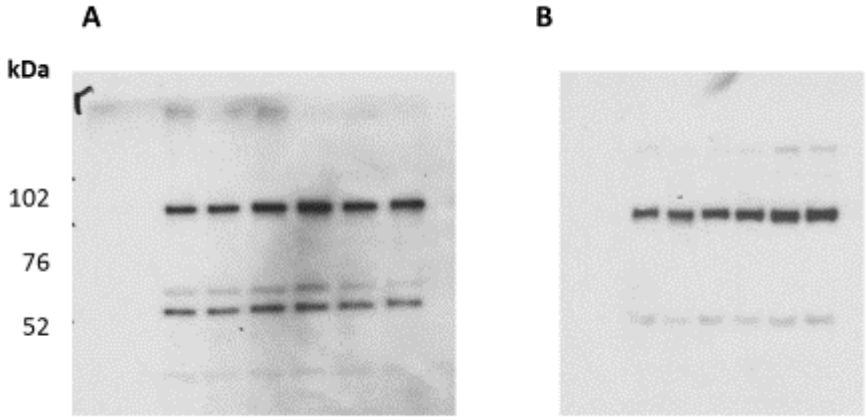


Figure 2.9 Two immunoblots performed simultaneously to show the effect of the type of gel on the relative abundance of oxidised cysteine as measured by the ratio of the dimeric (oxidised) band over the sum of the dimeric and monomeric bands as measured by scanning densitometry.
A – shows six independent samples run in a BioRad PROTEAN gel system.
B – shows the same six samples in A run using an Invitrogen Bolt® gel system.
All samples were of equal mass (15µg) and were run in non-reducing conditions.

Immunoblotting

After electrophoresis, protein is transferred from the gel to a stable membrane to allow repeated probing with primary or secondary antibodies. Polyvinylidene difluoride (PVDF) membranes (Amersham Bioscience Ltd, UK) membranes are activated by soaking in 100% methanol for 5 minutes prior to use. The activated PVDF membrane is placed in contact with the gel, packaged into a transfer system and the protein is transferred from gel to membrane under the influence of an electric field (Figure 2.10). Care is taken to ensure air bubbles are eliminated from the 'sandwich' of gel and membrane as this will ruin protein transfer. Transfer conditions for a BioRad semi-dry

system were a constant voltage of 100V for 1-2 hours; Invitrogen Bolt® transfer was performed at a constant voltage of 20V for 1 hour.

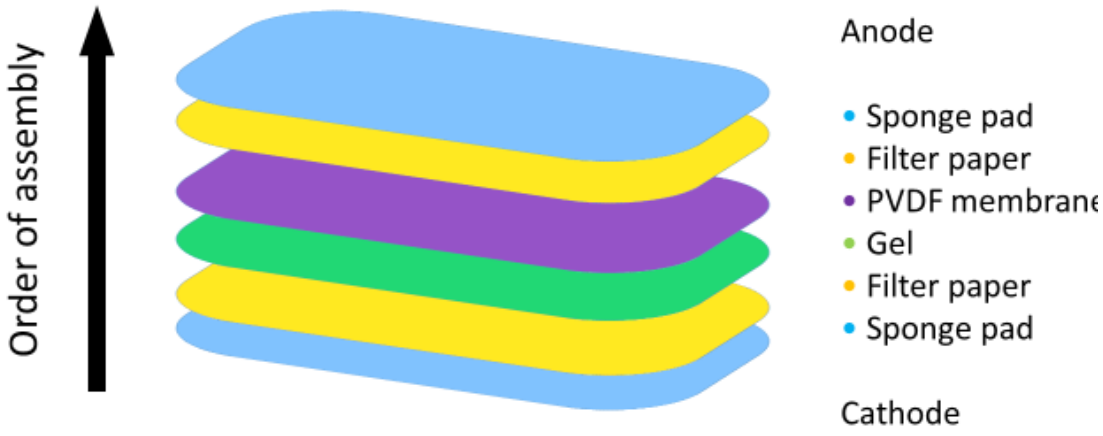


Figure 2.10 Schematic representation of the transfer of protein from gel to PVDF membrane

After transfer of protein to the membrane, a qualitative assessment of protein loading and transfer was made by using Ponceau S solution (P1710 – Sigma-Aldrich, USA) to stain the PVDF membrane reversibly to show protein bands. This allows for discrepancies in protein loading or errors in transfer of protein to be immediately identified and prompt repetition of the gel electrophoresis and subsequent transfer.

The membrane is blocked in 5% milk powder dissolved in TBST (TRIS-buffered saline with 1% Tween 20) for one hour at room temperature. The primary antibody was diluted in a 1% milk solution as per Table 2.7 (Chapter 2.5.4) with incubation at room

temperature or overnight at 4°C under constant agitation. After incubation, the primary antibody was removed by thorough washing with TBST and the membrane was then incubated with an appropriately diluted secondary antibody under constant agitation for one hour at room temperature and pressure. Finally, the secondary antibody was removed by thorough washing in TBST over 30 minutes. The immunological signal from the membrane was visualised with anti-IgG-horseradish-peroxidase and enhanced chemiluminescence (ECL Western Blotting Substrate 32106 – Pierce, USA). The probed membranes were exposed onto light-sensitive film (Hyperfilm ECL, Amersham, UK) and developed in dark-room conditions for subsequent analysis and storage as 'hard copy'.

Quantification

Comparison of the intensity of bands identified by immunoblotting may be performed by comparing the relative optical densities of the protein bands. In order to perform this, an immunoblot is scanned, stored in a digital format (ImageJ - National Institutes of Health, USA) and the optical density of the bands measured relative to background. In the case of the assessment of PKA RI run in non-reducing conditions, the ratio of dimeric protein bands to the sum of the two bands may be expressed to give a relative measure of cysteine oxidation. As the output is a figure relative to the total amount of PKA RI, there is no need for normalisation to a standard, house-keeping gene used as a loading control[77]. The use of antibodies on non-reducing gels may be compromised as commercially available antibodies are optimised to detect protein that has been run in reduced and denatured state. Indeed, the common house-keeping protein GAPDH is not recommended in redox studies due to its expression being relatively susceptible to cellular oxidative state[121].

2.5.3 Fractionation

The concept of ‘cellular compartmentalisation’ in cell biology helps to describe the distinct function and roles of membrane-bound regions of the cell, which include the nucleus, organelles (such as the mitochondria and ER/SR) and the cytosol. Compartmentalisation of signals appears to be one way in which to maintain signalling fidelity and specificity, especially in the case of the potentially widespread actions of cyclic nucleotide effectors and redox modifications[122-124].

Although biochemical analysis requires disruption of the cell, gentle fractionation techniques have been devised to separate the various membranous components of cells while preserving their individual functions. Fractionation has been used in two roles in this thesis. In Chapter 4, a cytosolic fraction was obtained to allow assessment of PKA signalling *in vitro* through the application of potential agonists of PKA signalling to a membrane-free preparation in which the cytosolic PKA FRET biosensor AKAR3ev was expressed. This allowed the functional assessment of the effects of H_2O_2 on PKA activity, without potential confounders arising from membrane-bound PKA. Fractionation was also used in Chapter 5, this time in a more traditional manner to identify the location of Type I PKA and an associated anchoring protein, AKAP10. The Qproteome® Mitochondria Isolation kit (37612 - Qiagen,USA) has been used to perform bench-top separation of cells into cytosolic and mitochondrial fractions. The protocol may be summarised as follows.

Cellular fractionation - Qproteome® Mitochondria Isolation

a) Qproteome Lysis buffer – 1ml
+ 10µl Protease Inhibitor per sample + 9.5mg maleimide (100mM)

b) Qproteome Disruption buffer – 1.5ml
+ 15µl Protease Inhibitor per sample + 14.5mg maleimide (100mM)

c) Lysis Buffer (Table 2.6)

1. Obtain a suspension of cells in a relevant Tyrode buffer
2. Centrifuge at 500 *g* at 4°C for 10minutes
3. Re-suspend the cell pellet in 1-2ml of ice cold Lysis Buffer (a)
4. Incubate for 10 minutes at 4°C using an end-over-end shaker
5. Centrifuge at 1000g for 10 mins at 4°C – D28 centrifuge
6. Remove supernatant – this constitutes the cytosolic fraction
   (Keep on ice if to be used shortly or flash freeze if to be used later).
7. Re-suspend pellet in 1.5ml ice-cold Disruption Buffer (b) by pipetting up and down using a 1ml pipette tip. Complete cell disruption by using a blunt-ended needle and syringe ≈10 times in a 5ml tube to avoid spillage of contents
8. Centrifuge lysate at 1000 *g* for 10 minutes at 4°C and transfer *supernatant* to clean, labelled 1.5ml tube.
   The pellet here corresponds mainly to the nuclear membranes
9. Centrifuge the suspension from the previous step at 6000 *g* for 10 minutes at 4°C
10. Supernatant – comprising a microsomal fraction - discard
    Pellet – mitochondrial fraction (keep on ice)
11. Add 30 µl Lysis Buffer (c) to each fraction
12. Mix the new suspension using an end-over-end shaker for 10 minutes
13. Centrifuge at 10 000 *g* at 4°C for 10 minutes to clarify the protein extract
14. This protocol gives two protein extractions labelled cytosol and mitochondria which are ready to be quantified.

Validation of fractionation

Fractionation of cells with a bench-top centrifuge and mechanical cellular disruption in a variety of lysis buffers may be susceptible to cross-contamination between fractions. In order to evaluate the efficacy of the fractionation protocol, fractionations were performed and marker proteins for each fraction were identified : GAPDH (cytosol)[125], oxidative phosphorylation enzymes (OXPHOS - mitochondria)[126] and SERCA2a (Endoplasmic / Sarcoplasmic Reticulum)[127]. Separation of cytosolic and mitochondrial compartments can be shown through the use of the antibody cocktail OXPHOS:GAPDH. OXPHOS in itself represents a cocktail of antibodies directed against five mitochondrial oxidative phosphorylation enzymes, to which anti-GAPDH antibody may be added to allow mitochondrial and cytosolic compartments to be identified in the same immunoblot.

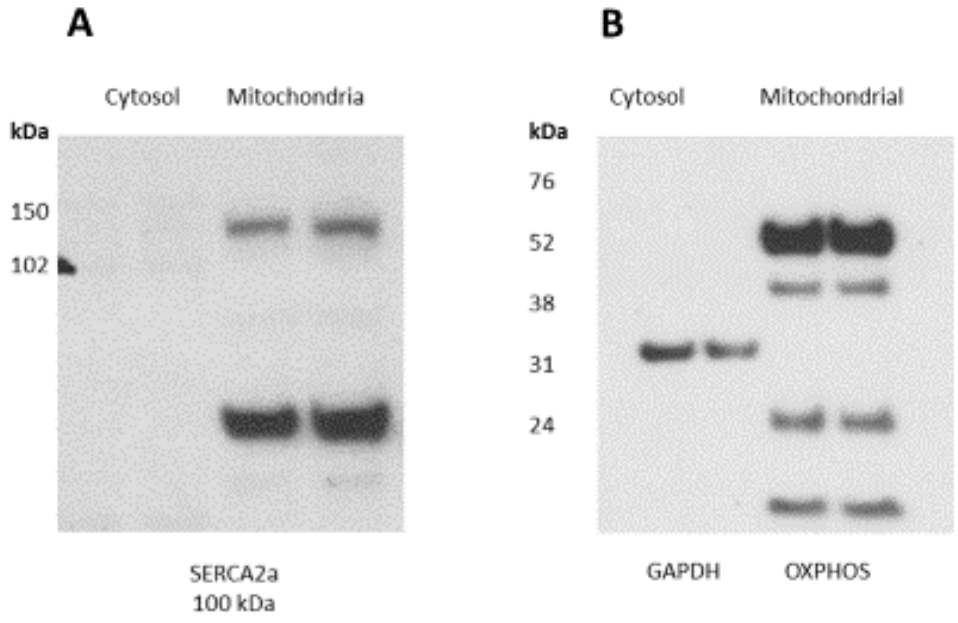


Figure 2.11 Immunoblot to show cytosolic and mitochondrial subcellular fractions derived from two repeats from cultured Human Embryonic Kidney (HEK) cell lines. A) SERCA2a – a marker of the endoplasmic reticulum and B) the cocktail of mitochondrial oxidative phosphorylation enzymes and GAPDH, the cytosolic marker.

Figure 2.11A shows that the cytosol does not contain any detectable SERCA2a, a marker of the SR/ER, but some SERCA2a is found in the ‘mitochondrial’ fraction. Indeed, Figure 2.11B shows that there is a distinct separation of cytosolic and ‘mitochondrial’ fractions in that the cytosolic marker, GAPDH, is found only in the cytosol. Equally the mitochondrial oxidative phosphorylation enzymes (OXPHOS) are not found in the cytosol. Even though the kit is marketed as being designed for obtaining a mitochondrial fraction, it is excellent at producing a cytosolic fraction, without apparent membranous contamination, with a mitochondrial fraction which has some degree of contamination. A more exhaustive examination of the purities of each fraction may include other markers of cellular compartments, in particular nuclear proteins such as Lamin A/B[128].

2.5.4. List of primary and secondary antibodies

Target protein	Dilution	Species	Supplier
PKA RI	1:3000	Mouse	BD Bioscience 610615
PKA RIα	1:3000	Mouse	BD Bioscience 610610
PKA RII	1:3000	Mouse	BD Bioscience 612242
GAPDH	1:1000	Mouse	Santa Cruz SC-166574
OXPHOS (Rodent)	1:7000	Mouse	MitoSciences MS604
OXPHOS (Human)	1:7000	Mouse	MitoSciences MS601
AKAP10	1:3000	Rabbit	Protein Tech 12356-1-AP
SERCA2 (C-20)	1:1000	Goat	Santa Cruz SC-8094
GFP	1:5000	Mouse	Santa Cruz SC-9996
Anti-Mouse	1:3000 - 1:6000	Goat	Promega W4021
Anti-Goat	1:3000 - 1:6000	Donkey	Promega V8051
Anti-Rabbit	1:3000 - 1:6000	Mouse	Promega W4011

Table 2.7 Primary and secondary antibodies used in Western immunoblotting analysis. Dilution, species and supplier details provided.

2.5.5 Comparison of PKA RI vs RIα antibodies

PKA Regulatory subunit Type 1 exists in two isoforms, α[129] and β[130-132]. Both proteins are 380 amino acids in length (≈50 kDa), of which ≈80% of the amino acids are identical[133]. The RIβ isoform is distributed mainly in the brain and spinal chord[131], whereas the RIα isoform is found in all other cell types including cardiomyocytes and hence is the more ubiquitous isoform of the RI subunit[134]. The difference in role between these two isoforms is not known but the aim of the study concerns the RIα subunit of PKA as it can form disulphide bonds in response to an oxidising stimulus. The D/D domain of RIα contains two cysteine residues, whereas RIβ contains three cysteine residues. However, the conformation of the cysteine residues in RIβ does not permit disulphide bond formation (Figure 2.12).

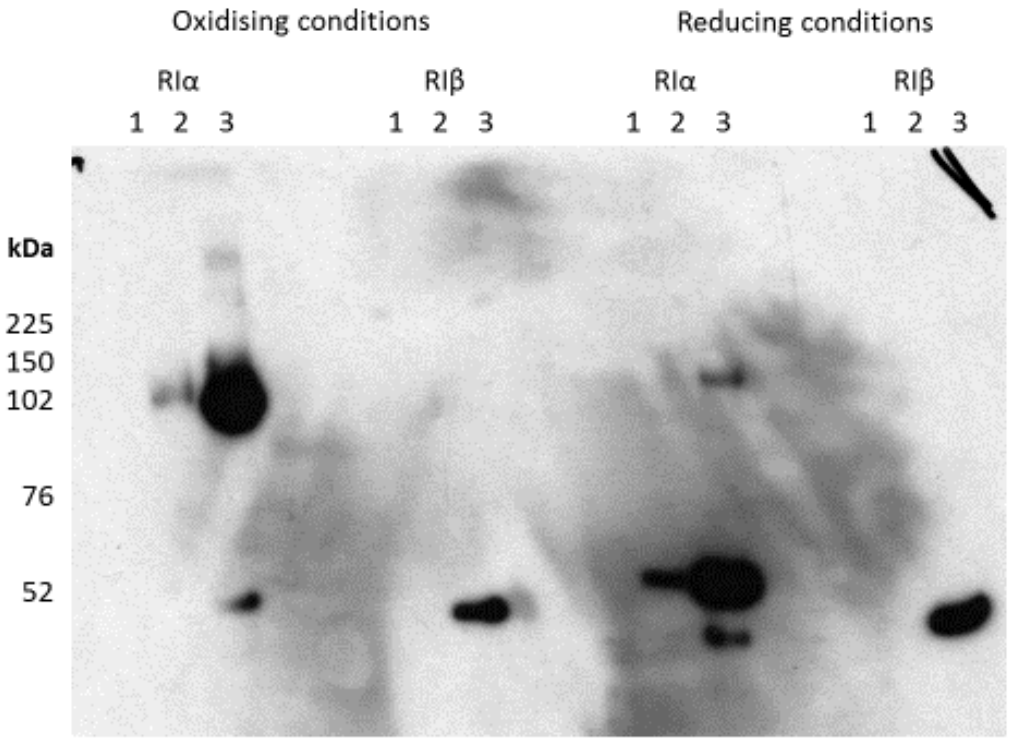


Figure 2.12 Immunoblot of serially diluted purified PKA RI α or β isoforms probed with PKA RI antibody. Lanes 1-3 represent serials dilutions by a factor of 10 from low to high concentration. The gel electrophoresis was performed in oxidising and reducing conditions. Primary antibody : PKA RI (610615 - BD Biosciences, UK)

Figure 2.12 shows the effect of oxidising and reducing conditions on synthesised RIα (ab41295 – Abcam, UK) and RIβ (ab41296 – Abcam, UK) protein when detected on immunoblot using a primary antibody directed non-specifically against PKA RI. Considering that purified protein has been used, the samples have been serially diluted by a factor of 10 from samples 3-1 from a nominal starting concentration of 1mg/ml to ensure a detectable signal. The immunoblot confirms that that only the RIα protein forms disulphide bonds in response to an oxidising stimulus, because of the absence of a band at approximately 100kDa in the RIβ lanes. The RI antibody perform as anticipated by detecting both RIα and RIβ proteins. A primary antibody that is specific for RIα has been described (610610 - BD Biosciences), which has been applied to the same experiment (Figure 2.13).

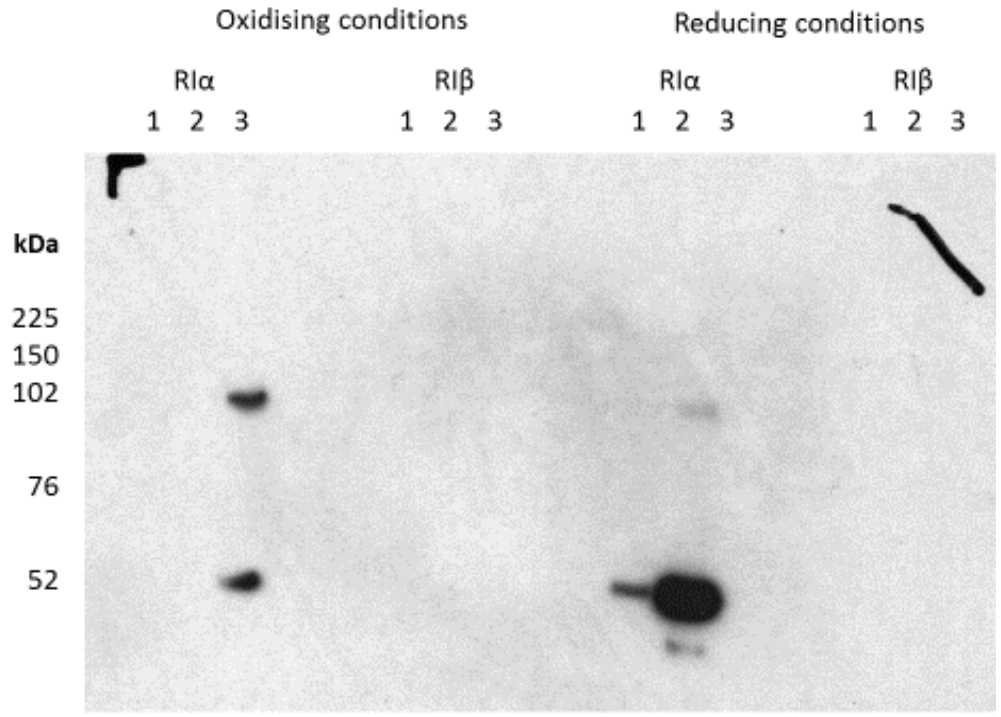


Figure 2.13 Immunoblot of serially diluted purified PKA RIα or β isoforms probed with PKA RIα antibody. Lanes 1-3 represent serials dilutions by a factor of 10 from low to high concentration. The gel electrophoresis was performed in oxidising and reducing conditions. Primary antibody : PKA RIα (610610 - BD Biosciences, UK)

Figure 2.13 shows that the RIα antibody is indeed specific for the RIα isoform, as no signal is identifiable in the lanes loaded with synthetic RIβ protein. Another observation is that the strength of signal derived from the band at ≈100 kDa attributed to oxidised PKARIα with disulphide bond formation is much weaker than observed with the non-specific antibody directed against PKA RI (Figure 2.12). From these observations, the apparently more sensitive, non-specific PKA RI antibody (610615 – BD Biosciences) was used for the remainder of the thesis. Signal derived from RIα can be assured in the experiments carried out due to the specific ability of RIα to undergo oxidation-dependent dimerization which manifests as a band of double weight (50 kDa →100 kDa), which RIβ cannot undergo. It should be remembered at this point that the monomeric representation of PKA RIα in gel electrophoresis is due to the usual reducing conditions that are applied to protein electrophoresis and for which antibodies ae optimised. Indeed, it should be remembered that the cysteine residues are not important for the normal dimerization of RIα subunits in the quaternary structure of the PKA holoenzyme[70]. Therefore, the ≈100kDa 'dimer' band represents the presence of two oxidised RIα subunits, compared to reduced single RIα subunits at ≈50 kDa.

2.6 Immunoprecipitation and 'pull-down'

Immunoprecipitation (IP) or 'pull-down' is the technique of precipitating a protein out of solution using an agent, such as an antibody, that specifically binds to that particular protein. This process can be used to isolate and concentrate a particular protein from a sample containing many thousands of different proteins. Immunoprecipitation requires that the antibody be coupled to a solid substrate at some point in the procedure. Figure 2.14 describes the series of steps involved in pull-down of GFP-fusion proteins, using agarose beads coated with an anti-GFP antibody (GFP-Trap®, Chromotek, USA). Co-immunoprecipitation describes the finding of another protein in association with the GFP-fusion protein, which by implication is likely to be bound to the GFP-fusion protein.

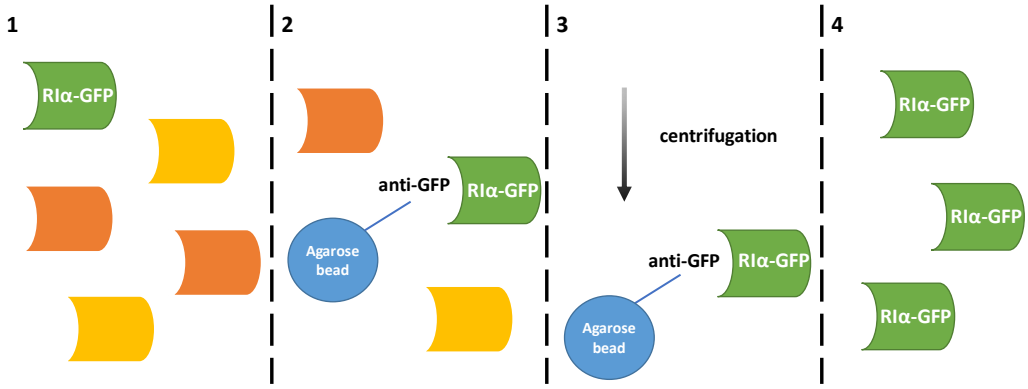


Figure 2.14 Cartoon to summarise the process of immunoprecipitation using anti-GFP-coated agarose beads.

In Figure 2.14, Step 1 shows an RIα-GFP subunit in solution with other proteins depicted by the orange and yellow symbols. Upon addition of agarose beads coated with an anti-GFP antibody in Step 2, binding between the beads and any protein that expressed GFP or a variant occurs – in this case the GFP-tagged RIα subunit. In Step 3,

there is centrifugation, to pellet the beads and allow removal of the superfluous, non-GFP-binding protein. Finally, in Step 4, protein is eluted from the beads by boiling the mixture, leaving a sample enriched for proteins that bind GFP directly. Proteins that form complexes with GFP-binding proteins may also be detected even though they do not bind cAMP directly – co-immunoprecipitation.

Specific protocol for pull-down with anti-GFP agarose beads

1. Extract protein as described in Chapter 2.5.1

2. Quantify protein in samples and prepare micro-centrifuge tubes each with 25µl beads (GFP-Trap®, Chromotek, USA) with an extra sample to remain as a negative control.

3. Add 400ug to each 25µl sample of beads. Ratio of beads to protein 400ug to 25µl beads for example and dilute to 500µl using lysis buffer.

4. Allow the protein and beads to mix on an end-over-end shaker at 4°C for three hours

5. Repeatedly pellet in a bench-top centrifuge and carefully remove the supernatant, being extremely careful not to touch the beads and wash the remaining beads in cold PBS four times.

6. Finally aspirate any remaining liquid, aspirate the beads using a fine insulin needle and syringe.

7. To dissociate the protein from the beads, apply 25µl SDS-based loading buffer and boil at 95°C to elute the protein.

8. After denaturation, briefly centrifuge and then aspirate contents using a fine loading tip and run the gel electrophoresis.

2.7 Fluorescence Microscopy

2.7.1 Fluorescence Resonance Energy Transfer Microscopy (FRET)

The visualization of real-time changes in cyclic nucleotide signalling within distinct cellular compartments was not possible until the development of live-cell imaging techniques that have improved spatial and temporal resolution over biochemical assays[135]. The first fluorescent biosensors for cAMP-PKA signalling were developed in the early 1990s[94] but were superseded by genetically encoded biosensors, principally those that make use of the phenomenon of Fluorescence Resonance Energy Transfer (FRET) to measure dynamic, ratiometric changes in cyclic nucleotide signalling [95]. FRET describes the non-radiative transmission of energy from a donor to an acceptor fluorophore. This process of energy transfer is highly dependent on the distance between the fluorophores and therefore can be modulated by the conformation of the protein structure to which the fluorophores are bound (Figure 1.5). In the case of cAMP-PKA signalling, sensors have been developed whereby binding of the cyclic nucleotide or phosphorylation by PKA leads to a change in protein conformation, which in turn modulates the degree of FRET. From the subsequent ratiometric change donor-emission spectra, relative changes in cAMP concentration or PKA activity can be inferred.

2.7.1.1 FRET Microscopy Equipment

FRET-based microscopy experiments per performed using a setup comprising an inverted microscope (Olympus IX71) using a PlanApoN, 60X, NA 1.42 oil immersion objective, 0.17/FN 26.5 (Olympus, UK). The microscope was equipped with a coolSNAP HQ monochrome camera system (Photometrics, USA) and a beam-splitter

optical device is required for the recording of dual wavelength emission of YFP and CFP (Dual-view simultaneous-imaging system, DV2 mag biosystem, Photometrics, USA). The FRET filter settings used throughout were: CFP excitation filter ET436/20x, dichroic mirror 455DCLP (Chroma Technology, Germany) in the microscope filter cube; dichroic mirror 505DCLP, YFP emission filter 545 nm, and CFP emission filter 480 nm (Chroma Technology, Germany) in the beam splitter. Images were acquired and processed using Meta imaging series 7.1, MetaFluor, (Molecular Devices, USA). FRET emission ratios were acquired every 5-10 seconds.

Cells were cultured on 15mm diameter sterilised borosilicate glass coverslips, which allow transfer to a perfusion chamber (Figure 2.15). The coverslips were held in place with a thin rim of silicone vacuum grease (18405 – Sigma-Aldrich, USA) in order to create a water-tight seal between the chamber and the coverslip. The RC-21 chamber in Figure 2.15 allowed the application of a stimulus to the bath of superfusate. Through the attachment of a vacuum pump to the outlet of the chamber (indicated by the steel aspiration needle on the right of the photograph), bath-applied stimuli could be removed with a period of washing with Tyrode solution.



Figure 2.15 Photograph of RC-21 (Warner Instruments, UK) chamber setup showing aspiration ducts to allow removal of bath applied stimuli during FRET microscopy experiments. (Image courtesy of Warner Instruments, UK).

Timing of fluorescence imaging experiments

The timing of imaging experiments depends upon the intensity of the fluorophore. Constructs with greater numbers of fluorescent subunits or brighter fluorophores will be observed earlier than those that are less bright. When assessing for fluorescence, be aware of the localization of the sensor as a guide to whether the sensor is being expressed or the cell is exhibiting autofluorescence (See Figure 2.16). NADPH has long been recognized as being autofluorescent[136], which can pose a problem with FRET biosensors as the emission spectrum of NADH is 477nM, which is similar to YFP-Venus (a common fluorophore used in FRET biosensors) at 530nM[137]. The pattern of NADH-based autofluorescence shows longitudinal striations to the cell, which differ from the classical transverse striations of cardiomyocytes.

a) b)

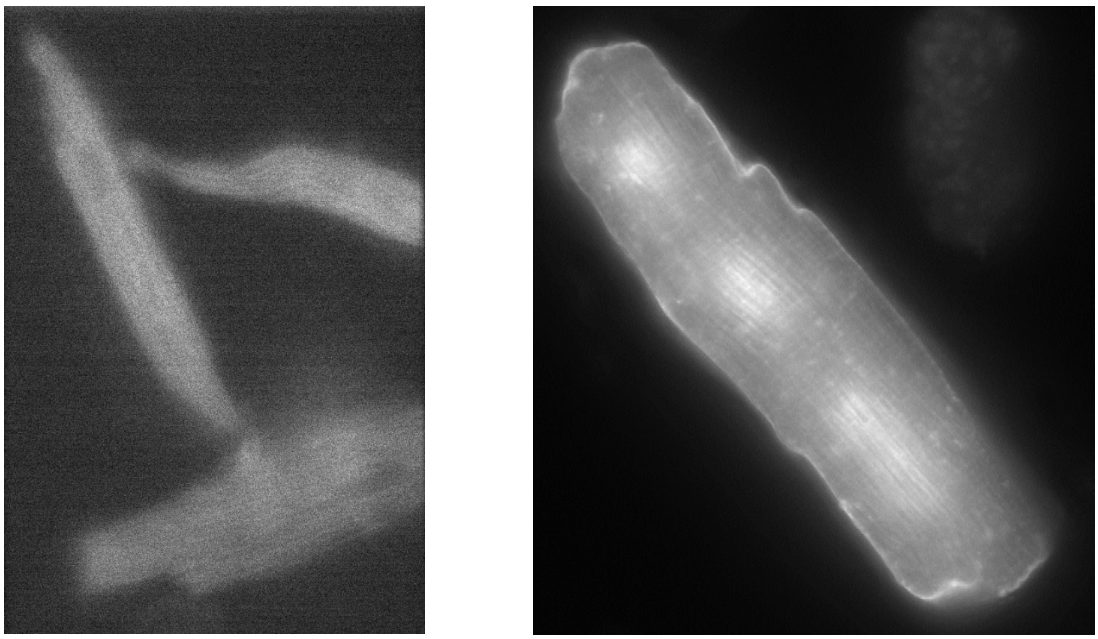


Figure 2.16 Fluorescence of primary adult mouse cardiomyocytes. Both images acquired using the same microscopy apparatus with the same excitation light intensity and an exposure time of 100ms.
a) Adult murine cardiomyocytes at 24 hours post isolation exhibiting autofluorescence.
b) Membrane-targeted EPAC-based sensor at 22 hours post isolation showing plasma and nuclear membrane localisation.

2.7.1.2 Pharmacological agents used to assess cAMP-PKA signalling dynamically in FRET imaging experiments

FRET-based biosensors allow the near real-time imaging of intracellular signalling events such as changes in intracellular cAMP concentration and PKA activity. These events may be examined through the use of known agonists and effectors of the signalling cascade. The intracellular concentration of cAMP may be elevated by two approaches, the stimulation of increased production of the cyclic nucleotide by adenylyl cyclase (AC) or inhibition of its breakdown by phosphodiesterases (PDEs). Downstream of cAMP, PKA activity may be blocked through the use of non-competitive and competitive inhibitors of PKA. Many of the pharmacological agents used are dissolved in Dimethyl-Sulphoxide (DMSO), which in high concentrations can induce disulphide bond formation between cysteine residues[138]. Since such events are a key part of the thesis, DMSO-contained vehicle controls are used through the experiments where needed.

Forskolin

Forskolin is a labdane diterpenoid (Molecular weight 410.5) that can be isolated from the roots of the plant *Coleus forskolin*. It activates Adenylyl Cyclase to stimulate the production of cAMP in most cells. The source of forskolin used in these studies was MP Biomedicals (190669). The powder was dissolved in Dimethyl Sulphoxide (DMSO) and stored in aliquots of 10mM at -80°C until use. For the purposes of the studies, a saturating dose of forskolin of 25μM was used as the aim was to show that a particular sensor was functioning appropriately to a rise in cAMP.

IBMX

3-Isobutyl-1-Methylxanthine (IBMX) is a competitive, specific but non-selective inhibitor of the phosphodiesterase (PDE) class of enzyme. Cyclic nucleotide PDEs degrade the phosphodiester bond in the second messengers cAMP and cGMP and therefore help to regulate the localisation, duration and amplitude of cyclic nucleotide signalling. The phosphodiesterase (PDE) family of enzymes catalyse the hydrolytic degradation of cAMP and cGMP. PDEs are encoded by 21 genes from which are derived eleven different families, designated PDE 1-11 according to their structure, kinetics, substrate specificity and regulatory mechanisms[139]. IBMX does not inhibit PDE 8 or 9, but for the purposes of this study, broad inhibition of PDE to raise intracellular cAMP through the use of IBMX at a saturating concentration of 100μM is an appropriate use of the compound. IBMX (Molecular weight 222.24) is obtained commercially from Tocris R&D Systems (UK) as a dry powder and reconstituted according to the manufacturer's instructions in DMSO and stored in stock aliquots at -80°C until use.

Inhibitors of PKA

A commonly used inhibitor of PKA activity is H89. Its mode of action is through competitive antagonism of ATP binding with the PKA catalytic subunit[140,141] (See Chapter 1.2.1) and therefore represents a different method on inhibition compared to endogenous PKI, which blocks kinase activity of the free catalytic subunit[37]. H89 has been developed to be readily cell-permeable at concentrations which suppress target phosphorylation in cells. Despite its ease of use, H89 does appear to lack specificity for PKA by having inhibitory actions on a variety of protein kinases[142]. Through the use of specific FRET-based biosensors for PKA activity of cAMP concentration, specificity of

output signal is obtained. However, indirect effects on other protein kinases on PKA could compound some observations. Nevertheless, H89 represents a reliable, highly cell-permeable inhibitor of PKA activity that, in in conjunction with AKAR FRET reporters of PKA activity, allows for the real-time assessment of relative PKA activity. H89 was purchased commercially from Tocris R&D Systems (UK) as a dry powder and was reconstituted according to the manufacturer's instructions in DMSO. Aliquots were stored at -80°C until use.

Protein Kinase Inhibitor (PKI) is an endogenous protein that inhibits the activity of PKA. In the early 1970s, the protein blocks the ability of PKA through selective inhibition of the free catalytic (C) subunit of PKA after cAMP-mediated dissociation from the regulatory (R) subunits[36, 37]. As it is an endogenous peptide, it operates very effectively when its expression is augmented within cells[143], however attempts to make exogenous peptide membrane-permeable have limited efficacy. For this reason, H89, a membrane permeable compound that inhibits PKA is suited to the purpose of driving a decrease in PKA activity as measured specifically by the AKAR class of FRET biosensor.

Hydrogen Peroxide (H_2O_2)

Hydrogen peroxide (H_2O_2) is a by-product of cellular metabolism and has been studied extensively. Entry into cells is readily achieved through passage via aquaporin channels[144], which allows for the use of exogenously applied H_2O_2, when a relevant intracellular source is not known[77]. Hydrogen peroxide was purchased from Sigma-Aldrich (USA) (21,676-3) with a molarity of 9.8M according to the manufacturer's product information. For the purpose of the studies, a concentration of 250μM H_2O_2

was chosen as a stimulus that greatly increased the presence of disulphide bonds between RI subunits but did not lead to cell necrosis during the approximate 10 minutes course of a FRET imaging experiment. The solution was stored at 4°C in dark conditions until use. The master solution was replaced frequently to avoid using degraded hydrogen peroxide.

2.7.1.3 FRET biosensors

There are a number of FRET biosensors for PKA activity. The A Kinase Activity Reporter (AKAR) class of FRET biosensor acts as a PKA phosphorylation target to relay changes in net PKA activity. It comprises one YFP (Venus) and one CFP fluorophore either side of a sensor domain that has the greatest sensitivity of AKAR FRET biosensors at the time of the study. A number of variants of AKAR have been produced, with varying properties related to sensitivity and kinetics of activation. AKAR3ev has been identified as the most sensitive of the currently available AKAR FRET biosensors[145]. AKAR4[99] is a very bright sensor but lacks some of the sensitivity of AKAR3ev, despite its more rapid kinetics of phosphorylation and dephosphorylation. EPAC-H187[101] for the detection of changes in cAMP concentration is excited by an argon laser at 488nm and its FRET was reported as the ratio of fluorescence measured at 480±10 nm and 530±10 nm.

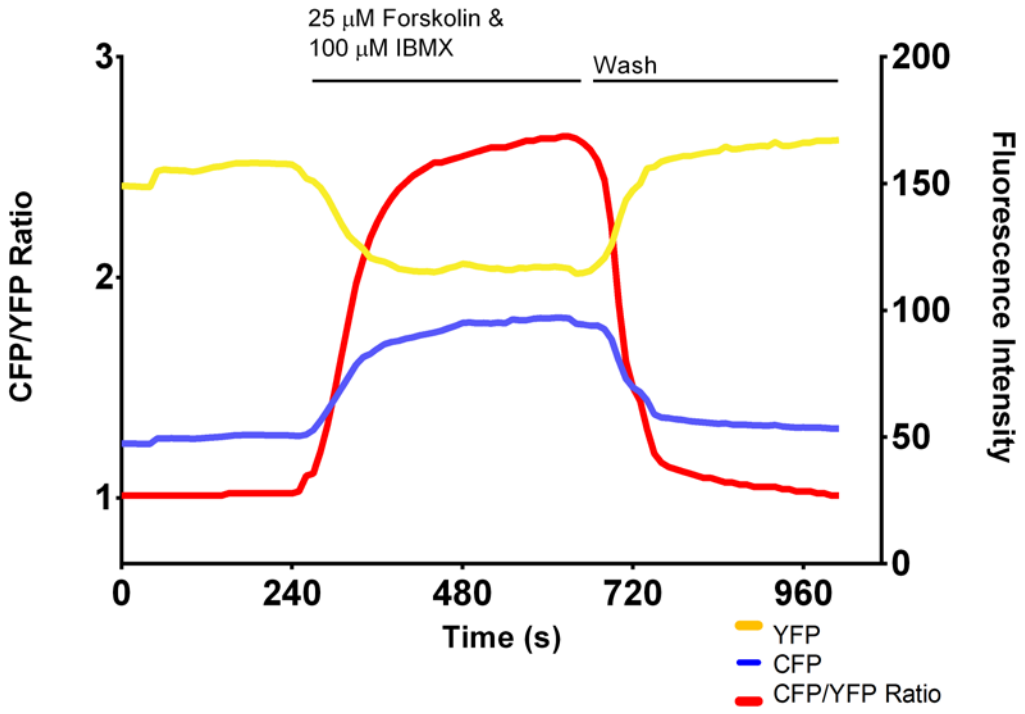


Figure 2.17 Graph to show an experiment involving cytosolic EPAC-based FRET biosensor to show the effects of an increase in cAMP due to forskolin and IBMX, with subsequent removal of the stimulus. The yellow and blue lines represent the changes in background-subtracted fluorescence intensity (right axis) of Yellow Fluorescent Protein (YFP) and Cyan Fluorescent Protein (CFP) respectively. The red line represents the CFP/YFP ratio, which has been normalised to the baseline during the first 240 seconds of the experiment (left axis).

Figure 2.17 shows an example experiment when the cAMP-FRET sensor EPAC H187 is expressed in adult mouse cardiomyocytes. Upon addition of forskolin and IBMX, the rise in [cAMP] binds the EPAC-based sensor and changes the conformation such that the CFP and YFP fluorophores separate. The separation of fluorophores results in a loss of FRET between the fluorophores. Therefore, excitation of CFP results in greater CFP emission at the expense of FRET to the YFP, with a concomitant fall in YFP intensity. The dynamic range of the biosensor is revealed by the addition of agents that maximally elevate the intracellular concentration of cAMP; forskolin to activate adenylyl cyclase to increase cAMP production; and IBMX to inhibit phosphodiesterases that hydrolyse

cAMP. The reversibility of the process is demonstrated the rapid reversal of the fluorescence intensities of YFP and CFP to baseline, upon removal of the forskolin and IBMX by means of the aspiration apparatus (Figure 2.15).

2.7.2 Fluorescence Recovery After Photo-Bleaching (FRAP)

2.7.2.1 Principles of FRAP

The technique of Fluorescence Recovery After Photobleaching (FRAP) represents is a method by which the diffusibility of fluorescently tagged proteins can be inferred by measuring the recovery of a cellular region in which a light source has bleached the local fluorescent protein. The quicker the recovery of the bleached region, the more mobile and less well anchored is the protein in question.

The initial rate of recovery, or rate constant (Figure 2.18a) is the most important, accurate and informative measurement of fluorescence recovery. It is accurate because it is concentration-independent. Even if photo-bleaching of the FRAP zone is incomplete, it does not affect the initial rate. It is informative because it measures how fast the unbleached fluorescent molecules move into the FRAP zone, as soon as the photo-bleaching event is over. The 'immobile fraction' is measured by determining the difference in plateaux achieved by the fluorescence in the bleached spot and in a region distant to the area of bleaching. This measurement is considered to represent the proportion of GFP-tagged protein that is trapped, for example behind a membrane or anchored very tightly to a subcellular structure[146].

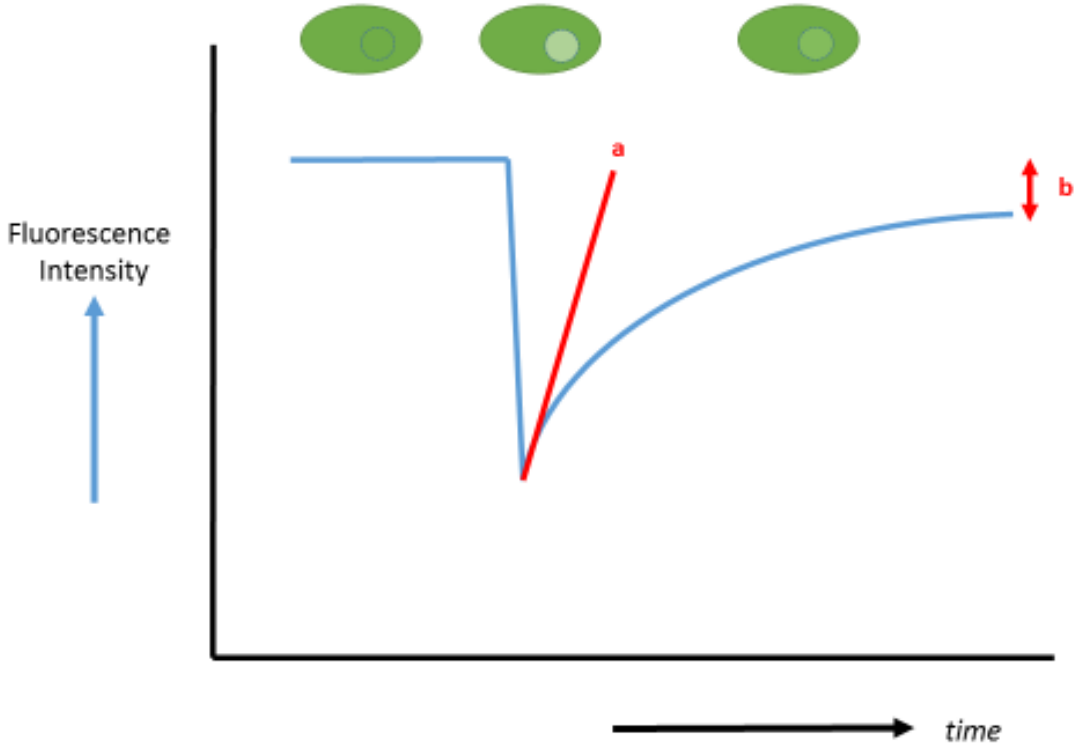


Figure 2.18 Schematic representation of a FRAP experiment showing bleaching and derivations of the mobile and immobile fractions. The blue line represents the change in fluorescence intensity in the chosen region (shown schematically in the green cells). The rate constant of the recovery of fluorescence is represented by the gradient 'a' – representative of the 'initial rate of recovery'. The difference between the baseline fluorescence and the fluorescence intensity at plateau after bleaching (b) represents the 'immobile fraction'.

2.7.2.2 FRAP Microscopy equipment

A Zeiss LSM 700 confocal imaging system recorded fluorescence in superfused cells (kind permission of Prof P Swietach, Department of Physiology, Anatomy and Genetics, Oxford, UK). GFP-expressing cells cultured in µ-Slide 4 Well Glass Bottom dishes (Ref: 80427; Ibidi, Munich, Germany) were excited at 488 nm and emission was recorded >520 nm. Experiments were conducted at room temperature and pressure.

Chapter 3

Ex vivo culture and adenoviral gene transduction of FRET reporters in adult mouse cardiomyocytes

3.1 Background

The visualization of real-time changes in cyclic nucleotide signalling within distinct cellular compartments was not feasible until the development of live-cell imaging techniques that have improved spatial and temporal resolution over biochemical assays[135]. The advent of transgenic mouse models that allow the constitutional or tissue-specific control of gene expression has been a highly valuable tool in biomedical science. It has aided the modelling of human disease in mice and also allowed the manipulation of cell-signalling systems. Therefore, being able to use cardiomyocytes from genetically modified mice in conjunction with the real-time imaging technique afforded by FRET biosensors may provide significant opportunities to answer biological questions. Indeed, animals with transgenic FRET biosensors have been generated[147]. However, this approach is limited by the time-consuming development of a transgenic animal, which is a significant barrier to the use of novel constructs of sensor. Variations of sensor may be related to the characteristics of fluorophores used[148] or the addition of particular targeting sequences to localise a FRET sensor at a particular subcellular location[99]. Adenoviral gene transfer may represent a relatively straightforward and flexible approach to using FRET biosensors in primary adult mouse cardiomyocytes. Adenoviral gene transfer is readily achievable in certain cell types, such as the neonatal rat cardiomyocyte[149], however the model is not frequently subjected to transgenic modification. Adult murine cardiomyocytes are not only difficult to subject to gene transduction[109], whether plasmid or adenoviral, they also present a significant challenge to maintain in culture for a sufficient length of time to allow expression of the sensor[111].

Equally, how suitable a model of cardiomyocyte function cultured cells are after 24 hours with adenoviral infection is not clear. In primary cell culture, it has been shown that the rate of loss of contractile function in rodent cardiomyocytes is species-dependent, with up to 50% of mouse cardiomyocytes losing the ability to contract after 24 hours in culture, whereas >75% of rat cardiomyocytes can contract after 48 hours of culture[108]. Chemical supplementation of the culture conditions, such as with sub-micromolar concentrations of cytochalasin D[150], have been reported to improve cardiomyocyte viability but the effects in conjunction with adenoviral gene transfer are not known.

In order to be able to use the live-cell fluorescent imaging technique of FRET to evaluate the effects of H_2O_2 on the activity of the PKA RIα holoenzyme and make use of the 'redox-dead' knock-in mouse model, a protocol for the adenoviral gene transfer of FRET reporters to adult mouse myocytes needed development and validation.

The aim of this chapter is to describe the conditions required to facilitate adenoviral gene transfer of FRET biosensors into adult mouse cardiomyocytes; whether Cytochalasin D is associated with improved viability and to assess whether viral infection is associated with altered cardiomyocyte function. Much of the information contained within this chapter has been published as part of a chapter entitled 'Adenoviral transduction of FRET-based biosensors for cAMP in primary adult mouse cardiomyocytes' in the book *Methods in Molecular Biology : cAMP signaling,* for which I was the lead author[151].

3.2 Methods

3.2.1 Cardiomyocyte Isolation, Infection and Culture

Primary adult mouse cardiomyocytes were isolated from wild-type C57/BL6 mice using a Langendorff perfusion method as described in Chapter 2.1.1. The C57/BL6 strain of mouse was chosen as it is the same background strain in which the 'redox-dead' mice, to be used in later studies of redox state on PKA RI activity, was generated. In addition to the protocol outlined earlier, the following steps were required after plating the cells on laminin-coated glass coverslips in order to culture adult mouse cardiomyocytes after transient exposure to adenovirus.

After isolation and washing of the cells to remove cellular debris and fibroblasts from the isolation, the cells were suspended in Modified Eagle Medium (MEM - M1018, Sigma-Aldrich, USA). The medium has a molarity of glucose of 5.5mM and is supplemented with 9mM NaHCO3, 1% L-glutamine, 1% penicillin/streptomycin. The cells were cultured in a standard laboratory incubator maintained at 37°C and supplemented with 5% CO_2. The rationale for the use of MEM-based culture medium was based upon observations by Li *et al* 2003[109] in which the expression of the Coxsackie Adenovirus Receptor (CAR) by adult mouse cardiomyocytes, which is responsible for allowing entry of the adenovirus into the cell, was enhanced compared to when other culture media were used such as M-199.

Two FRET-reporter constructs have been used in the thesis, AKAR3ev[145] to detect PKA activity and Epac H187[101] (referred to as H187 hereon) to detect changes in cAMP concentration. At the time of the study, AKAR3ev had been identified as the most sensitive PKA activity sensor available[145], which was considered a particularly valuable

attribute when trying to detect potentially small changes in PKA activity in response to non-classical stimuli such as H_2O_2. The constructs were cloned into an adenoviral vector constructed for mammalian tissue expression (CMV promoter) and amplified commercially (Vector BioLabs, Philadelphia USA) to a titre of 10^{10} Particle Forming Units (PFU) per millilitre. The ratio of viral particles to target cell for infection, the so-called Multiplicity of Infection (MOI), is an important determinant of efficacy of gene transfer[109]. From the available literature, an MOI of 100 was chosen[111] as a high ratio of virion (PFU) to cell in order to drive effective gene transfer. For example, 1µl (1×10^{-6} l) of a viral preparation with a titre of 10^{10} viral particles per ml is applied to culture of 100,000 (10^5) cells; i.e. a ratio of 10^7 viral particles to 10^5 cells. Transient exposure to virus was performed over three hours before removal of the virus by washing in serum-free MEM-medium. Incubation was continued at 37°C in 5% CO2 and gene expression was achieved within 24 hours. Cells destined for examination at 0 hours were used after the plating or viral infection step as appropriate. Experiments were conducted at room temperature and pressure using the appropriate microscopy equipment in a Tyrode Buffer solution with 1.2mM [Ca^{2+}].

Cytochalasin D (Sigma-Aldrich, USA - C8273), an alkaloid mycotoxin known to inhibit actin polymerisation, has been found to preserve structural integrity and contractile function at sub-micromolar (e.g. 0.5 µM) concentrations in adult rat cardiomyocytes[150]. The principal mechanism of action is thought to be via actions on the cytoskeleton that prevent the loss of T-tubules that has been observed in cultured rodent ventricular cardiomyocytes[108]. The adenovirally mediated expression of FRET biosensors has not been described in adult mouse cardiomyocytes and the effect of cytochalasin D on this process was not known. Cytochalasin D was added to the culture

medium after three hours of incubation with virus, when cells were washed carefully three times with fresh medium.

3.2.2 Measurement of viability and contractility of cardiomyocytes

In order to determine whether the application of virus or cytochalasin D significantly affects myocyte function, important outcome measures of cardiomyocyte integrity are viability as measured by the ability of the cell to contract upon depolarisation. A myocyte contractility recording and analysis system (Ionwizard, Ionoptix, USA) was used to determine measures of cardiomyocyte contractility. This was achieved through acquisition of images of cardiomyocytes under 1 Hz electrical field stimulation, from which changes in sarcomere length over time could be derived. Fractional shortening (FS) describes relative percentage change in sarcomere length during a period of contraction, in this instance due to 1Hz electrical field stimulation. The measurement acts as a descriptor of the inotropic capacity of the cell. Conversely, 'Tau' (τ) is the exponential decay time constant that characterises the speed of recovery (relaxation or calcium reuptake) of the cardiomyocyte. A greater tau value equates to a longer recovery or time to return to baseline. A sample trace to show the derivation of these values is shown in Figure 3.1.

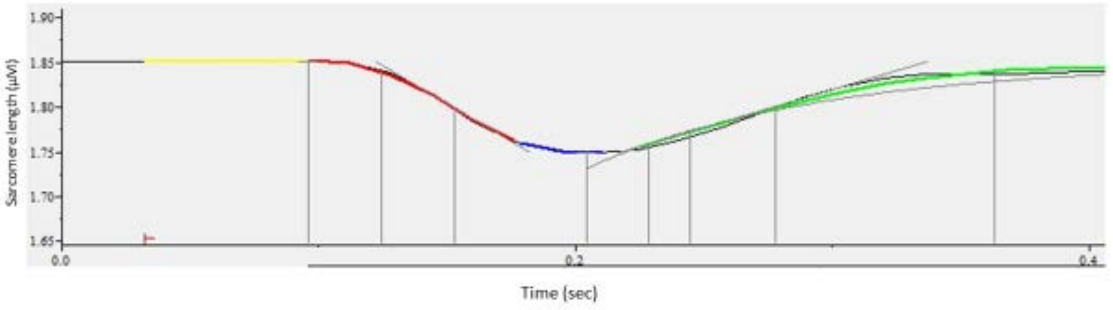


Figure 3.1 Sample raw trace from Ionoptix® software of the contraction of an adult mouse cardiomyocyte. Fractional shortening is derived from the baseline (yellow) and nadir (blue).

The green line shows a curve fit for the determination tau.

Viability was determined by simply counting the proportion of contractile cells under 1Hz electrical field stimulation compared to non-contractile cells that had the chrematistic morphology of adult mouse ventricular cardiomyocytes. The cells were plated on laminin-coated glass coverslips as described in Chapter 2.1.1 and bathed in a Tyrode solution pH corrected to 7.4 and supplemented with 1.2mM Ca^{2+}. All experiments were carried out at room temperature and pressure to ensure consistency with the experimental conditions encountered during FRET microscopy experiments.

3.2.3 Statistical analysis

The experimental data were collected and interpreted using one-way or two-way analysis of variance (ANOVA) with repeated measures (with Tukey's *post hoc* correction) according to the experimental design. All statistical analysis was conducted using GraphPad Prism 6.07 (GraphPad Software, La Jolla California USA).

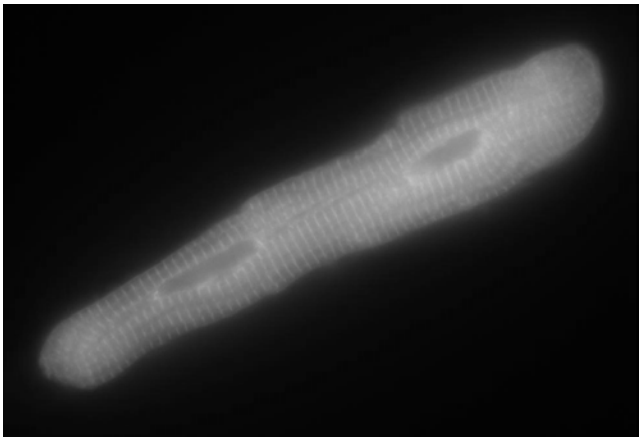
3.3 Results

3.3.1 Adenoviral gene transfer

The first aim of this part of the project was to show whether adenoviral gene transfer of a FRET biosensor was achievable in primary adult mouse cardiomyocytes. By using previously published protocols and a fastidious approach to cardiomyocyte isolation as described in detail in Chapter 2.1, reliable adenoviral gene-transfer and subsequent expression of FRET biosensors was achieved (Figure 3.1a). Figure 3.1b is a graphical representation of an example experiment to show a functioning FRET biosensor to detect PKA activity in an adult mouse cardiomyocyte. The yellow and blue lines represent the changes in background-subtracted fluorescence intensity (right axis) of Yellow Fluorescent Protein (YFP) and Cyan Fluorescent Protein (CFP) respectively that constitute the FRET sensor. The red line represents the YFP/CFP ratio, which has been normalised to the baseline during the initial 60 seconds of the experiment (left axis). The dynamic range of the biosensor was revealed by the addition of agents that maximally elevate the intracellular concentration of cAMP and hence PKA activity; forskolin to activate adenylyl cyclase to increase cAMP production; and IBMX to inhibit phosphodiesterases that hydrolyse cAMP. The resultant increase in cAMP concentration activates PKA in a classical manner to allow the AKAR3ev FRET biosensor to be activated – as show by the increase in FRET ratio. As is often the case with the AKAR FRET reporters, the divergence of fluorescence intensity of the fluorophores, i.e. the FRET, is more pronounced in the CFP channel than the YFP channel. At the end of the experiment, H89, a non-selective inhibitor if PKA, was used to show that that change in PKA activity was reversible.

Figure 3.2 shows an example experiment when the cAMP-FRET sensor EPAC H187 is expressed in adult mouse cardiomyocytes. Panel A shows the bright expression of the sensor associated with the striations of the cardiomyocyte. Panel B shows the results from a FRET imaging trace conducted in the cell. Upon addition of forskolin and IBMX, the rise in [cAMP] binds the EPAC-based sensor and changes the conformation such that the mTurquoise2 and tandend Venus fluorophores separate. The separation of fluorophores results in a loss of FRET between them. Therefore, excitation of mTurquoise2 results in greater mTurquoise2 emission at the expense of FRET to the Venus fluorophore, with a concomitant fall in Venus emission intensity. The dynamic range of the biosensor is revealed by the addition of agents that maximally elevate the intracellular concentration of cAMP; forskolin to activate adenylyl cyclase to increase cAMP production; and IBMX to inhibit phosphodiesterases that hydrolyse cAMP. The reversibility of the process is demonstrated the rapid reversal of the fluorescence intensities of the Venus and mTurquoise and fluorophores to baseline, upon removal of the forskolin and IBMX by means of the aspiration apparatus (Figure 2.15).

A)



B)

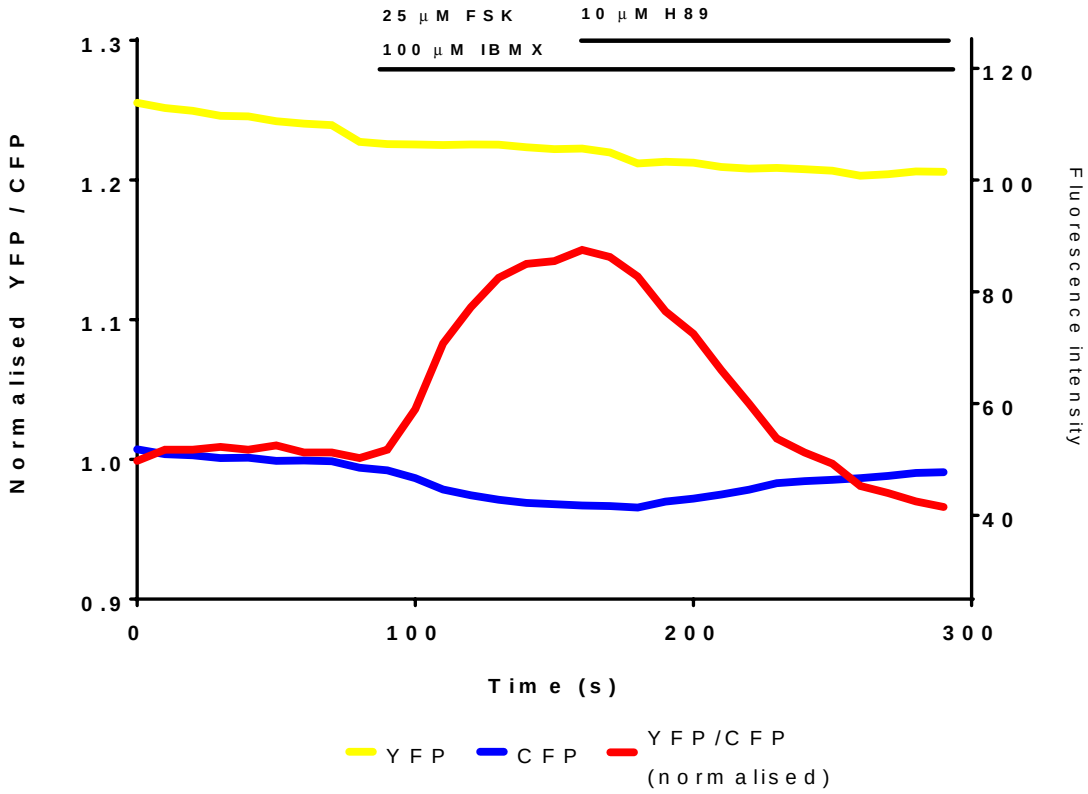
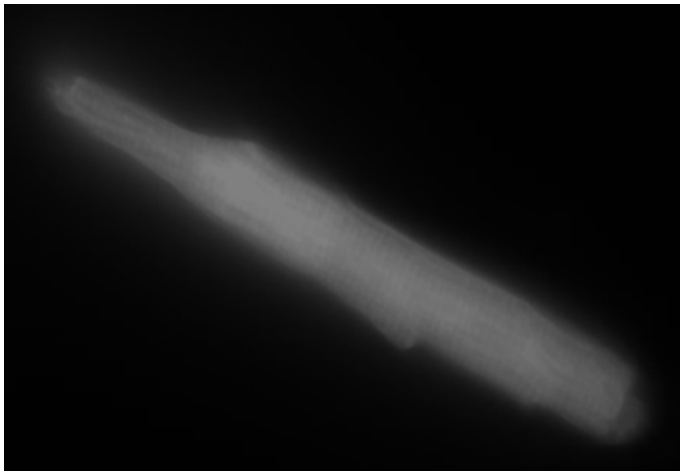


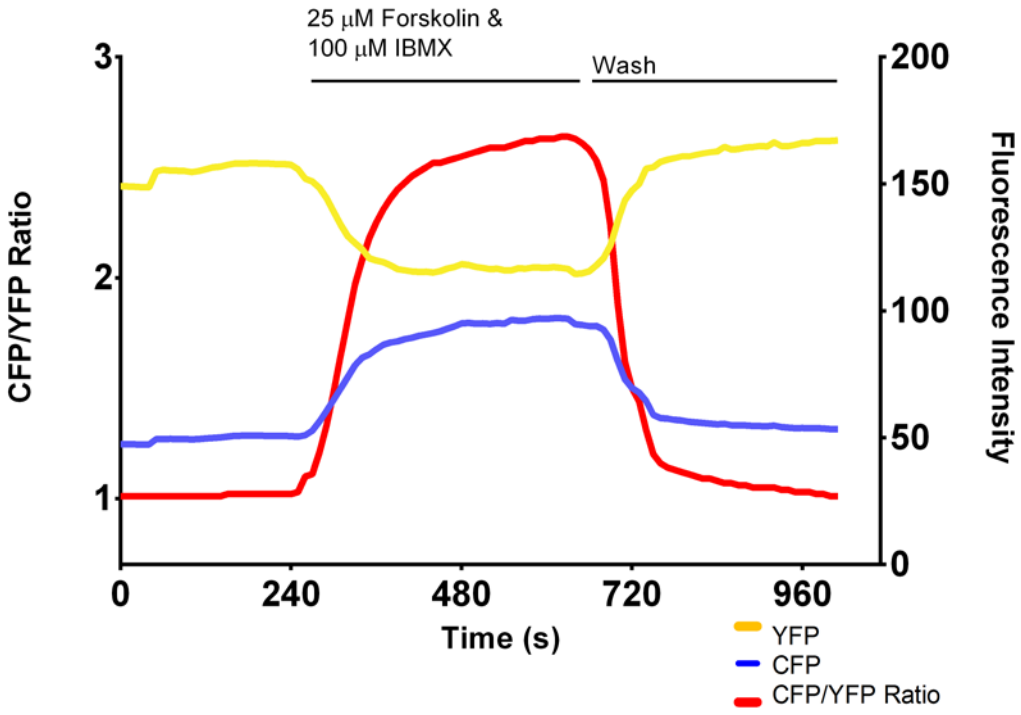
Figure 3.2

a) Primary adult mouse cardiomyocyte expressing a cytosolic AKAR3ev sensor for PKA activity after approximately 24 hours in culture.

b) Graph to show an experiment involving cytosolic AKAR FRET biosensor expressed in a primary adult mouse cardiomyocyte to show changes in PKA activity.

A)





B)

Figure 3.3 Graph to show an experiment involving cytosolic EPAC-based FRET biosensor to show the effects of an increase in cAMP due to forskolin and IBMX, with subsequent removal of the stimulus. The yellow and blue lines represent the changes in background-subtracted fluorescence intensity (right axis) of Yellow Fluorescent Protein (YFP) and Cyan Fluorescent Protein (CFP) respectively. The red line represents the CFP/YFP ratio, which has been normalised to the baseline during the first 240 seconds of the experiment (left axis).

3.3.2 Effects of cell culture and viral infection on viability of cardiomyocytes

Once a protocol had been identified to produce adult mouse cardiomyocytes reliably expressing FRET biosensors, the next step was to determine the effects on cell survival of transient adenoviral infection with subsequent 24 hours of culture and whether cytochalasin D was associated with improved functional characteristics of the cells.

Viability of primary adult mouse cardiomyocytes was determined by their ability to contract in response to 1Hz of electrical field stimulation. Cells with a morphology consistent with adult mouse cardiomyocytes (striated, angular cells that are often binucleate) were counted and the proportion of those cells that contracted in response to field stimulation was recorded. Figure 3.3 shows how the proportion of contractile cells at Time 0 was approximately 63%, which had fallen by half to approximately 27% after 24 hours in culture, consistent with previously published observations[108]. One-way ANOVA with repeated measures confirmed the statistical significance of the fall in viability over 24 hours (p = 0.003) and showed that there was no effect of viral infection over the course of a culture. To address this, the one-way ANOVA with multiple comparisons did not reveal an interaction between viral infection and viability after culture.

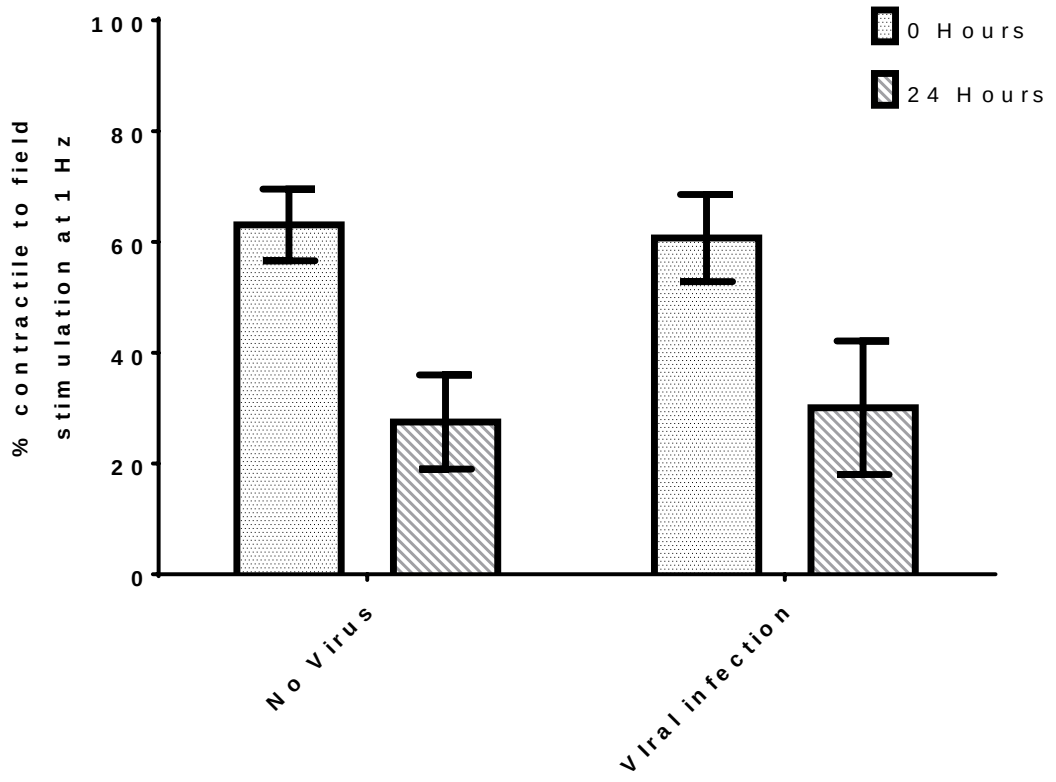


Figure 3.4 Graph to show viability of primary adult mouse cardiomyocytes with and without adenoviral infection with a FRET biosensor before and after 24 hours in culture conditions. One-way ANOVA with repeated measure based on time in culture revealed a decrease in the number of contractile (viable) cardiomyocytes after 24 hours in culture. There was no interaction due to adenoviral infection. (p = 0.003). Data presented as a mean + SEM. n = each group comprises 4 isolations with 6-12 cells per isolation.

3.3.3 Effects of viral infection and Cytochalasin D on contractile properties of primary adult mouse cardiomyocytes

In order to achieve expression of fluorophores in adult mouse cardiomyocytes after adenoviral gene transfer, approximately 24 hours in culture is required[109]. The aim of the forthcoming experiments was to identify what effects cell culture with or without adenoviral infection and cytochalasin D had on cardiomyocyte contractile properties of fractional shortening (FS), to describe cardiomyocyte inotropic potential, and the parameter τ, which describes the time taken for a myocyte to relax after contraction.

Figure 3.4 shows the effects of transient adenoviral infection on Fractional Shortening (FS) with and without cytochalasin D.

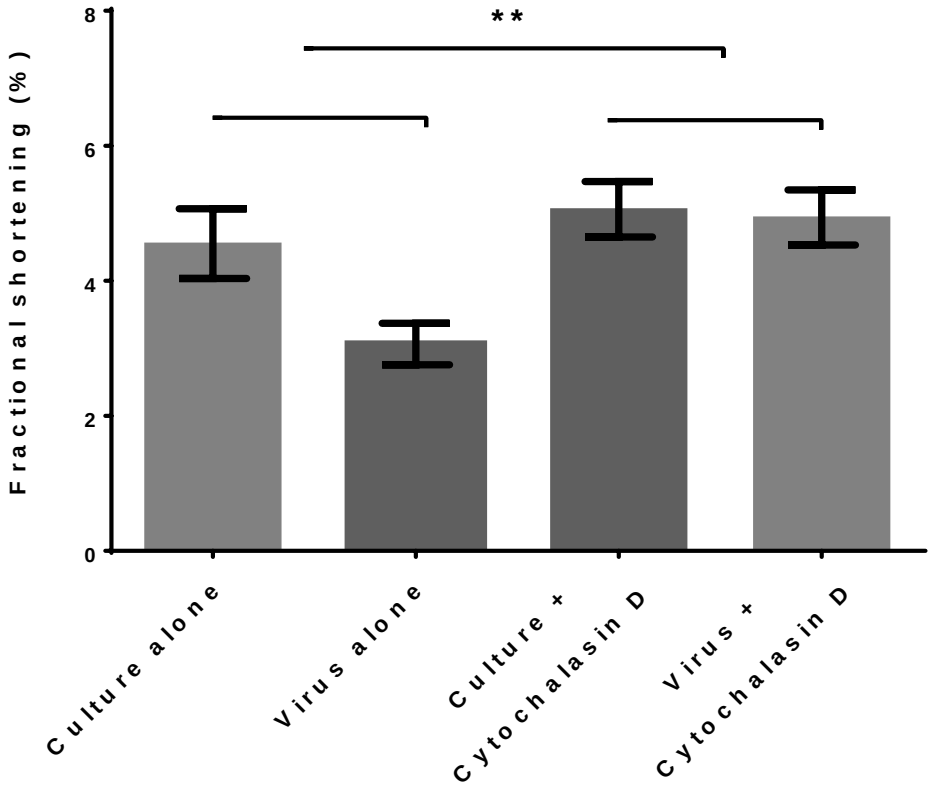


Figure 3.5 Graph to show the effects of adenoviral infection and 0.5µM cytochalasin D on Fractional Shortening (FS) in primary adult mouse cardiomyocytes. Two-way ANOVA reveals that viral infection compared to culture alone causes a decrease in fractional shortening as well as and a significant effect of cytochalasin D in restoring the deleterious effect of adenoviral infection (** p = 0.0028). The bracket on the graph is drawn to convey the analysis of cytochalasin D across two groups. Data presented as a mean + SEM. n = each group comprises 4 isolations with 6-12 cells per isolation.

Figure 3.4 describes the effects of adenoviral infection with and without supplementation with 0.5µM cytochalasin D in cultured primary adult mouse cardiomyocytes. Two-way ANOVA with repeated measures (with Tukey's *post hoc* correction) showed that virally infected cells exhibit a reduction in contractile function

as a decrease in FS from 4.5% to 3%. Secondly, the ANOVA reveals that supplementation with 0.5µM cytochalasin D maintains contractile shortening, obviating the deleterious effects of viral infecton alone (p = 0.0028 - brackets on graph – Figure 3.4).

Figure 3.5 shows the effects on *tau (τ)* of transient adenoviral infection with and without cytochalasin D in comparison to a control group of primary adult cardiomyocytes cultured for 24 hours without intervention.

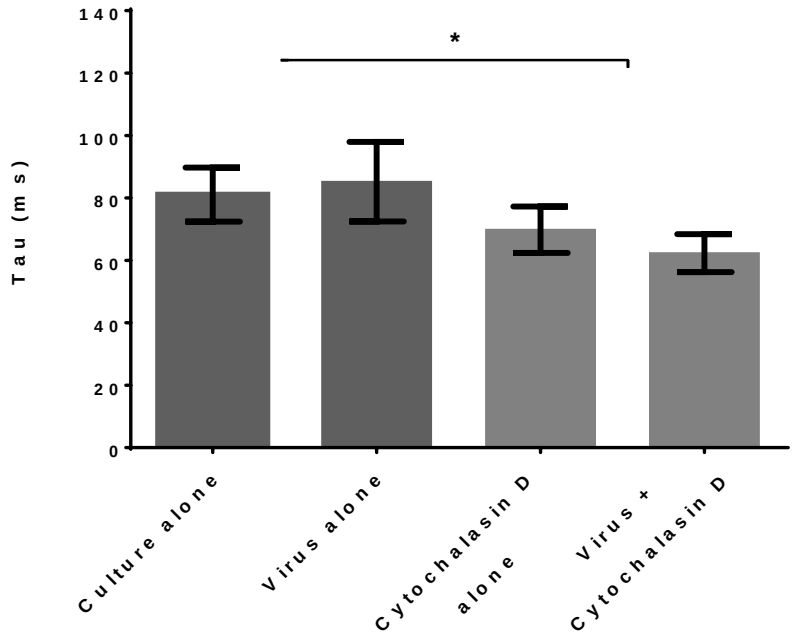


Figure 3.6 Graph to show the effects of adenoviral infection and 0.5µM cytochalasin D on Fractional Shortening (FS) in primary adult mouse cardiomyocytes. The bracket on the graph is drawn to convey the analysis of cytochalasin D across two groups - the addition of 0.5µM cytochalasin D is associated with a significant mean reduction in Tau (τ) compared to untreated groups. Data presented as a mean + SEM. *n* = each group comprises 4 isolations with 6-12 cells per isolation.

Two-way ANOVA reveals that the addition of 0.5µM cytochalasin D is associated with a smaller value of Tau (τ) reducing the mean from 80ms to approximately 60ms. This

decrease in Tau, i.e. quicker recovery, is consistent with an improvement in myocyte relaxation due to more rapid uptake of Ca^{2+} by the Sarcoplasmic Reticulum.

3.4 Discussion

The first aim of this part of the project was to refine and validate a protocol for the adenoviral transfer of genes encoding FRET-based biosensors to detect changes in cAMP-PKA signalling. Adenovirus-mediated gene transfer encoding for fluorescent proteins has been described[109, 111]. However, such a process to drive expression of functional FRET biosensors of PKA-cAMP signalling had not been demonstrated in adult mouse cardiomyocytes. Indeed, reflecting the difficulty of the process, a transgenic mouse expressing FRET biosensors had been developed[103] in spite of the expensive time-consuming development of such a model. By being able to examine cAMP-PKA signalling using real-time FRET imaging in adult mouse cardiomyocytes, this allowed the use of this imaging technique with the transgenic 'redox-dead' knock-in mice to be used as a control in subsequent chapters.

By being careful in the isolation of adult mouse cardiomyocytes, combined with transient exposure to adenovirus prior to culture for approximately 24 hours, a reliable protocol was achieved. Figures 3.1 and 3.2 show that adult mouse myocytes are able to express functional FRET biosensors and allow detection of changes in cAMP-PKA signalling. These data show that functional FRET biosensors can be expressed after adenoviral gene transfer in primary adult mouse cardiomyocytes and indeed, such cells have the functional capacity for cAMP-PKA signalling. The overall efficiency of adenoviral gene-transfer and resultant expression of biosensor in primary adult mouse cardiomyocytes was low at approximately 20% of total cells surviving 24 hours in

culture, though adequate for the purposes of FRET imaging where one cell is used per experiment.

The next step was to identify what effect cell culture following transient adenoviral gene transfer had on the function of cardiomyocytes after 24 hours. Many primary cells die as they are harvested from tissue and fail to survive in the unusual environment afforded by cell culture conditions. Indeed, survival rates of 1-10% are often cited for primary cells in culture[152]. Figure 3.3 shows that transient exposure to adenovirus in the culture is associated with a decrease in inotropic potential as measured by a fall in Fractional Shortening. This effect was abolished with the addition of 0.5μM Cytochalasin D. In addition, the measure of myocyte recovery, *tau*, was shortened in the presence of Cytochalasin D (Figure 3.5). Together, these observations confirm prior observations that the culture of adult mouse cardiomyocytes is associated with a loss of function of the cells, particularly after adenoviral infection. However, the addition of 0.5μM Cytochalasin D is associated with improved measures of contractility and recovery, which extends observations made in rat cardiomyocytes[150].

In summary, the data presented here describe for the first time cultured primary adult mouse cardiomyocytes that express FRET biosensors (for cAMP and PKA activity) that show signalling integrity in cultured adult mouse cardiomyocytes, and which retain their ability to contract after approximately 24 hours in culture, a process that is supported through the addition of 0.5μM Cytochalasin D. These data therefore allow the further investigation of the effects of cellular redox state on PKA signalling in adult mouse cardiomyocytes. Moreover, the cellular model allows for the potential use of cells from ‘redox-dead’ mice which contain a transgenic modification of PKA RIα that

renders it unable to be oxidised to form disulphide bonds – a putative mechanism of PKA activation[77]. Therefore, the combination of the technical capacity to use adenovirally infected adult mouse cardiomyocytes with a transgenic mouse represents a unique opportunity to study the effects of redox state on PKA activity.

Chapter 4

Effects of disulphide bond formation between RIα subunits on PKA activity

4.1 Background

Numerous protein kinases contain redox-sensitive structures that have been reported to affect the activity of the enzyme, including Protein Kinase G (PKG)[72] and Protein Kinase C (PKC)[71]. PKA RIα, which contains two conserved cysteine residues at positions 17 and 37 of the dimerization and docking domain (D/D) of the regulatory subunit, has been known to undergo redox-dependent dimerization for many years[70, 153]. The tetrameric holoenzyme of PKA comprises two R subunits and redox-dependent dimerization is not necessary for assembly of the R subunit dimer in the holoenzyme[49, 103], but the formation of redox-dependent disulphide bonds between RIα subunits has been associated with downstream phosphorylation of putative PKA targets as well as an increase in the amplitude of contraction of rat ventricular myocytes[77]. The biochemical and functional effects were inhibited by H89, an ATP analogue that inhibits PKA by competing with ATP at the ATP-binding site of the kinase, to inhibit target phosphorylation Therefore, H89 has inhibitory effects on numerous protein kinases, leading to a lack of specificity of action (See Chapter 2.7.1.2). Nevertheless, these observations suggested that PKA RIα activity, as measured by downstream effects, is increased in response to oxidation. These effects were abolished by H89 and not associated with an increase in intracellular cAMP, suggesting a cAMP-independent activation of PKA.

Since these observations were made, a transgenic mouse which possesses a mutation of cysteine 17 to serine (C17S) to prevent redox-dependent dimerization has been developed[103]. Only one of the two redox-sensitive cysteines needs to be mutated in order to prevent redox-dependent dimerization as the regulatory subunits assemble in an anti-parallel manner[68]. Furthermore, the fluorescence imaging technique of FRET has

developed to permit real-time measurement of changes in signalling in live cells. The AKAR class of FRET reporter comprises a PKA substrate domain sandwiched between two fluorophores (Fugure 1.4). Phosphorylation of the AKAR reporter alters the conformation of the protein, which causes a change in distance between the fluorophores which leads to a change in FRET. Therefore, the AKAR FRET sensor acts as a ratiometric marker of PKA activity. The transgenic mouse and the availability of FRET reporters, which can now be used reliably in adult mouse cardiomyocytes, as described in Chapter 3, allow the direct assessment of changes in PKA activity after an oxidative stimulus is applied to cells which can possess either redox-sensitive of insensitive (redox-dead) endogenous PKA RIα. The aim of the following investigation is to determine whether there is increased PKA activity as measured using FRET reporters, in adult mouse cardiomyocytes following application of exogenous hydrogen peroxide. If the original observations were supported, the subsequent aim would be to use FRET sensors targeted to subcellular domains to attempt to measure discrete effects of redox modulation of PKA signalling.

4.2 Methods

4.2.1 Adult mouse cardiomyocyte FRET reporter analysis

Adult mice aged between 8 and 14 weeks were obtained from the ‘PKA Redox Dead’ colony of C57/BL6 mice, whose maintenance is described in Chapter 2. The animals used were either homozygous for C17S, rendering their PKA RIα insensitive to oxidative disulphide bond formation, or their wild-type littermate controls as determined by PCR-based genotyping of ear notches (Chapter 2.1).

The isolated cardiomyocytes were cultured on laminin-coated glass coverslips and incubated transiently for three hours with an adenoviral preparation of AKAR3ev[145]. The cells were stored in an incubator maintained at 37°C with an atmosphere comprising 95% O_2 and 5% CO_2. After approximately 18-24 hours in culture, when fluorescent cells were visible using a bench-top fluorescent microscope, individual cover slips were removed from their culture medium and washed gently with a Tyrode solution containing 1.4 mM Ca^{2+}. This allowed cells to be studied without optical interference from phenol red in the culture medium. The coverslip was mounted into an appropriate stage adapter and FRET experiments were performed immediately using the solution exchange apparatus as described in Chapter 2.7.

The experimental protocol for the FRET study was arranged as follows. Each experiment began with a baseline period of two minutes to allow a stable baseline trace to be obtained. Next, Tyrode buffer supplemented with 250μM H_2O_2 was applied to the chamber accompanied by simultaneous aspiration of the baseline Tyrode buffer solution (Table 2.1). The hydrogen peroxide solution was applied for eight minutes to ensure sufficient time has elapsed to induce PKA RIα dimerization as originally described in the functional and biochemical effects of hydrogen peroxide on adult rat ventricular cardiomyocytes[77]. After eight minutes, the H_2O_2 containing solution was exchanged for the baseline buffer solution. This ‘wash’ or removal of the potential stimulus for PKA was intended to show whether any activation was reversible. After a two-minute wash period, a combination of saturating doses of the adenylyl cyclase activator, Forskolin, and the non-selective phosphodiesterase inhibitor, IBMX, was applied to generate a maximal concentration of cAMP. This final experimental manoeuvre acts as a positive control to demonstrate that the intracellular apparatus of cAMP-PKA signalling was

intact and that the FRET reporter for PKA activity performed as expected and underwent maximal FRET change. All experiments were carried out at room temperature and pressure. Raw data of fluorescent intensities were obtained from the MetaFluor software of the fluorescence microscopy setup (Chapter 2.7) and FRET ratios were calculated. Data and statistical analysis, where applicable, were plotted using GraphPad Prism 6.07 (GraphPad Software, La Jolla California USA).

4.2.2 *In vitro* assessment of the effects of H_2O_2 on PKA activity in the cytosolic compartment of HEK-293 cells

In summary, HEK-293 cells were transfected with AKAR3ev plasmid 12 hours prior to cell lysis and protein extraction, once FRET biosensor expression had been observed. Using a commercially available cellular fractionation kit QProteome Mitochondrial Cell Compartmentation Kit (Qiagen, MN, USA), which was validated in Chapter 2.5.3, a cytosolic fraction was obtained. By placing the HEK-293 cytosolic fraction on a glass coverslip, which contains most of the AKAR3ev FRET reporter, an *in vitro* measurement of FRET ratio could be measured.

4.2.3 Statistical analysis

The experimental data were collected and interpreted using one-way analysis of variance (ANOVA) with repeated measure or two-way ANOVA according to the experimental design. All statistical analysis was conducted using GraphPad Prism 6.07 (GraphPad Software, La Jolla California USA).

4.3 Results

4.3.1 Effects of exogenously applied 250μM H_2O_2 on PKA activity in adult mouse cardiomyocytes expressing AKAR3ev FRET biosensor

In order to have an impression of the sensitivity of AKAR3ev in adult mouse cardiomyocytes, cells expressing the sensor were exposed to a range of concentrations (625nM to 25μM) forskolin to activate adenylyl cyclase to produce cAMP (Chapter 2.7.1.2). The % change in FRET was plotted against the concentration of forskolin using a logarithmic axis and the results are shown in Figure 4.1.

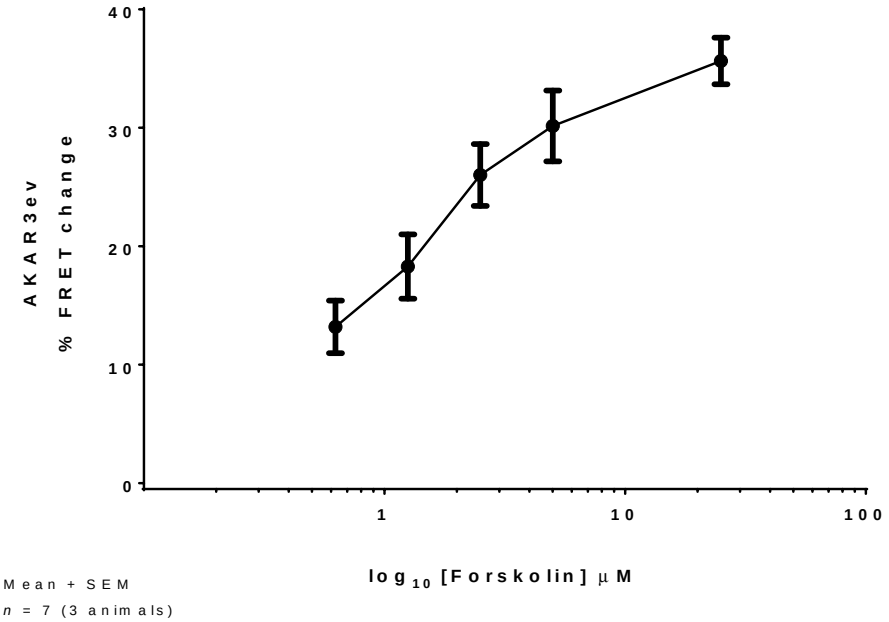


Figure 4.1 Dose-response curve showing FRET changes for AKAR3ev expressed in adult mouse cardiomyocytes that have been exposed to a range of concentrations of forskolin. Data are expressed as means + SEM.

The data in Figure 4.1 indicate that AKAR3ev expressed in adult mouse cardiomyocytes show a maximal FRET change of ≈35% consistent with published observations of ≈45% maximal FRET change[145]. Furthermore, AKAR3ev is able to

detect changes in PKA activity even with very low, sub-micromolar doses of forskolin. However, it should be remembered that cAMP-PKA signalling is an amplificatory cascade so small changes in cAMP generated by low doses of forskolin can lead to significant downstream PKA activity. In order to perform a dose-response curve using cAMP, analogues of the cyclic nucleotide would need to be introduced into cells expressing the sensor using a patch pipette.

In order to demonstrate that the addition of 250μM H_2O_2 induces disulphide bond formation in adult mouse cardiomyocytes and that disulphide bond formation does not occur in 'redox-dead' knock-in mice, which lack the C17 residue to form such bonds, freshly isolated cardiomyocytes from the two groups were incubated for five minutes with 250μM H_2O_2. Protein was extracted from whole cell lysates, run in non-reducing conditions and blotted for PKA RI – the data are shown in Figure 4.2 with two repeats per condition. In this experiment, under basal conditions, disulphide bonds forming RIα dimers are seen in wild-type but not redox-dead samples (n=2). After incubation with 250μM H_2O_2, the proportion of dimeric protein increase in the wild-type samples compared to basal conditions. Even in the presence of an oxidising stimulus, the redox-dead samples do not exhibit dimeric bands.

After demonstrating that the FRET biosensor is sensitive to small increases in cAMP and that incubation of primary adult mouse cardiomyocytes induces disulphide bond formation between RIα subunits with no effect in redox-dead animals, the next step was to examine whether hydrogen peroxide was associated with increased PKA activity in wild-type compared to 'redox-dead' animals.

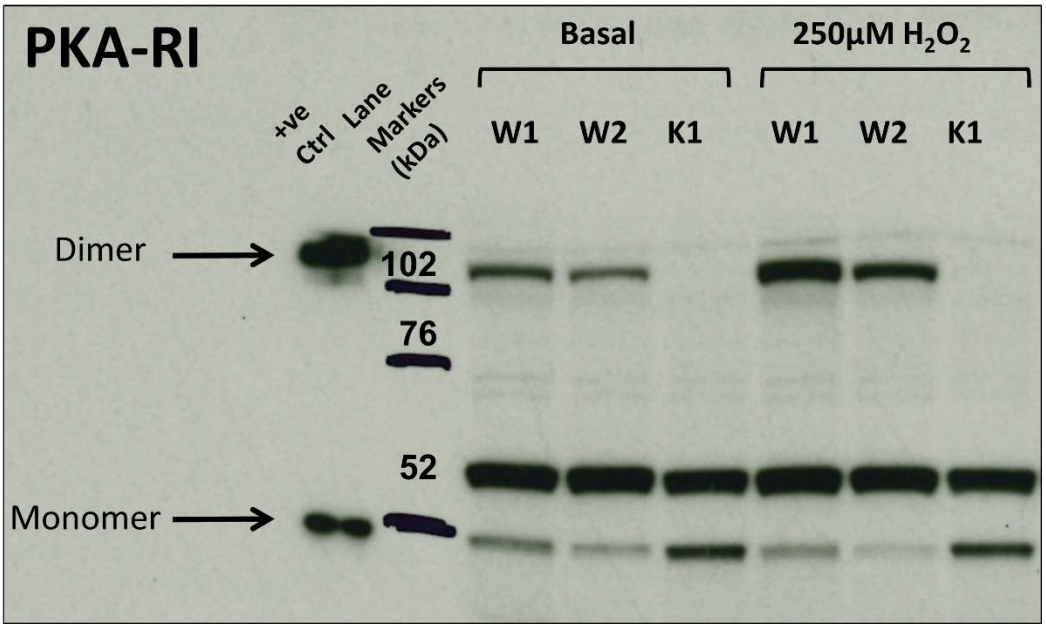


Figure 4.2 Immunoblot of PKA RI in whole cell lysates from adult mouse cardiomyocytes to show the presence of disulphide bonds between RIα-subunits (dimers) compared to reduced monomeric subunits in cells from wild-type (W1 and W2 – n=2 animals) and 'redox-dead' (K1) animals with and without incubation with hydrogen peroxide.

Figure 4.3 describes the effect of 250µM H_2O_2 on primary adult mouse cardiomyocytes derived from 'redox-dead' and wild-type littermate controls expressing AKAR3ev, a FRET-based PKA activity reporter. The first observation to be made from the data in Figure 4.3 was that both the wild-type and the 'redox-dead' knock-in animals exhibit increased PKA activity in response to a rise in cAMP secondary to the application of forskolin and IBMX. The 'redox dead' possess the C17S mutation in PKA RIα making them incapable of forming disulphide bonds between RIα subunits in response to oxidising agents and, in effect, equivalent to being in a persistent chemically reduced state. Therefore, if an oxidant such as hydrogen peroxide (250µM H_2O_2) were added to the cells, which is known to induce disulphide bond formation between PKA RIα subunits, then increased PKA activity as measured by an increase in FRET ratio would be expected to be observed. The data presented in Figure 4.3 show a drifting baseline

but without any significant divergence in response between the cells from the wild-type or 'redox-dead' animals during exposure to 250µM H_2O_2. The benefit of using the 'redox-dead' mouse is evident as it represents an ideal negative control, which prevents misinterpretation of a wandering FRET trace. Therefore, these data do not support the hypothesis that redox-dependent dimerization of PKA RIα is associated with an increase in activity of the PKA holoenzyme as measured by the AKAR FRET reporter of PKA activity.

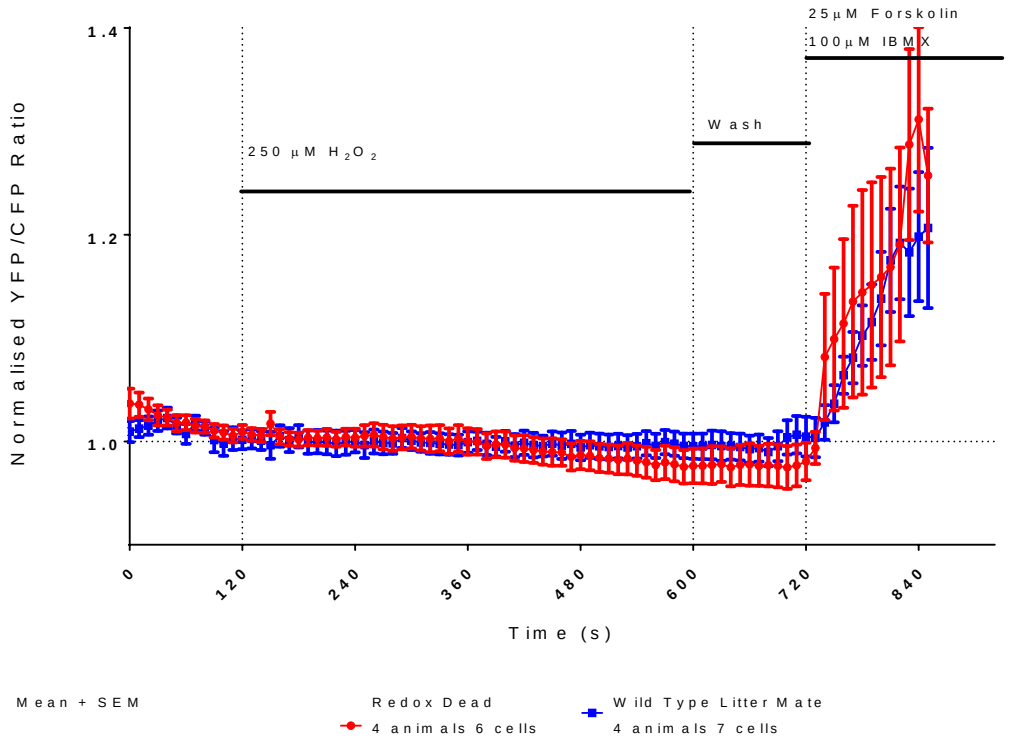


Figure 4.3 Graph to show the FRET ratio in response to the incubation with 250µM H_2O_2on adult mouse cardiomyocytes from wild-type and redox-dead animals expressing the AKAR3ev FRET biosensor. Lines denotes mean + SEM. The addition of forskolin and IBMX act as a positive control to show that the cells under investigation possess functional kappa signalling apparatus.

4.3.2 Effects of 250µM H_2O_2 on cAMP concentration in adult mouse cardiomyocytes expressing the H187 FRET biosensor

The data in Figure 4.4 describe the effects of 250µM H_2O_2 on adult mouse cardiomyocytes expressing the H187 FRET sensor which reports changes in cAMP concentration – a higher ratiometric value denoting increased cAMP concentration. The graph does not show a fall in cAMP concentration over the course of the experiment. The lack of change in PKA activity seen in Figure 4.3 therefore does not appear to be due to a concomitant decrease in cAMP to offset an increase in cAMP-independent PKA activity.

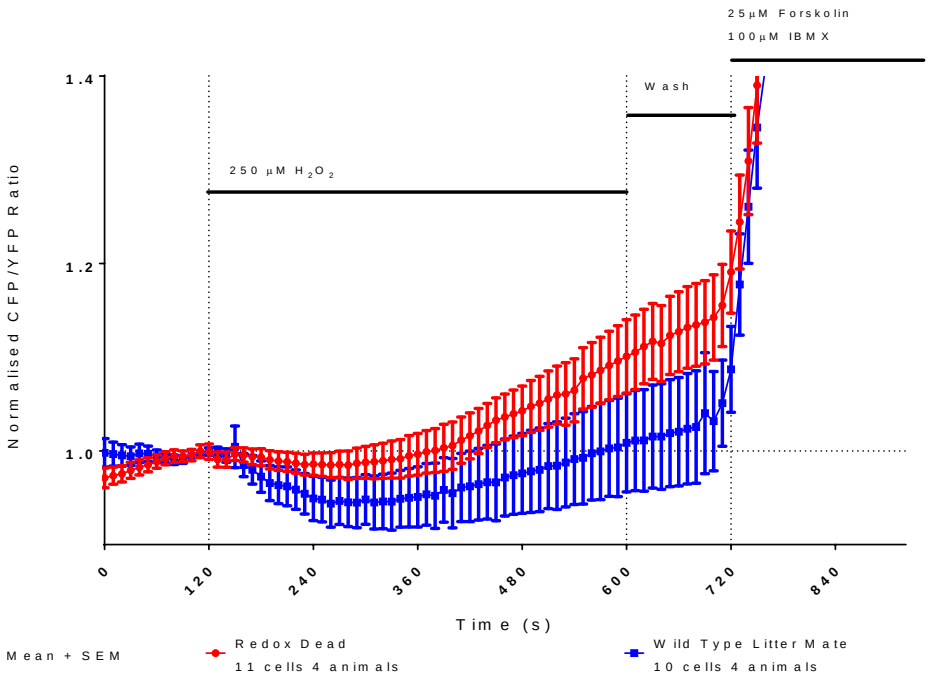


Figure 4.4 Graph to show the FRET ratio in response to the incubation with 250µM H_2O_2 on adult mouse cardiomyocytes from wild-type and redox-dead animals expressing the H187 FRET biosensor. The addition of Forskolin and IBMX act as a positive control to show that the cells under investigation possess functional kappa apparatus. Lines denotes mean + SEM.

4.3.3 Effects of 30μM H89 on adult mouse cardiomyocytes expressing AKAR3ev FRET biosensor

Figure 4.5 shows that, at baseline, some oxidation of PKA RIα is present in freshly isolated wild-type adult mouse cardiomyocytes and this increased during time in culture to 24 hours, when FRET experimentation takes place. Therefore, cells expressing FRET biosensors represent conditions in which PKA RIα is either heavily oxidised (wild-type) or not oxidised (redox-dead).

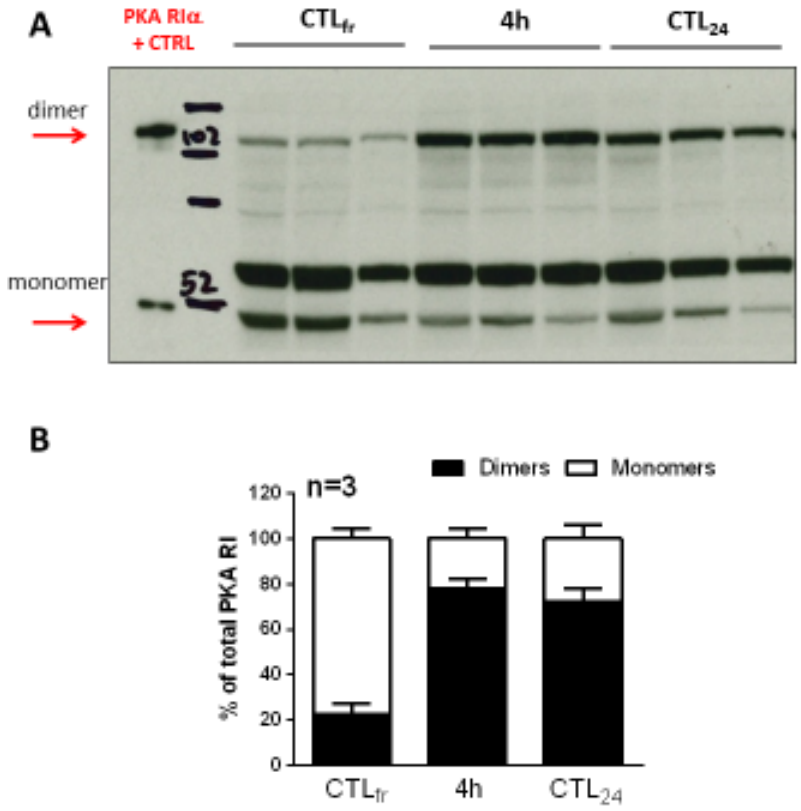


Figure 4.5
CTL$_{fr}$ = Control (untreated) cells freshly isolated. 4h = cells incubated for four hours with no exogenous treatment. CTL$_{24}$ = Control (untreated) cells incubated for 24 hours.
A – shows an immunoblot performed in non-reducing conditions (BioRad Protean) of samples of protein derived from primary adult mouse cardiomyocytes (n = 3).
B – shows the proportion of total PKA that is oxidised (dimeric) compared to reduced (monomeric) calculated using optical densitometry of the immunoblot in A. Error bars represent the SEM about the means show in the bars.

Adapted from Dr N Rozmaritsa, Casadei laboratory.

Therefore, one may expect an increase in basal PKA activity in the wild-type animal to be revealed upon addition of H89. To test this hypothesis, 30μM H89, an inhibitor of PKA activity, was used to compare basal PKA activity in cardiomyocytes isolated from redox-dead vs wild-type expressing the AKAR3ev FRET sensor (Figure 4.6). As H89 is such a potent inhibitor of PKA activity, that cannot be washed out of the cells, a positive control stimulus of forskolin and IBMX to show functional cAMP-PKA signalling apparatus was not feasible. No difference in basal PKA activity was found between wild-type and redox-dead groups, which does not support the hypothesis that disulphide bond formation between RIα subunits is associated with increased PKA activity.

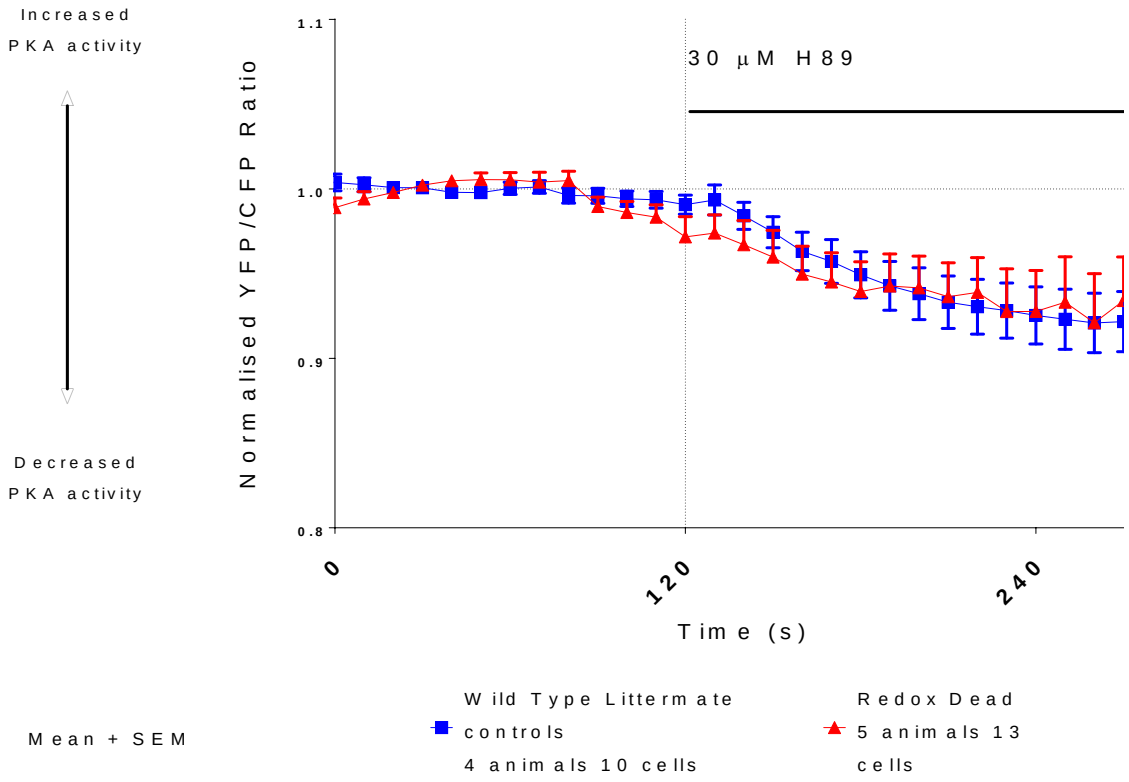


Figure 4.6 Graph to show the effects of the PKA inhibitor H89 on adult mouse cardiomyocytes from 'wild-type' or 'redox dead' animals expressing the AKAR3ev FRET biosensor. De fall in the FRET ratio below the normalised baseline of 1 denotes an inhibition of PKA activity. Lines denotes mean with standard error of the mean.

4.3.4 *In vitro* measurement of PKA activity in a cytosolic fraction of HEK cells expressing the AKAR3ev sensor

One possible criticism of the approach used in cardiomyocytes is that the AKAR sensor is not expressed in a localised manner and hence oxidation of RIα subunits in PKA holoenzymes may result in activation of the enzyme in particular cellular compartments that are not detectable by the indiscriminately expressed AKAR sensor as used in the adult cardiomyocytes.

The original categorisation of PKA Regulatory subunits into Type I and Type II was based on cellular fractionation if cardiomyocytes in which RI associated with a supernatant fraction and RII with a membranous fraction[154]. Although it is now recognised that RI subunits can be associated with membranous compartments of the cell, the original distinction remain helpful as the majority of RI is found in the cytosol. Therefore, the cytosol may be considered to be a functional compartment which contains endogenous PKA RIα which in cell lines is present in both oxidised and reduced forms.

By using a commercially available kit to separate HEK-293 cells transfected with the AKAR3ev biosensor, into cytosolic and membranous fractions, it has been possible to assess the effects of H_2O_2 on PKA activity in an isolated cellular compartment of the cytosol – free from confounding effects of membrane-bound PKA. Figure 4.7A shows PKA RI (non-reducing conditions) showing monomers and dimers of PKA RI in the

cytosol. Panels B and C show the presence of markers of the endoplasmic reticulum (SERCA2a) and four of the mitochondrial oxidative enzymes (OXPHOS). Importantly, these membranous components are absent from the cytosol.

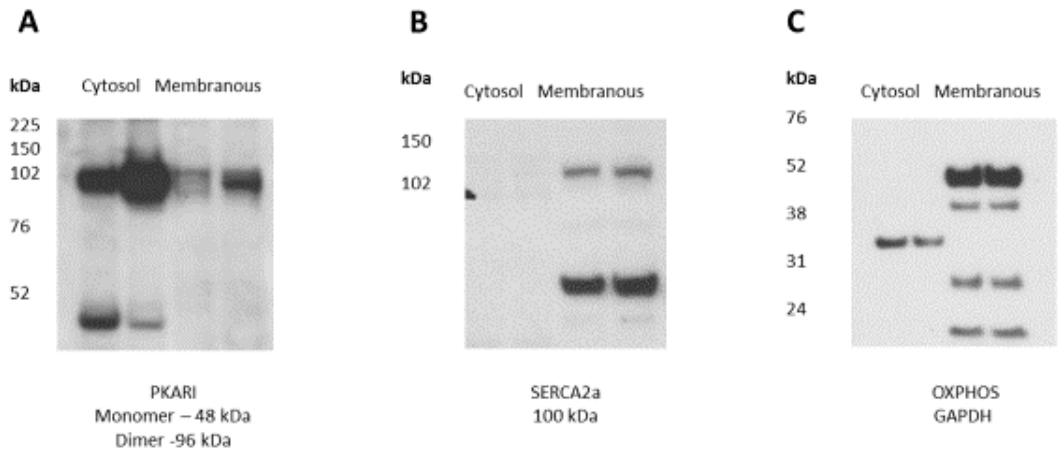


Figure 4.7 Immunoblot run in non-reducing conditions to show cytosolic and membranous subcellular fractions derived from two repeats from cultured Human Embryonic Kidney (HEK) cell lines. The first lane of each pair is from untreated cells, with the second of the pair being from cells treated with 250μM H_2O_2
A) PKA RI
B) SERCA2a – a marker of the endoplasmic reticulum
C) the cocktail of mitochondrial oxidative phosphorylation enzymes and GAPDH, the cytosolic marker.

In Figure 4.7A, bands are visible in the membranous fraction that suggest that PKA RIα dimers are selectively enriched in this fraction compared to reduced PKARI (monomers). However, running the cytosolic and membranous samples in reducing conditions does not abolish the band at ≈100 kDa, which may have been consistent with oxidised RIα subunits (Figure 4.8). It is possible that the bands at ≈100 kDa may indeed represent two subunits of PKA RIα but the inability to reduce them signifies that they do not require disulphide bonds and hence are not relevant to this thesis.

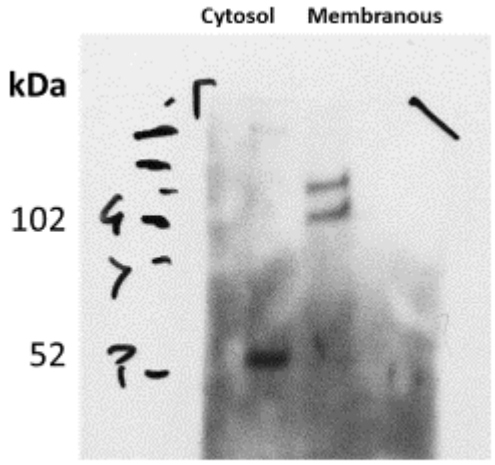


Figure 4.8 Immunoblot run in reducing conditions for PKA RI in cytosolic and membranous fractions derived from HEK-293 cells. The persistence of bands at ≈100kDa in reducing conditions, demonstrate that the protein does not require disulphide bonds and hence not relevant to this thesis.

Figure 4.9 shows the effects of 250μM H_2O_2 and the PKA inhibitor H89 on PKA activity in the cytosolic fraction of HEK-293 cells as measured by the AKAR3ev FRET biosensor. These data reveal a small background PKA activity at baseline as shown by application of H89 as well as an expected rise in PKA activity upon addition of cAMP. The addition of cAMP acts as positive control to show that the classical cAMP-PKA signalling apparatus and the AKAR3ev reporter remain functional in the isolated cellular fraction of the cytosol. Application of 250μM H_2O_2 was not associated with increased PKA activity compared to baseline. The combination of H_2O_2 and H89 was performed to see if any rise in PKA activity, if present, were abolished by H89. A two-way ANOVA analysis of the cells with and without H_2O_2 treatment; and with and without H89 treatment (i.e. using the first four conditions shown in the Figure 4.9), shows that H89 was associated with a significant decrease in FRET ratio consistent with revealing some background PKA activity at baseline ($p = 0.003$).

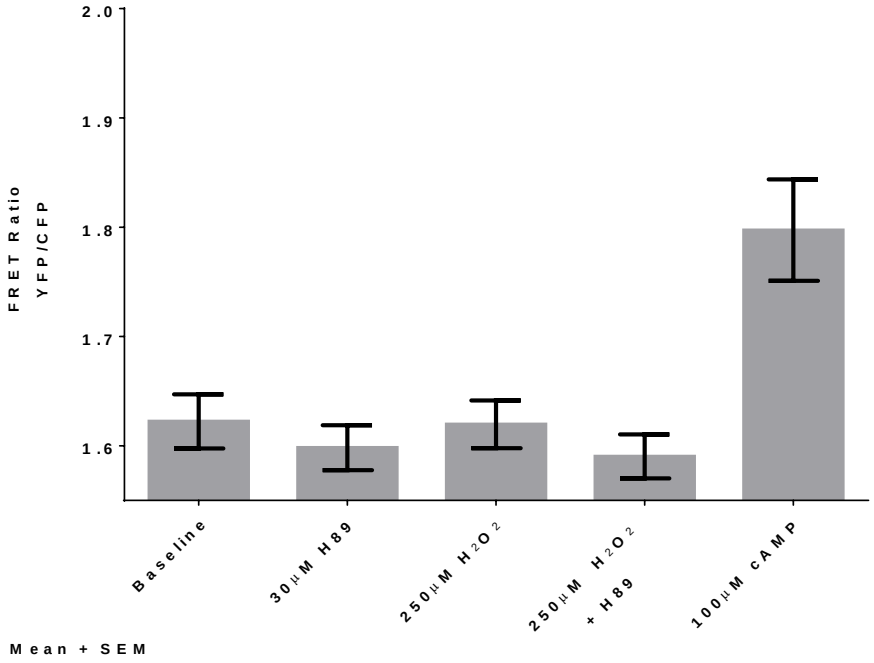


Figure 4.9 Bar graph to show steady-state *in vitro* PKA activity in a variety of conditions. n=4. Error bars denote SEM. *n*=6 (18 cells). A higher FRET ratio indicates greater PKA activity.

4.4 Discussion

The simple observation that both the wild-type and the 'redox-dead' knock-in animals exhibit increased PKA activity in response to a rise in cAMP secondary to the application of forskolin and IBMX is an important one. From this observation, PKA RI that lacks the ability to form disulphide bonds behaves in a similar fashion to wild-type PKA RI and therefore consistent with the hetero-tetrameric structure of PKA being conserved in spite of a lack of disulphide bond formation. This interpretation is supported by the biochemical observation that chemical reduction of PKA RI, that abolishes disulphide bonds between RI subunits, does not inhibit R subunit homodimer formation as part of the PKA holoenzyme[70].

The notion of redox modulation of protein kinases is well established. However, the effect of redox state on individual protein kinases varies from one to another and appears to depend on the structure of the kinase in question. For example, PKG[72] and PKC[71] have been reported to show increased catalytic activity in response to oxidising stimuli, whereas the formation of disulphide bonds between the RII subunit and the catalytic subunit of PKA have been associated, predictably, with decreased PKA activity as such bonding would inhibit the release of inhibitory RII subunits from the catalytic subunits[155] (Figure 1.3). However, the mechanism of action of the redox modification differs.

Functional and biochemical targets of PKA activity have been described in association with oxidative dimerization of the RIα subunit. However, direct evidence of PKA RIα activation in response to disulphide bond formation within the D/D between the C17 and C37 residues has not been shown. The experiments described in this chapter replicate in adult mouse cardiomyocytes the conditions subjected to an adult rat model in which the oxidant-induced activation of PKA Type I was proposed[77]. However, the data presented here do not support the hypothesis that there is increased PKA activity in response to RIα subunit oxidation. The AKAR class of FRET reporter is well-suited to the investigation of this question as it provides a direct measure of changes in PKA-dependent phosphorylation, rather than relying on surrogate markers of activity, such as downstream phosphorylation targets like Troponin I[77]. The observation that a significant proportion of PKA RIα was oxidised at baseline and during the culture (Figure 4.3) gave rise to the need for the experiment outlined in Figure 4.4. In this experiment, the inhibitor of PKA activity was used to examine differences in basal PKA activity in cultured primary adult mouse myocytes in which PKA RIα had become

heavily oxidised, compared to cells from redox-dead animals, in which PKA RIα subunits cannot form disulphide bonds. No difference between the groups was observed. These data suggest that disulphide bond formation between RIα subunits is not associated with increased PKA activity. However, the lack of effect may have been due to a lack of sensitivity by the AKAR3ev FRET biosensor or because of adaptive changes in the constitutive 'redox-dead' knock-in mouse.

Cell culture is a vital tool in cell biology that allows primary or secondary cells to be maintained over a period of time to allow experiments to be conducted. In the experiments performed in this thesis, the culture of primary adult myocytes is essential for allowing adenoviral gene transfer of FRET biosensors to take place. However, the often elevated partial pressure of oxygen to which cells in culture are exposed may affect many cellular processes. For example, the use of trypsin to help disaggregate cells has been associated with a decrease in the intracellular concentration of reduced glutathione (GSH), which protects cysteines from oxidation[156, 157]. *In vivo* partial pressures of O_2 in the deep tissues of mammals are approximately 1-10 mmHg (0.5 – 2 kPa) compared to the ≈150 mmHg (20 kPa) found in cell culture conditions due to the ambient gaseous composition of 95% air / 5% CO_2 in most incubators. This hyperoxia in turn leads to increased production of hydrogen peroxide[158]. Furthermore, the steps involved in maintaining cell culture, such as replacement of culture medium, that has been saturated with air may generate a hyperoxic stimulus to cells, which have become relatively hypoxic as O_2 has been consumed from the pre-existing culture medium. Since the effects of oxidative stress are difficult to mitigate, the use of the 'redox-dead' transgenic mouse in which the oxidation of C17 of the PKA RIα D/D is not possible, acts as a vital experimental comparator.

There are limitations to the approach employed in cardiomyocytes in examine PKA activity. In particular, the lack of specificity of the AKAR reporter both in respect to the source type of PKA (I or II) and the effects of RIα oxidation in a particular subcellular localisation, which may be missed by a reporter that is expressed, untargeted, in the cytosol. To address this limitation, a cytosolic fraction from HEK cells, expressing AKAR3ev was obtained and shown to be free from membranous contamination. Therefore, this represents a functional compartment analogous to the cytosol in whole cells. Addition of cAMP to the lysate confirmed that phosphorylation of AKAR by PKA was possible (Figure 4.6). The addition of 250μM H_2O_2 to the lysate was not associated with a change in steady-state FRET ratio that would have been consistent with increased PKA activity. These experiments do not account for a concomitant action of hydrogen peroxide on phosphatases that dephosphorylate PKA targets, i.e. opposing PKA activity, which may diminish the degree of PKA activity recorded by a FRET biosensor[80]. However, such a circumstance requires activation of two enzymes to counter-balance each other over the same time course and if this were the case would call into question the function of such an apparently futile signalling mechanism.

The premise that oxidation 'activates' the PKA holoenzyme, is in essence, that oxidation of RIα subunits reduces their affinity for the catalytic subunits of the tetramer, leaving them free to phosphorylate their targets. Therefore, a perhaps more definitive experiment would be to perform affinity-binding studies, for example with a Biacore assay[159], between RIα subunits in an oxidised or reduced form, with respect to catalytic subunits.

The oxidation of PKA RIα in response to hydrogen peroxide was first described in the 1980s[68] but its role has not been determined. Across the mammalian proteomes, cysteine residues occur with a probability of ~2.25%, which is significantly lower than would be expected by random probability alone (3.3%). In PKA RIα, the C17 and C37 residues are conserved between phyla including *Homo sapiens*, *Bos taurus* and *Caenorhabditis elegans*[49], which suggests that they play a role in PKA RIα function. However, the series of experiments presented in this chapter do not support the hypothesis that redox-dependent modification of PKA RIα constitutes a cAMP-independent activation of PKA Type I.

Chapter 5

Effects of disulphide bond formation in RIα subunits on PKA holoenzyme localisation

5.1 Introduction

The redox state of conserved cysteine residues has been implicated in the sub-cellular localisation of signalling proteins in both eukaryotes and prokaryotes[160, 161]. This represents an evolutionarily ancient signalling mechanism by which the cell can sense, and ultimately respond to its redox state. The suggestion that PKA signalling may be modulated in a cAMP-independent manner by oxidative modification of the R-subunits of PKA[77] may be explained by a change in localisation of the enzyme with respect to its modulators or targets rather than through a direct effect on the catalytic activity of the PKA Type I holoenzyme.

The redox state of PKA RIα has been implicated in a mechanism that influences localisation of the enzyme with respect to other components of the signalling cascade. Classically, PKA RII subunits are associated with discrete regions of the cell primarily through binding of the dimerization-docking domain (D/D) of the regulatory (R) subunit to A-Kinase Anchoring Proteins (AKAPs)[162]. However, it has been shown in lymphocytes that RI subunits, which are normally considered to be free within the cytosol have the potential for dynamic recruitment to subcellular locations by binding to a small number of AKAPs[45] (Chapter 1, Table 1.1). By bringing together clusters of associated proteins, AKAPs can form complexes of signalling molecules that together have specific, localised functions. For example, there are numerous isoforms of phosphodiesterase (PDE) and phosphatase which differ in their enzyme kinetics or substrate specificity, which when combined with the differing properties of PKA Type I or Type II, may give rise to a variety of permutations of the signalling complex, or signalosome.

AKAP10 (also known as Dual-specific A-kinase anchoring protein 2 or D-AKAP2), possesses the ability to bind RI or RII subunits of the PKA holoenzyme[50, 51]. PKA signalling via AKAP10 has been implicated in the balance of cell growth and differentiation[163]. Mutations in AKAP10 have been associated not only with colorectal[164] and familial breast[165] cancer but also with heart rate variability[166]. In terms of subcellular localisation, AKAP10 has been associated with mitochondria[56]. Using an *in vitro* biochemical assay, it has been shown that the conserved cysteine residue at position 17 (C17) in the RIα subunit of PKA alters the affinity of binding of this regulatory subunit for AKAP10[49]. However, whether the redox state of the cysteine is important or conversely the structural conformation induced by cysteine at this site in the peptide sequence with respect to downstream signalling has not yet been evaluated in cells.

The first aim of this part of the project was to observe whether mutations in the dimerization-docking domain (D/D) of PKA RIα were associated with changes in diffusibility of the subunit within the cell. Dual-specificity AKAPs, such as AKAP10, bind at the region directly flanked by the C17 and C37 cysteine residues. The original observation that the C17 residue of the PKA RI D/D was important for binding to AKAP10 made using a solely biochemical analysis, with no assessment of whether this observation was relevant in living cells[49]. If mutation of the C17 subunit of the D/D of the PKA RI subunit were associated with diminished binding to an AKAP, such as AKAP10, the RI subunit would be expected to be less tightly bound to a large AKAP complex and hence be more mobile, or diffusible, within the cell. Some the specificity of PKA signalling is determined by the binding of PKA to an AKAP within a signalling complex, or signalosome, in associated with other signalling mediators. The

composition of such signalosomes contributes to the kinetics and targeting of second messenger signalling in the cell. Therefore, the propensity for PKA to be bound to a particular signalosome may represent a mechanism by which different downstream targets of PKA are phosphorylated – a process that would imply classical cAMP activation of PKA but modulated by the redox state of the cell. Although such a mechanism is not related to direct modulation of PKA activity, the redistribution of PKA within a cell to different effector sites, may explain how redox modulation of the signalling cascade could influence PKA signalling in a manner consistent with the original functional experiments[77].

To test this hypothesis, the imaging technique of Fluorescence Recovery After Photo-bleaching (FRAP) has been employed to assess the mobility of GFP-tagged, exogenously expressed PKA RIα subunits and associated mutants. FRAP is a method by which the diffusibility of fluorescently tagged proteins can be inferred by measuring the recovery of fluorescence signal within a cellular region in which a light source has been used to bleached the local fluorescent protein. The more rapid the recovery of the bleached region of the cell, the more mobile and less well anchored is the tagged protein, the so-called 'initial rate of recovery' or rate constant. Furthermore, an 'immobile fraction' of trapped, bleached GFP-tagged protein can be identified, which may suggest that a protein is attached to a relatively immobile subcellular structure such as an organelle.

Mutations to conserved residues within the D/D of PKA RIα that influence binding to AKAP10 have been identified. For the purposes of this investigation, mutations at

position 17 and 24 were used[49]. These mutations allowed comparison of data observed in HeLa cells with FRAP to be compared to data from the 'redox-dead' mouse which expresses PKA RIα C17S. The H24A mutation in the RI D/D was chosen as it had been reported to have a similar effect to the C17 mutation on binding to AKAP10.

Localised, endogenous sources of hydrogen peroxide

The original observations that oxidation may lead to a cAMP-independent activation of PKA RI signalling[77] relied on the application of exogenous hydrogen peroxide (H_2O_2) to cells in order to induce disulphide bond formation between PKA RI subunits. In this situation, H_2O_2 gains entry to the cell by diffusion through aquaporin channels[144]. A limitation of this approach is that the exogenous application of H_2O_2 may exert a variety of potentially confounding effects on the assessment of cell signalling.

A number of protein kinases including PKG[72], PKC[71] and even PKA RII[155] have been associated with altered activity in response to oxidising stimuli. Apart from the modulation of kinases, H_2O_2 has been found to exert a wide variety of actions on protein structure, such as SUMOylation[167], as well as lipid structure. Such indiscriminate actions may therefore provide confounding observations depending on the relative abundance of these kinases in different cell types. Furthermore, in order to identify a physiological role of oxidative modification of PKA RI, rather than merely as a biochemical epiphenomenon, an endogenous source of H_2O_2 is needed to investigate this putative signalling mechanism in more detail. The second aim was to identify whether PKA RI disulphide bond formation could be driven by an endogenous, physiological stimulus.

Given the wide range of possible targets of oxidative modification by H_2O_2, specificity may be achieved through co-localisation of source of production and the intended target. This concept has been supported by the observation that the antioxidant peroxiredoxin (Prx1) is transiently phosphorylated near to a membrane oxidant source in response to growth factor stimulation[168]. The NADPH Oxidase (Nox) class of enzyme is the major source of receptor-induced generation of H_2O_2 in cells. In particular, Nox4 is an H_2O_2-producing oxygen sensor that reports cellular oxygen levels[169]. Nox4 differs from other Nox isoforms in that its product is H_2O_2 rather than superoxide anion ($O_2^{\cdot}$)[27] and is constitutively active without recruitment of regulatory subunits from the cytosol. Nox4 has been found to be expressed in a variety of cells, including cardiomyocytes, where the predominant subcellular localisation is in the mitochondria[21]. Nox4 has been implicated in cardiac apoptosis in the context of hypertrophic stimuli[21] as well as in the context of atrial fibrillation[170], heart failure[20] and ischaemia reperfusion injury[171, 172].

An important site of redox-modification of proteins is the mitochondria. These organelles are evolutionarily ancient structures that are thought to be derived from prokaryotes that have become incorporated symbiotically into the larger eukaryotes[173]. The vast majority of mitochondrial proteins are encoded by the nucleus of the cell and hence transport systems are necessary to allow proteins to gain entry to the organelle. Mitochondria comprise two aqueous, membrane-limited compartments, the matrix and the inter-membrane space (IMS). The localisation and functional relevance of PKA RI to mitochondria is a current controversy in the field[122]. PKA activity has been described outside mitochondria[174], in the IMS[52] and in the matrix[175]. Whether these are mutually exclusive or inter-related pathways of PKA signalling is not known. Functionally, PKA

RI has been associated with the regulation of mitochondrial dynamics and the elimination of certain reactive oxygen species. The mitochondrial E3 ligase March5 has been found to co-immunoprecipitate with PKA RI[176]. The ligase is located on the outer mitochondrial membrane and catalyses the ubiquitination of a number of proteins, including SOD1, an enzyme that catalyses the dismutation of superoxide anion $O_2^{-}\cdot$ to H_2O_2. Taken together, these observations may provide a link between mitochondrial PKA signalling and an AKAP whose binding to PKA R-subunits depends upon the cysteine residue at position 17 (C17) of the D/D of PKA RI[177].

Recently, it has been shown that PKA RI redox-dependent disulphide bond formation occurs in response to a physiological stimulus in the form of Nox4 activation in murine vascular endothelial cells[103]. Since Nox4 is found in cardiomyocytes[20], experiments were devised to identify whether known activators of Nox4 activity, such as the peptide hormones insulin[28] and Vascular Endothelial Growth Factor (VEGF)[178], can induce disulphide bond formation between RI subunits of PKA in adult mouse cardiomyocytes. Nox4 is located at mitochondria, particularly in cardiomyocytes and is an important source of intracellular H_2O_2[28]. The reported mitochondrial localisation of Nox4 and AKAP10 may then be further investigated to elucidate a potential redox-sensitive PKA RI signalling cascade with downstream effects on cell viability.

Eukaryotic organisms require extracellular signalling to survive. A variety of extracellular pathways including AKT, MAPK and JAK signalling pathways mediate these signals. The binding of growth factors to their receptors results in the activation of a series of pathways that lead to a wide variety of physiological events such as cell growth or proliferation. For example, in neonatal rats oxidative stress has been found to

induce ERK-dependent signalling cascades to promote cardiomyocyte survival[179]. Through oxidative modification of protein cysteine residues, H_2O_2 signalling may provide an important link between extracellular growth factor signals and the complex intracellular networks of growth factor signalling. In support of a possible role of oxidative modulation of PKA-signalling in cell growth and survival, it should be noted that AKAP10 also been implicated in the biology of cell growth and survival in the context of cancer[165, 180].

Vascular Endothelial Growth Factor (VEGF) is a peptide hormone that was first identified as a growth factor critical to the development of tissues such as endothelium and the endocardium. However, a role of paracrine VEGF in cardiomyocyte biology has recently been described[181] whereby upon binding cardiac VEGF receptors[178, 182], mitogen-activated protein (MAP) kinases are triggered, promoting cellular growth and survival[183]. In support of this, myocardial function has been found to be preserved by VEGF in an animal model of myocardial infarction[178].

Since the 1970s insulin has been found to stimulate the intracellular production of H_2O_2[184] in eukaryotic cells via the Nox family of enzymes[185]. Rather than being a by-product of signal transduction, H_2O_2 elicits insulinomimetic signalling actions in eukaryotic cells[186]. In particular, the Nox4 isoform of the Nox family acts as the major source of insulin-derived H_2O_2 production[24]. Although best known for its role in glucose homeostasis, insulin is a growth hormone with numerous actions in cardiomyocytes which promote cellular growth and survival[187]. However, the role played by insulin and reactive oxygen species in cardiomyocyte signalling is complex.

Conversely, insulin has been found to protect against H_2O_2-induced cardiomyocyte apoptosis or programmed cell death[188].

The third aim of this part of the project was to test the hypothesis that growth-factor dependent activation of Nox4 can lead to PKA RI oxidation. Primary cardiomyocytes from wild-type adult mice were incubated for 30 minutes with insulin and VEGF both with, and without the pharmacological inhibitor of Nox4, GKT137831[189]. By identifying physiological, endogenous stimulants of PKA RIα oxidation, a functional role for this post-translational modification may then be identified.

In summary, the aims of the experiments described in this chapter are :

1. A) Identify whether loss of C17 in the D/D of PKA RI is associated with increased diffusibility in a HeLa cell line.
   B) To identify whether the diffusibility could be modified by acute changes in redox state of the cell or the co-expression of AKAP10.

2. To identify whether known modulators of Nox4-derived H_2O_2 could alter disulphide bond formation between PKA RI subunits in adult mouse cardiomyocytes.

5.2 Methods

5.2.1 Cell culture, plasmid generation and transfection

HeLa cell cultures were prepared according to standard protocols (Chapter 2.2.1). Culture conditions comprised Dulbecco's Modified Eagle Medium (DMEM), supplemented with 10% Foetal Calf Serum with incubation in a humidified 5% CO_2 incubator set at 37°C. Passages were completed using 0.1% Trypsin (Sigma-Aldrich, USA) to prepare cells to be approximately 75% confluent for transfection. Transfection was performed using the transfection agent FuGENE HD (Promega, USA) to allow the introduction of plasmid DNA into HeLa cell lines and expression of GFP-tagged RIα subunits. In summary, plasmid DNA was mixed at a ratio of 1μg to 2μl FuGENE HD transfection reagent in serum-free DMEM. The mixture was allowed to incubate for 20 minutes and then applied to samples of HeLa cells cultured in flasks appropriate to the experiment to be performed.

In order to assess the effects of mutations within the RIα-subunit of PKA, pCDNA3-mouse PKA-RIα-mEGFP was obtained as a gift from Haining Zhong (Addgene plasmid # 45525)[114]. After amplification and Sanger sequencing (Source Bioscience, UK) to check validity of the construct, mutations were introduced using site-directed mutagenesis – see Table 5.1 below for summary of mutations and Chapter 2.3 for a full protocol describing site-directed mutagenesis. The C17S mutation was chosen to abolish the capacity of RIα to form intermolecular disulphide bonds with other RI subunits and is the same mutation as found in the 'redox-dead' mouse model. For the second mutation at position 24, histidine, a positively charged, aromatic amino acid, was replaced with alanine, a nonpolar, aliphatic amino acid in order to provide a contrast in chemical properties and is as used elsewhere in the literature[49]. AKAP10

cDNA was obtained commercially (SC324657; Origene, USA), amplified and the resulting sequence verified by Sanger sequencing (SourceBioscience, UK) using custom-designed primers.

PKA RIα Wild-type

5′ tgc gag ctc tat gtg cag aag cac aat atc cag gcc ctg aag gac tcc atc gtg cag ctg tgc 3′

PKA RIα Cys17Ser

5′ **A**gc gag ctc tat gtg cag aag cac aat atc cag gcc ctg aag gac tcc atc gtg cag ctg tgc 3′

PKA RIα His24Ala

5′ tgc gag ctc tat gtg cag aag **GC**c aat atc cag gcc ctg aag gac tcc atc gtg cag ctg tgc 3′

PKA RIα Cys17Ser; His24Ala

5′ **A**gc gag ctc tat gtg cag aag **GC**c aat atc cag gcc ctg aag gac tcc atc gtg cag ctg tgc 3′

Table 5.1 Summary of plasmid sequences of human wild-type PKA RIα and mutations that give rise to C17S; H24A and C17S:H24A mutants. Mutated bases shown in bold and capitalised.

For FRAP imaging, HeLa cells were cultured in Ibidi glass-bottomed culture dishes (80427; Ibidi, Germany), transfected as above and incubated overnight until fluorescence was clearly visible with a bench-top microscope. At this point, FRAP experiments were conducted as described in the following section.

The second use of transfected HeLa cells was for immunoblot analysis of whole cell lysates to demonstrate the effects of H_2O_2 on the formation of disulphide bonds in the PKA RIα mutants described above. These protein extracts were also used to perform

co-immunoprecipitation experiments. In order to maintain similar levels of expression between transfection wells, variability was minimised by diluting samples of prepared cDNA plasmid to reduce the effects of pipetting errors.

5.2.2 Fluorescence recovery after photo-bleaching (FRAP)

A HeLa cell line was used to express plasmids encoding PKA RIα-GFP as the relatively flat morphology of the cells made them ideal for fluorescence imaging studies. HeLa cells were cultured on specialised microscope slides (80427; Ibidi, Germany) and then transfected with PKA RI-GFP plasmids and/or AKAP10. After approximately 12 hours in culture, the cells were imaged using a confocal microscope (LSM700, Carl Zeiss Inc).

For experiments requiring H_2O_2, the dishes containing the cells were incubated with 250µM H_2O_2 for 5 minutes prior to imaging. FRAP requires the identification of a cellular region of homogeneously expressed GFP-tagged protein that is then bleached. The recovery and attainment of plateau of the fluorescence intensity was then recorded through serial image acquisition. The rate constant of fluorescence recovery was then calculated using a custom-designed algorithm (kind gift of Dr Pawel Swietach, Oxford University). These data provide a numerical description of the 'initial rate of recovery' of the fluorescence, i.e. freely diffusible GFP-tagged protein which may show differences in diffusion related to altered affinity for binding to anchoring proteins. The 'immobile fraction', i.e. GFP-tagged protein that is anchored very tightly to a relativey immobile structure such as a membrane, is measured by determining the difference in plateaux achieved by the fluorescence in the bleached spot compared to baseline before

bleaching was performed (Figure 5.1 - b). The data were then analysed using commercially available statistical software GraphPad Prism 6.07 (GraphPad Software, La Jolla California USA).

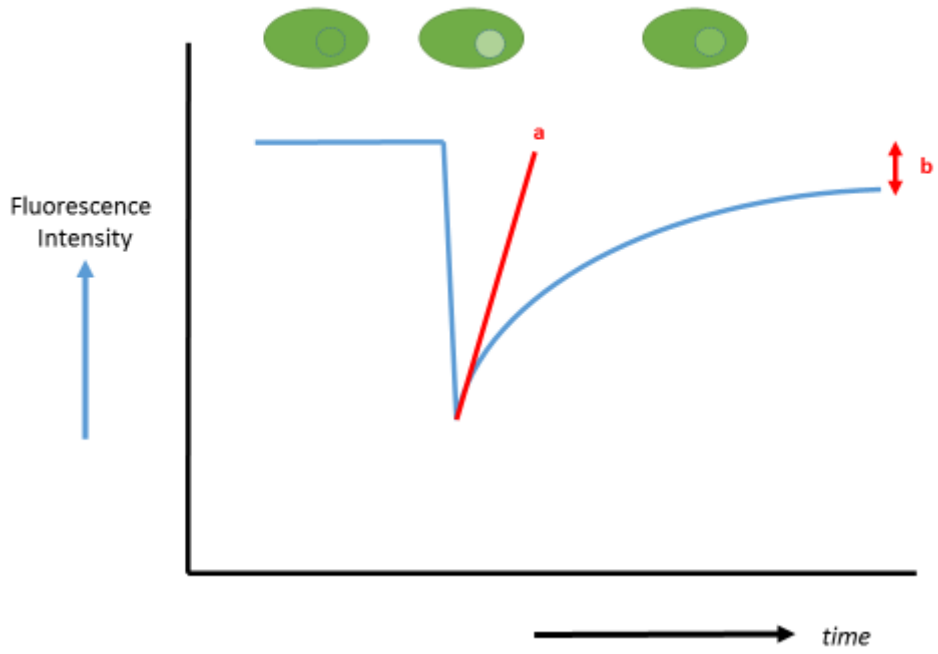


Figure 5.1 Schematic representation of a FRAP experiment showing bleaching and derivations of the mobile and immobile fractions. The blue line represents the change in fluorescence intensity in the chosen region (shown schematically in the green cells).

The rate constant of the recovery of fluorescence is represented by the gradient 'a' – representative of the 'initial rate of recovery'.

The difference between the baseline fluorescence and the fluorescence intensity at plateau after bleaching (b) represents the 'immobile fraction'.

5.2.3 Protein preparation from whole cell lysates and subcellular fractions

Whole cell lysates and cellular fractionation

Whole cell lysates from cell lineswere obtained by first washing cultured cells in sterile PBS to remove culture medium. The cells were then mechanically scraped from T25 flasks and then suspended in RIPA lysis buffer (Table 2.6) supplemented with protease and phosphatase inhibitors, for 30 minutes at 4°C on a rotating wheel. A detailed protocol describing cellular fractionation with control immunoblots is provided in Chapter 2.5.3. In summary, cells were washed in PBS and subjected to mechanical disruption with blunt-ended needles in disruption buffers of varying strength with repeated rounds of benchtop centrifugation to separate subcellular fractions (Chapter 2.5.3). Protein concentrations of whole cell lysate or fractionation samples were then determined using a protein serial dilution standard curve.

5.2.4 Immunoblotting and immunoprecipitation

Protein extraction

The effect of mutation in the D/D of the PKA RIα-GFP subunits was observed for three different mutants compared to wild-type control (Table 5.1). Therefore, four T25 flasks, comprising approximately five million cells, were each infected with equal masses of plasmid DNA as described in Chapter 2.5. After incubation, the cells were observed to have a high degree of GFP-fluorescence. The flasks of cells were washed with sterile PBS and were lysed using RIPA supplemented with protein and phosphatase inhibitors. The whole cell lysates were clarified with benchtop centrifugation to remove cellular debris and the supernatant was quantified using a benchtop spectrophotometer in comparison to a serial dilution of protein standard in a Bradford assay.

Co-immunoprecipitation

Co-immunoprecipitation of an R subunit of PKA and an AKAP has been used previously to highlight differences in binding affinity between the two proteins[166]. The rationale for the experiment was to use agarose beads coated with an anti-GFP antibody (GFP-Trap®, Chromotek, USA) to pull-down GFP-tagged RIα subunits (Wild-type and mutants) and from this lysate to probe for endogenous AKAP10 (i.e. to see if AKAP10 co-immunoprecipitates with RIα). If the affinity between AKAP10 and a GFP-tagged RIα subunit were affected by the mutations, then it may be expected that less AKAP10 would be identified in the immunoprecipitate on immunoblotting. 400µg of total protein was loaded with 20µl of GFP-antibody-tagged beads (GFP-trap, ChromoTek GmbH, Germany) and placed on a rotating mixer for four hours at 4°C. Details of the steps required to elute protein from the beads and quantify it ready for immunoblotting are described in detail in Chapter 2.6 and 2.5.2).

Immunoblotting

Protein extracts were separated by gel electrophoresis using the Invitrogen Bolt Bis-Tris system and associated pre-cast gels (4-12%) or Bio-Rad Mini-PROTEAN gels (4-20%). The reason for the use of two different systems for gel electrophoresis is for consistency of comparison between proteins analysed in non-reducing conditions. As discussed in Chapter 2.5.5, different gel chemistries can affect the generation of disulphide bonds as the protein passes through the gel. Therefore, as in previous studies that analysed the ratio of monomers and dimers between RI subunits, Bio-Rad gels were used. For proteins that were assessed in standard denaturing, reduced conditions, the Invitrogen electrophoresis and blotting system was used.

After gel electrophoresis, the proteins were transferred to PVDF membranes (GE Amersham) and blocked with 5% milk in TBST. The membranes were incubated with primary antibody for two hours at room temperature or overnight at 4°C. A primary antibody against GFP was used to identify the effects of hydrogen peroxide on the ability of the transfected RIα subunits to form disulphide bonds as shown by monomers (reduced cysteines) compared to dimers (oxidised cysteine residues that from disulphide bonds i.e. cystine). After washing with PBS-Tween, secondary antibody was applied that was raised against the host of the primary antibody. After incubation for one hour at room temperature, the membrane was washed and then incubated with an enhanced chemiluminescent reagent (GE, Amersham) for one minute. The membranes were then processed using an automated developer onto photo-sensitive film. Hard copy films were scanned using a desktop scanner and stored as TIFF images for analysis with ImageJ image processing software (National Institutes of Health, USA). As performed in previous studies[77], the ratio of monomers (reduced cysteines) to dimers (PKA RI with disulphide bonds) as measured by scanning densitometry of immunoblot bands using ImageJ software constitutes an outcome measure of PKA RIα oxidation.

5.2.5 Isolation of adult mouse myocytes and preparation for assessment of effects of endogenous growth hormones

Primary mouse cardiomyocytes were isolated from adult C57/BL6 mice using the protocol described in Chapter 2.1.1. This protocol produces a pellet of approximately one million viable cardiomyocytes with minimal contamination with fibroblasts and dead myocytes. The pellet of freshly isolated cardiomyocytes was then divided into six groups based on test conditions (Figure 5.2) and kept in micro-centrifugation tubes

agitated gently at room temperature. Treatments were added and after 30 minutes of incubation, the cells underwent bench-top centrifugation. The resultant pellet was then lysed, protein extracted and gel electrophoresis performed as described earlier.

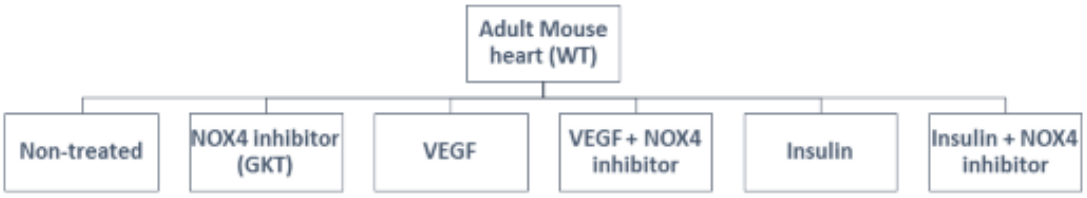


Figure 5.2 Experimental design of effects of VEGF, Insulin with and without the Nox inhibitor GKT137831

5.2.6 Growth hormones as potential drivers of endogenous H_2O_2 production

Recombinant murine Vascular Endothelial Growth Factor (VEGF) (Insight Biotechnology, UK) recombinant insulin (Sigma-Aldrich, USA) and a Nox4 inhibitor GKT137831 (Genkyotex, Switzerland) were obtained from commercial suppliers. GKT137831 is an inhibitor of NOX4/1[189] with limited effect on NOX5/2 and minimal effect on Xanthine Oxidase[190]. In experiments involving cultured cells, concentrations of up to 20µM[189, 191] have been used. Based on a review of the literature to find concentrations that had been shown to be relevant to cells from adult mouse cells, concentrations were chosen as per the following Table 5.2. An assay of hydrogen peroxide production by cells with and without the inhibitor, Gkt137831, was attempted but the kit used lack sensitivity to detect small changes in H_2O_2 production (Amplex Red Hydrogen Peroxide Assay kit, Thermofisher, USA). In order to reduce the possibility of false negative results with Gkt137831, a dose at the high end of

previously observed efficacy was chosen from published observations in the literature[189-191]. Prolonged periods of incubation over 30 minutes with the inhibitor, or growth hormones, were not possible as adult mouse cardiomyocytes have a very short survival time in culture such that 50% of myocytes may not survive a few hours, which could give rise to misleading biochemical analysis. Finally, the minor inhibition of Gkt137831 on Nox1[190], a producer of superoxide, would be expected to produce a false positive rather than a false negative result.

	Non-treated	**VEGF (Mouse)**	**Insulin**	**GKT137831**
Supplier	-	Insight Biotechnology	Sigma	Genkyotex
Concentration	-	50ng/ml[103]	50nM[28]	20μM[189, 191]
Preparation	DMSO vehicle control	DMSO solvent	DMSO solvent	DMSO solvent

Table 5.2 Summary of reaction conditions for effects Nox4 modulation on PKARIα oxidation.

The pellet of freshly isolated adult mouse cardiomyocytes was divided equally into six treatment groups : Non-treated, VEGF, VEGF + GKT137831, Insulin, Insulin + GKT137831 and GKT137831 alone (Figure 5.2). The cells were suspended in 1ml of Tyrode solution that had been supplemented with 1.4mM calcium and pH-corrected. 2μl of a 500x stock of each pharmacological condition was added, with DMSO as required for samples not involving GKT137831, which is dissolved in DMSO. The tubes containing each experimental condition were agitated at room temperature for 30 minutes. Then the samples underwent benchtop centrifugation at 1000 *g* at 4°C to form a pellet, after which cell lysis and protein extraction with supplemented RIPA lysis buffer (Table 2.6) was performed as for other whole cell lysates.

The sample size for each experimental group was calculated after five independent animals were used. Based on this variance, a final sample size of nine would give enough power to the study to identify differences in ratio of PKA RI monomer to dimer of ≈5%. Statistical analysis was then performed using commercially available statistical software GraphPad Prism 6.07 (GraphPad Software, La Jolla California USA) with One or Two-way Analysis of Variance (ANOVA) as appropriate.

5.3 Results

5.3.1 Effects of mutations in the PKA RIα D/D and exogenous H_2O_2 on the ability to form disulphide bonds between PKA RIα subunits

Using site-directed mutagenesis, plasmid constructs were generated to form the following variants of wild-type murine PKA RIα-GFP WT, H24A, C17S and C17S-H24A (double mutant). The mutations were chosen to demonstrate the necessity of the cysteine residues for disulphide bond formation. The amino acid residue at position 24 was chosen as a conserved site to assess for the effects of non-cysteine mutations on the function of the RIα subunit[49]. The H24A mutation had been found to impair binding of RIα to AKAP10 in an *in vitro* biochemical assay, to a similar degree as the C17 mutation[49]. Plasmids were expressed in a HeLa cell line and the cells were exposed to 250μM H_2O_2 for 5 minutes prior to cell lysis and protein extraction. The lysate was then quantified and underwent SDS-based gel electrophoresis in non-reducing conditions, followed by probing with anti-GFP primary antibody (Figure 5.3). The aim was to demonstrate the formation of dimeric protein in response to cellular treatment with 250μM H_2O_2. This experiment demonstrates how protein derived from PKA-RIα wild-type or with the H24A mutation forms disulphide bonds, as shown by the presence

of dimers at ≈100kDa. When the C17S mutation is introduced to either of these variants, disulphide bond formation is abolished.

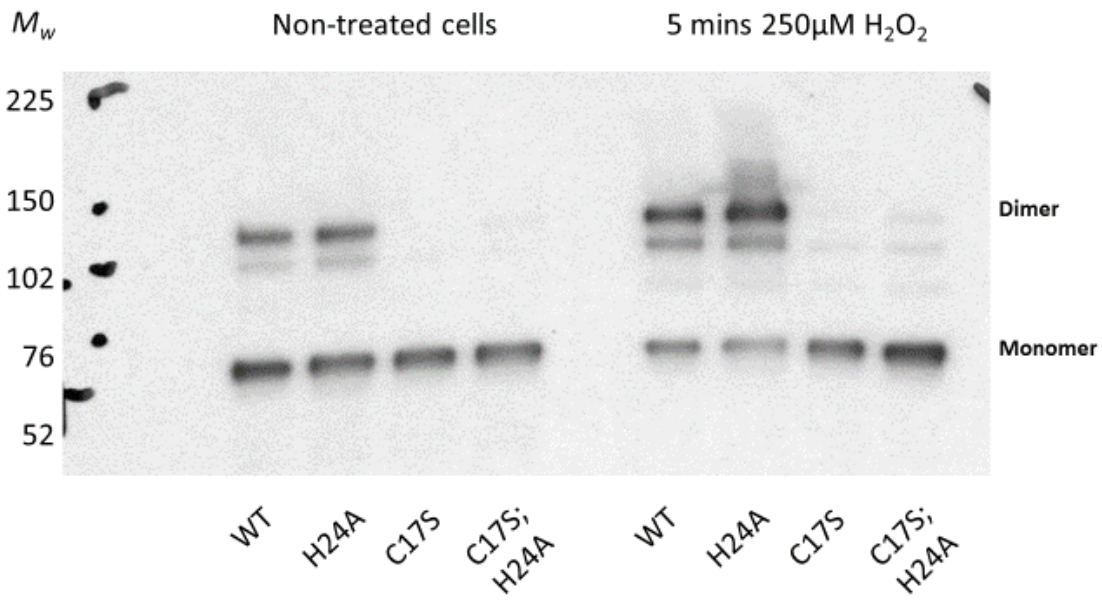


Figure 5.3 Primary antibody directed against GFP against protein from whole cell lysates from HeLa cells expressing PKA-RIα-GFP mutants. Band at ≈100kDa represents two RIα subunits bound by a disulphide bond. The bands at ≈50kDa represent monomeric PKA RIα.

Furthermore, the blot shows that there is a mixed population of proteins with and without disulphide bonds in untreated cells. The treatment of cells with five minutes of incubation with 250µM H_2O_2 drives disulphide bond formation between PKA RIα-GFP subunits as shown by the increased proportion of dimers in samples from treated cells compared to untreated cells.

5.3.2 Diffusibility of GFP-tagged RI subunits in HeLa cells as measured by Fluorescence Recovery After Photo-bleaching (FRAP)

Having validated the relevant biochemical properties of the expressed PKA RIα-GFP and its mutations, FRAP imaging experiments were performed in HeLa cells that expressed the wild-type, C17S, H24A and C17S-H24A mutants of PKARIα-GFP.

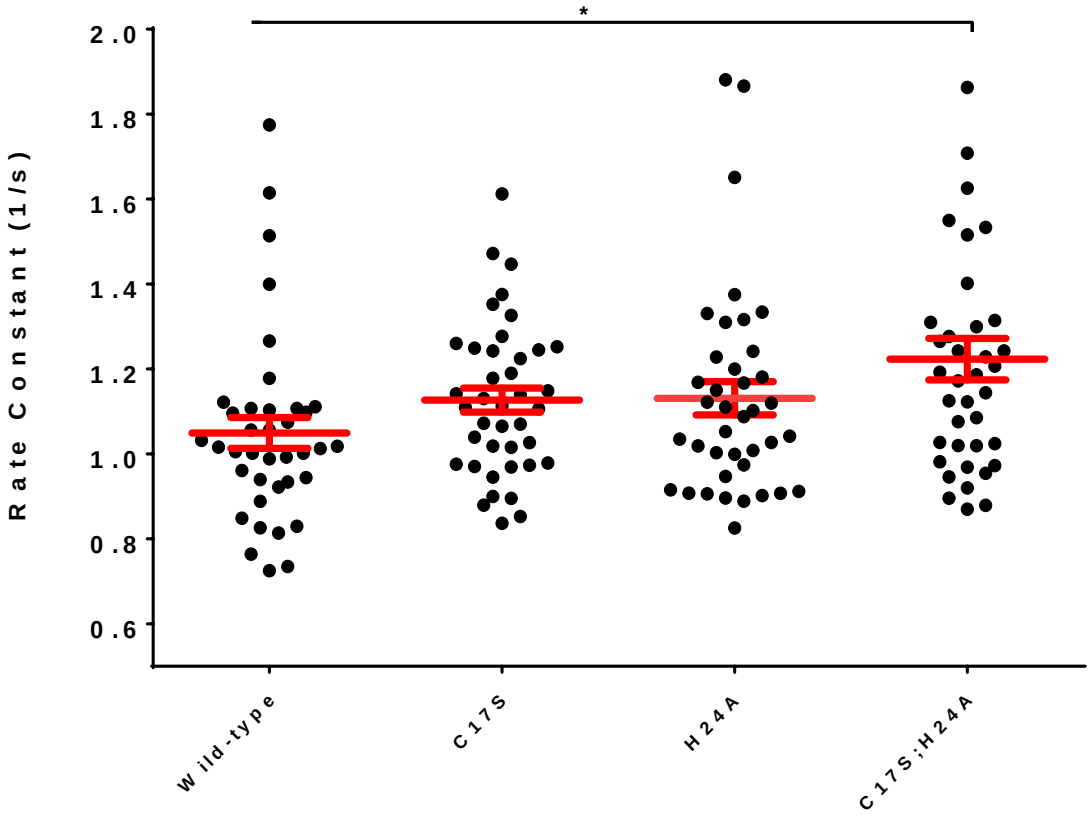


Figure 5.4 Scatter dot-plot to show rate constants for diffusibility of PKA RI-GFP constructs expressed in *n=38* HeLa cells in each group. The red lines represent the mean + SEM. One-way ANOVA was performed on the data with Tukey's *post-hoc* test for multiple-comparison, which revealed a statistically significant difference in means (*) between Wild-type and dual C17S; H24A mutations (*p=0.0216)*

The observations in Figure 5.4 showed a trend increase in rate constant for the mutant proteins compared to wild type, consistent with increased diffusibility or reduced

anchoring of RI. The effect appeared to be cumulative as the presence of both C17S and H24A mutations as the double mutant (C17S-H24A) was associated with a significant increase in rate constant compared to wild type.

To test the hypothesis that disulphide bond formation between RI subunits decreases binding affinity to anchoring proteins (AKAPs) an experiment was conducted which compared the rate constants of wild-type RI-GFP and C17S RI-GFP constructs in the absence and presence of H_2O_2 - in order to accentuate differences between RIα constructs that can and cannot form disulphide bonds (Figure 5.5).

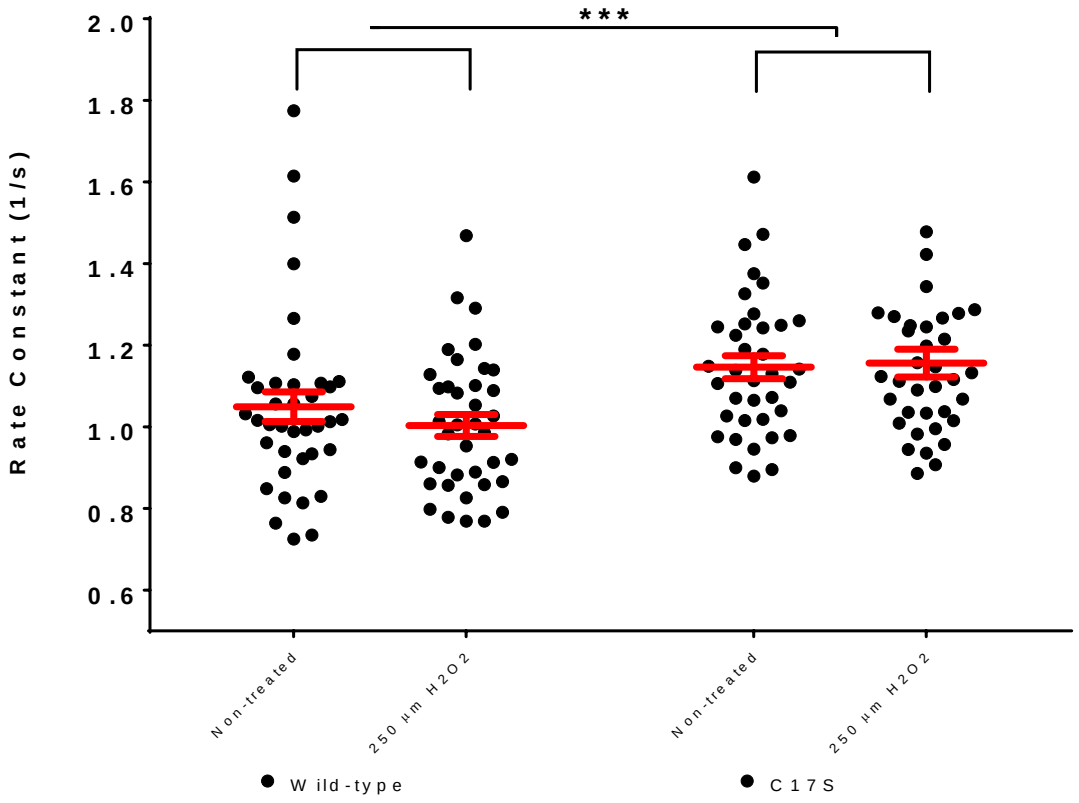


Figure 5.5 Rate-constants from *n=38* HeLa cells expressing wild-type PKA RI-GFP or C17S PKA RI-GFP that were exposed to 250µM H_2O_2 or -non-treated. The red lines represent the mean + SEM. 2-way ANOVA revealed a statistically significant difference between genotypes (*** *p=0.0002*) but no effect of treatment with hydrogen peroxide.

The data in Figure 5.5 show that the genotype with an inability to readily form disulphide bonds (C17S PKA RIα-GFP) compared to wild-type PKA RIα-GFP exhibits a significantly greater rate constant, which is consistent with more rapid diffusion and hence less anchoring.

In vitro observations have suggested that the presence of PKA RIα-subunit disulphide bonds alter the affinity of the R-subunit for the anchoring protein AKAP10[49]. The FRAP experiments have suggested very small differences in affinity in cells compared to the approximately three-fold difference in affinity described by biochemical assay. One explanation for this may be that the over-expression of PKA RIα-GFP constructs in cells saturates the available AKAP for binding, leaving a pool of mobile PKA RIα-GFP free to diffuse and mask differences in binding affinity. Therefore, an experiment was devised whereby wild-type and C17S variants of RIα-GFP were both co-expressed with AKAP10 in order to provide substrate for binding in an attempt to improve the availability of potential binding partners (Figure 5.6).

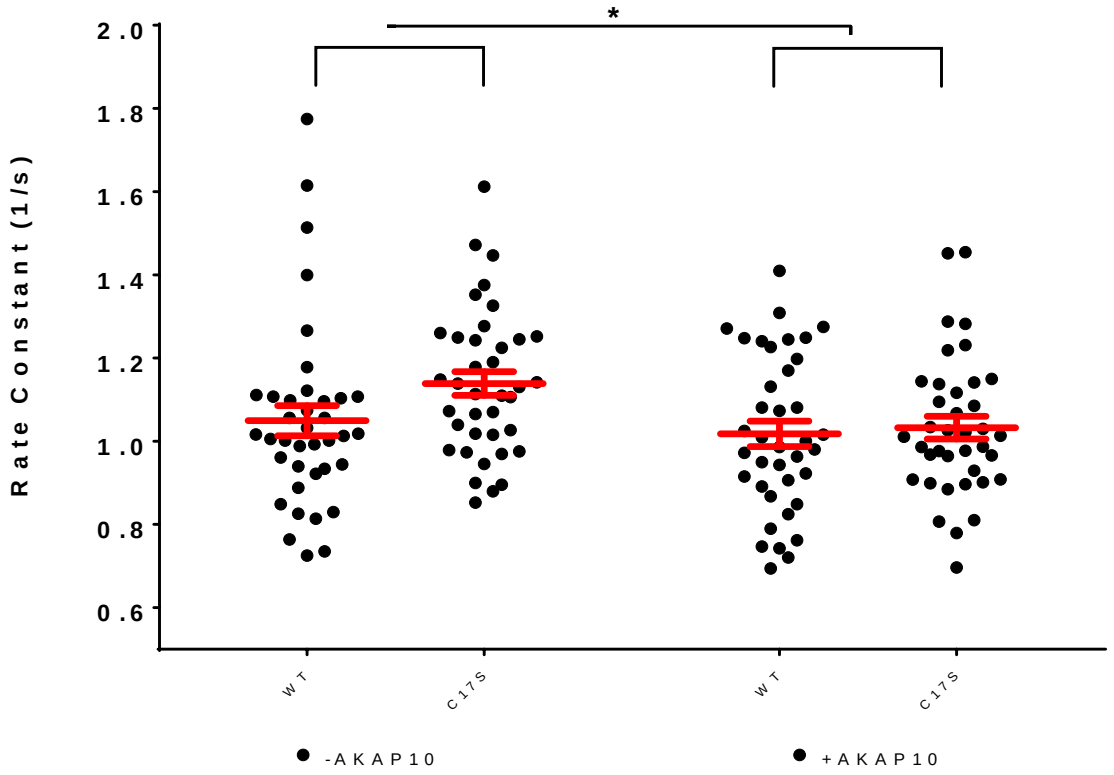


Figure 5.6 FRAP rate-constants from *n=38* HeLa cells expressing wild-type PKA RIα-GFP or C17S PKA RI-GFP. The second pair of conditions are cells in which AKAP10 is co-expressed with the PKA RIα-GFP variant. Two-way ANOVA matching for both factors revealed a statistically significant reduction in rate constant (* *p = 0.0191*) due to the presence of AKAP10 but no interaction between the C17S mutation and AKAP10. The red lines represent the mean + SEM.

The data presented in Figure 5.6 support the hypothesis that by providing substrate in the form of AKAP10, to allow binding of PKA RIα, a decrease in rate constant is observed. However, no interaction between the C17S mutation and AKAP10 was observed, which suggests that, by itself, the mutation does not affect binding to AKAP10 in these conditions. There appears to be a trend towards an increased rate constant associated with the C17S mutation, but this is not statistically significant. Finally, the rationales of the experiments in Figures 5.5 and 5.6 were combined in order to accentuate any difference in diffusibility in oxidising conditions combined with co-expression of a known potential binding partner, AKAP10.

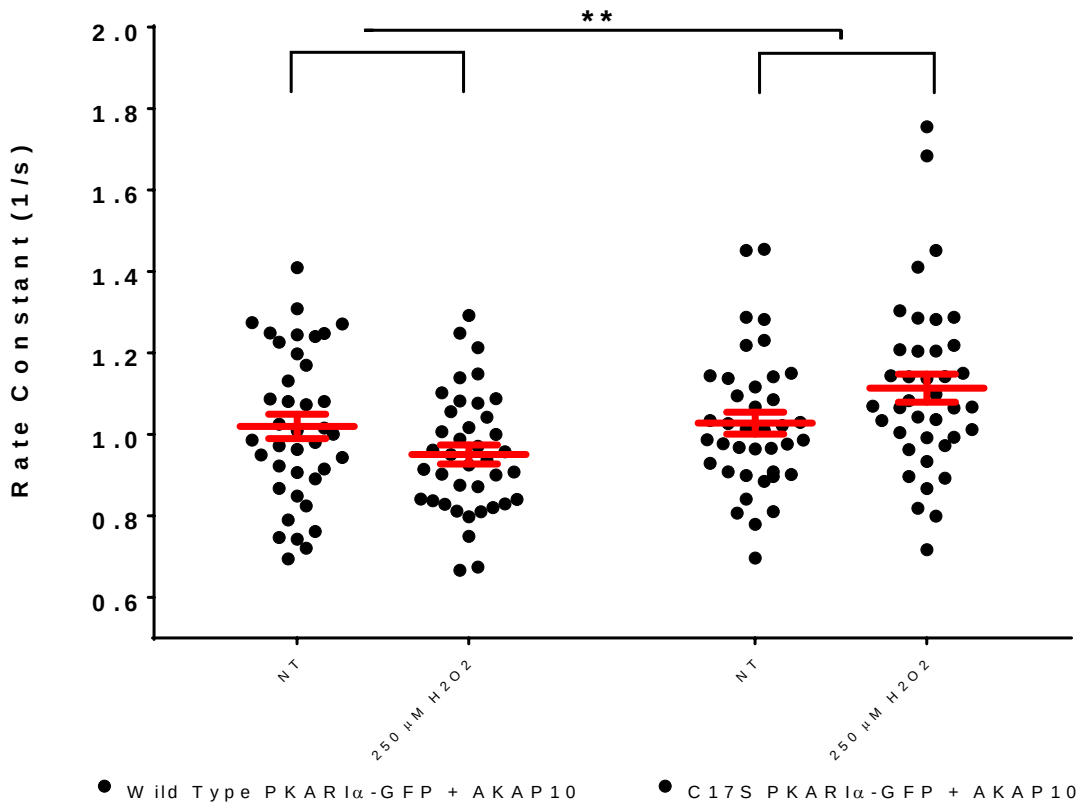


Figure 5.7 FRAP rate-constants from *n=38* HeLa cells expressing wild-type PKA RI-GFP or C17S PKA RI-GFP, both of which are co-expressed with AKAP10. The red lines represent the mean + SEM. 2-way ANOVA with Tukey's *post-hoc* correction of multiple comparisons revealed a statistically significant difference between WT vs C17S (genotype) (*p=0.0026*) and an interaction between H_2O_2 treatment and genotype *(p=0.0147)*

The data presented in Figure 5.7 are consistent with the observations made in Figure 5.5 in that the wild-type genotype, which can form disulphide bonds between RIα subunits, exhibits a slower rate constant compared to the C17S mutant that does not form disulphide bonds (*p=0.0026*). There is a statistical interaction between the effect of hydrogen peroxide treatment and the genotype *(p=0.0147)*. This interaction is consistent with the redox-sensitivity of the cysteine residues of the RIα subunit of PKA that influences mobility and, by inference, anchoring via an AKAP. This observation supports the hypothesis that the redox state of the residue is important for the

diffusibility of RI, rather than the presence of cysteine over another amino acid residue such as serine having steric effects on protein structure.

5.3.3 Anchored GFP-tagged RI subunits as determined by measurement of immobile fraction of RI-GFP after Fluorescence Recovery After Photo-bleaching.

The biological significance of the 'immobile fraction' may be interpreted as a measurement of GFP-tagged protein that is anchored to a sub-cellular structure such as a membrane or organelle that renders the protein relatively fixed. The derivation of the 'immobile fraction' is shown in Figure 5.1 and was calculated for the wild-type and three mutants of PKA RIα-GFP that have been used in this study C17S, H24A and C17S-H24A (Figure 5.8). No difference in immobile fraction and hence trapping within the cell was observed.

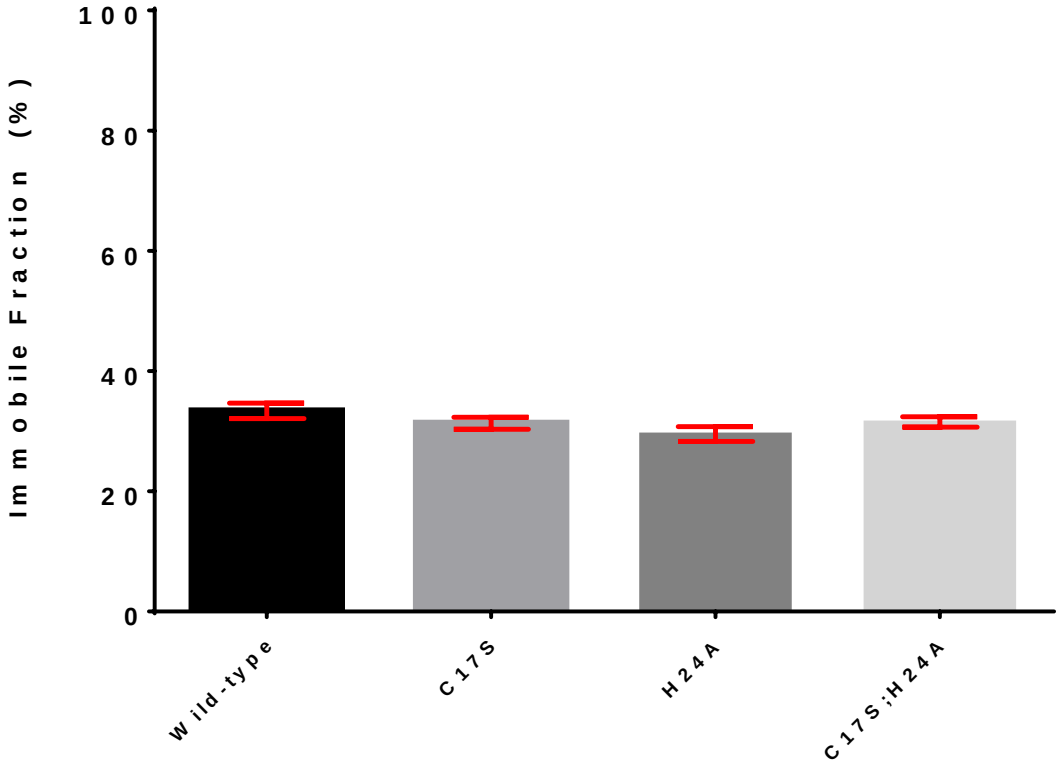


Figure 5.8 Bar chart to represent the immobile fraction found in FRAP experiments involving PKA RIα-GFP and mutants expressed in HeLa cells. *n* = 38. The red lines represent the mean + SEM. One-way ANOVA with Tukey's *post-hoc* test for multiple-comparison revealed no statistically significant difference in means.

In order to identify the effect of oxidation on the proportion of PKA RIα-GFP that becomes relatively fixed within the cell, hydrogen peroxide was added to cells that expressed wild-type PKA RIα-GFP and the C17S mutant, which is unable to form disulphide bonds between RI subunits (Figure 5.9). No difference in immobile fraction and hence trapping within the cell was observed upon treatment with hydrogen peroxide.

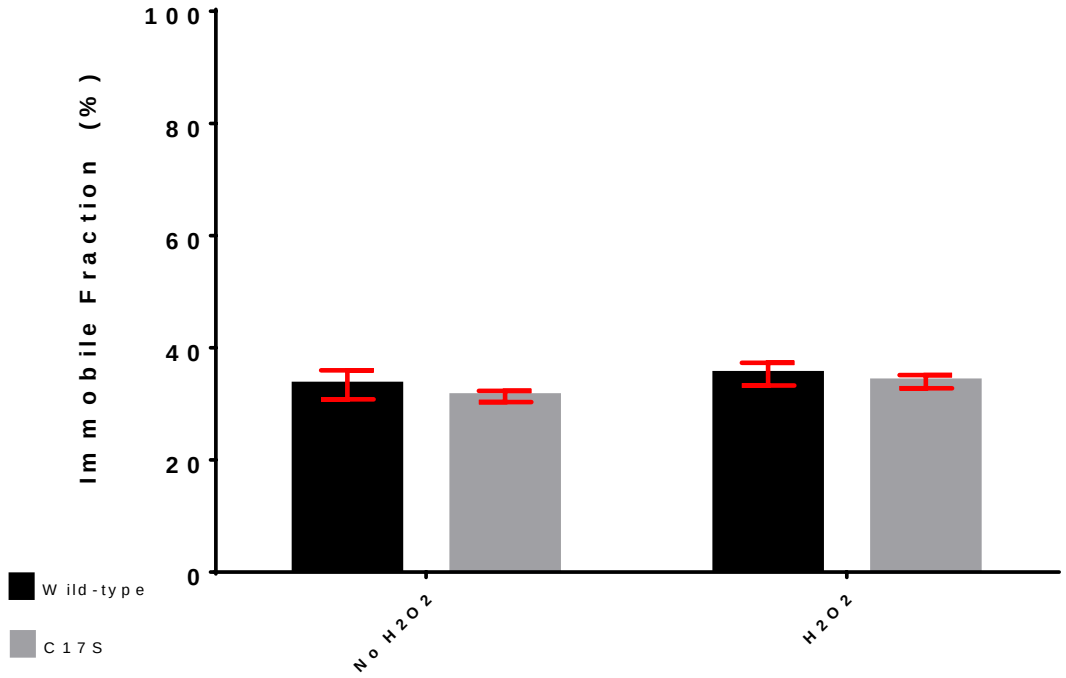


Figure 5.9 Bar chart to represent the immobile fraction found in FRAP experiments involving wild-type and C17S variants of PKA RIα-GFP expressed in HeLa cells. *n* = 38. The red lines represent the mean + SEM. One-way ANOVA Tukey's *post-hoc* test for multiple-comparison revealed no statistically significant difference in means.

Similarly, to examine the effect of increased availability of AKAP on the proportion of relatively fixed PKA RIα-GFP, AKAP10 was co-expressed with PKA RIα-GFP (wild-type and C17S mutant) (Figure 5.10). No difference in immobile fraction and hence trapping within the cell was observed.

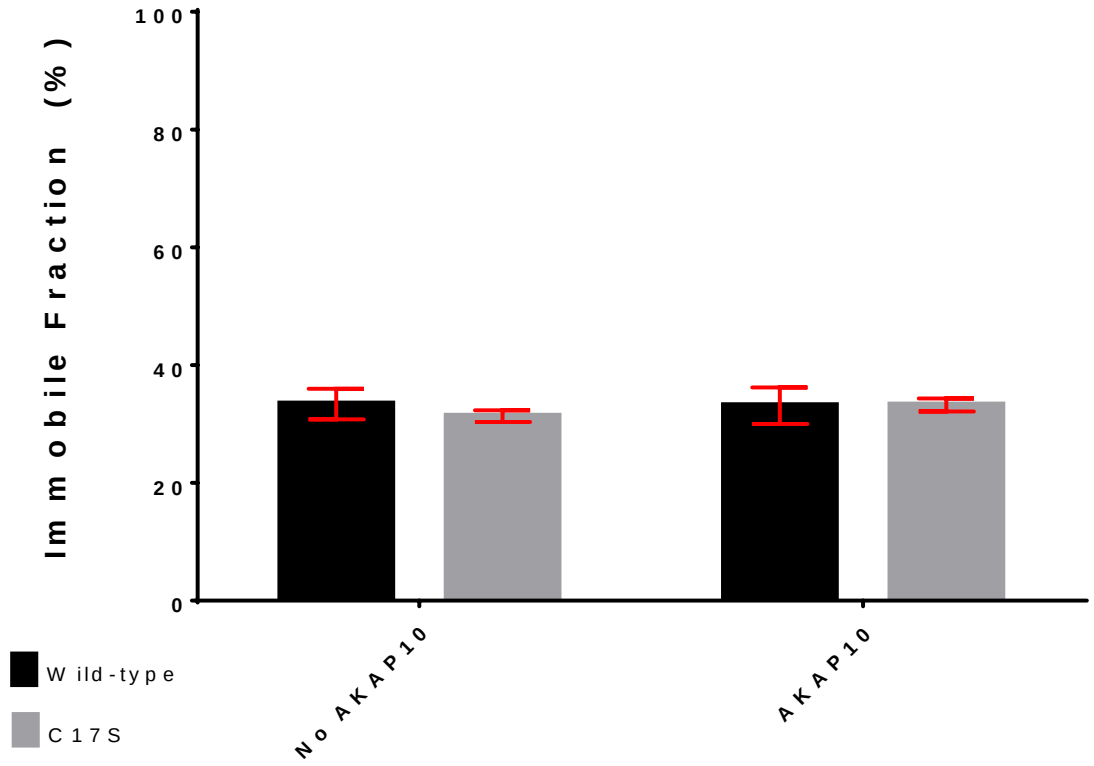


Figure 5.10 Bar chart to represent immobile fraction found in FRAP experiments involving PKA RIα-GFP and mutants and without co-expression with AKAP10 in HeLa cells. *n* = 38. The red lines represent the mean + SEM. One-way ANOVA was performed on the data with Tukey's *post-hoc* test for multiple-comparison, which revealed no statistically significant difference in means

Finally, in order to examine if there is a small, combined effect of 250μM H_2O_2 and the presence of substrate in the form of AKAP10, both wild-type and C17S variants of PKA RIα-GFP were co-expressed in HeLa cells and exposed to hydrogen peroxide before measurement of the immobile fraction (Figure 5.11). The co-expression of AKAP10 with PKA RIα-GFP was not associated with any significant change immobile fraction, which implies that the AKAP was not associated with strong anchoring, for example to a membrane, within the cell.

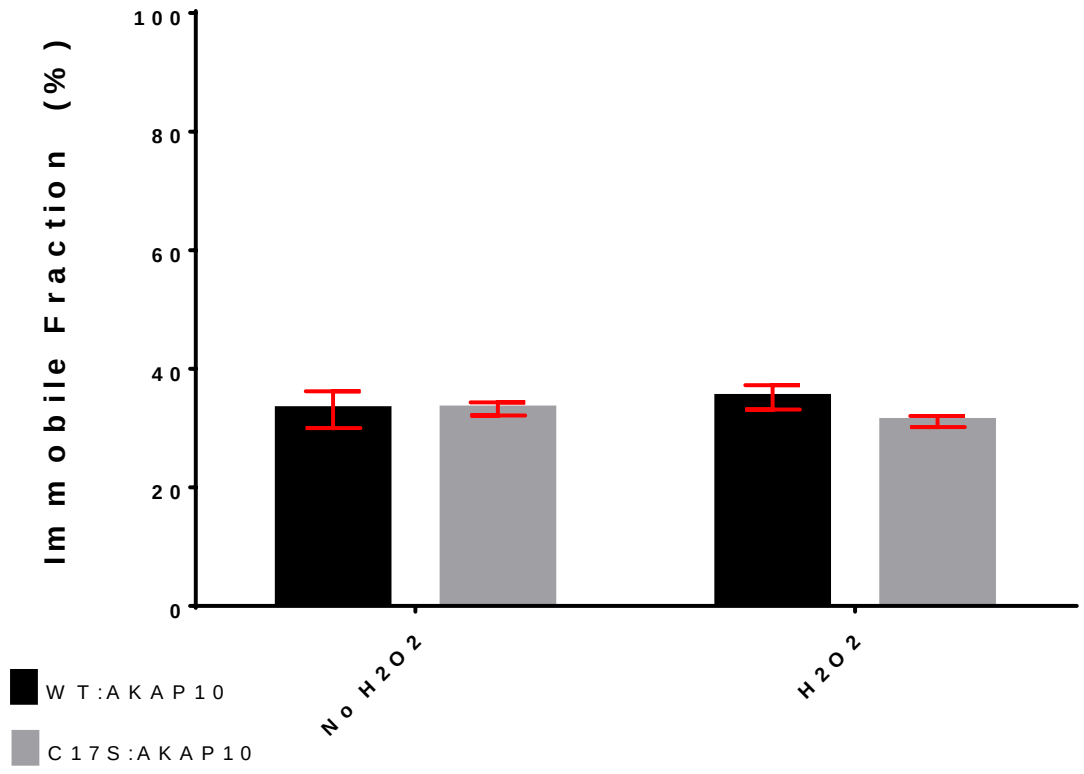


Figure 5.11 Bar chart to represent immobile fraction found in FRAP experiments involving PKA RIα-GFP and mutants co-expressed with AKAP10 and treated with H_2O_2 or control. *n* = 38. One-way ANOVA was performed on the data with Tukey's *post-hoc* test for multiple-comparison, which revealed no statistically significant difference in means. The red lines represent the mean + SEM.

5.3.4 The effects of R-subunit mutation on co-immunoprecipitation of GFP-tagged RI subunits with AKAP10

If the affinity of PKA RI for AKAPs such as AKAP10 is affected by the presence or absence of mutations of the D/D, it may be expected that the amount of AKAP10 that co-immunoprecipitates with PKA RIα depends on the primary protein structure (amino acid sequence) of the D/D. From the published biochemical observations[49] and the FRAP data described earlier in the chapter, it may be hypothesised that less AKAP10 will co-immunoprecipitate with PKA RIα-GFP mutants C17S and H24A if their affinity for AKAP10 is indeed diminished compared with wild-type PKA RIα-GFP. Such an approach has been attempted previously to investigate PKA RII:AKAP binding[166].

Therefore, immunoblots were performed on GFP pulldowns to observe whether there were changes in the relative quantity of AKAP10 pulled down in association with (co-immunoprecipitated) PKA RIα-GFP and whether this was affected by the mutated forms used in the FRAP experiments (Figure 5.12). If mutations in the D/D of PKA RIα-GFP were associated with increased mobility and by inference diminished binding to anchoring proteins such as AKAP10, less endogenous AKAP10 may be expected to co-immunoprecipitate with the PKA RIα-GFP mutants. The data suggest that AKAP10 is an important AKAP for binding to RI subunits, but the different mutations do not exhibit a preferential AKAP10-binding affinity as measured by this technique.

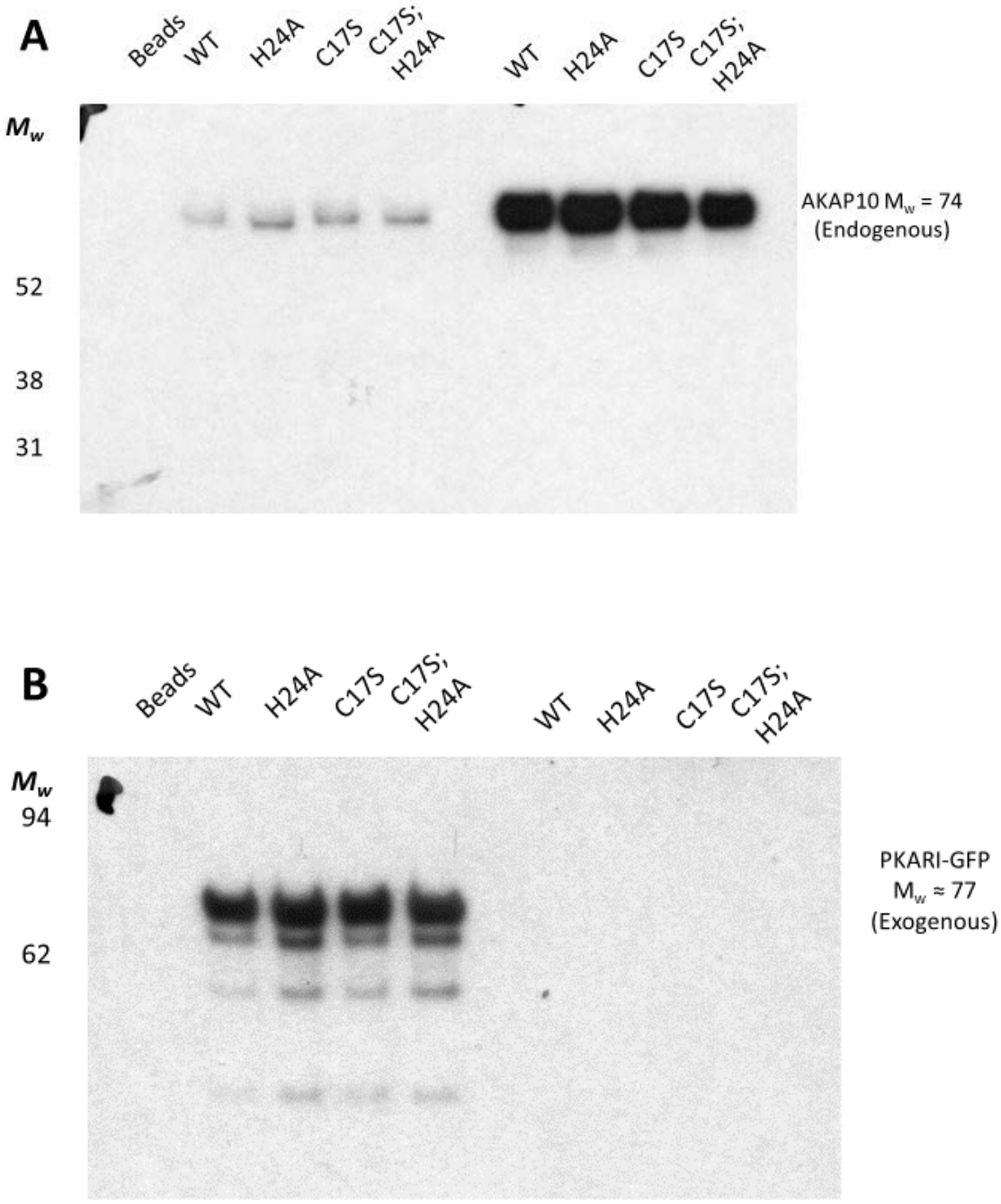


Figure 5.12 A) Immunoblot to show AKAP10 in samples after GFP-bead pull-down (left) and in whole cell lysate (right) B) Immunoblot to show GFP control, which shows even loading of GFP in each of the pull-down lanes. GFP is not shown in the whole cell lysate as the excess of GFP in the pull-down lanes meant only brief exposure was required to show those lanes unsaturated on the immunoblot. The samples are run in normal, reduced conditions as a monomer:dimer ratio was not required from the data.

5.3.5 Localisation of AKAP10 by subcellular fractionation

The data from the FRAP experiments suggested that AKAP10 did not affect the immobile fraction and hence did not appear to be relatively fixed as may be expected from a membrane-bound organelle. This observation does not support the published data that AKAP10 is membrane-bound organelle, principally to the mitochondria[56, 122]. Subcellular fractionation of HeLa cells has been used to isolate cytosolic and mitochondrial subcellular compartments. Figure 5.13A shows an immunoblot that has been probed with a cocktail of antibodies directed against the cytosolic marker, GAPDH, and the mitochondrial oxidative phosphorylation (OXPHOS) enzymes, in order to demonstrate distinct separation of these cellular fractions with respect to mitochondrial and cytosolic components. Lane 1 is a positive control lane for AKAP10 and is clear in Panel A because of the over-expression of the protein in this sample. Lane 2 shows the presence of GAPDH (M_w = 37 kDa) and Lane 3 shows the variety of specific mitochondrial enzymes (OXPHOS) – see Table 2.7. Panel B shows the heavy staining of AKAP10 in the positive control (Lane 1). A corresponding band is observed in Lane 2, but not Lane 3. From the information in Panels A and B, it can be concluded that AKAP10 can be attributed to being a mainly cytosolic AKAP, rather than mitochondrial as previously described[56].

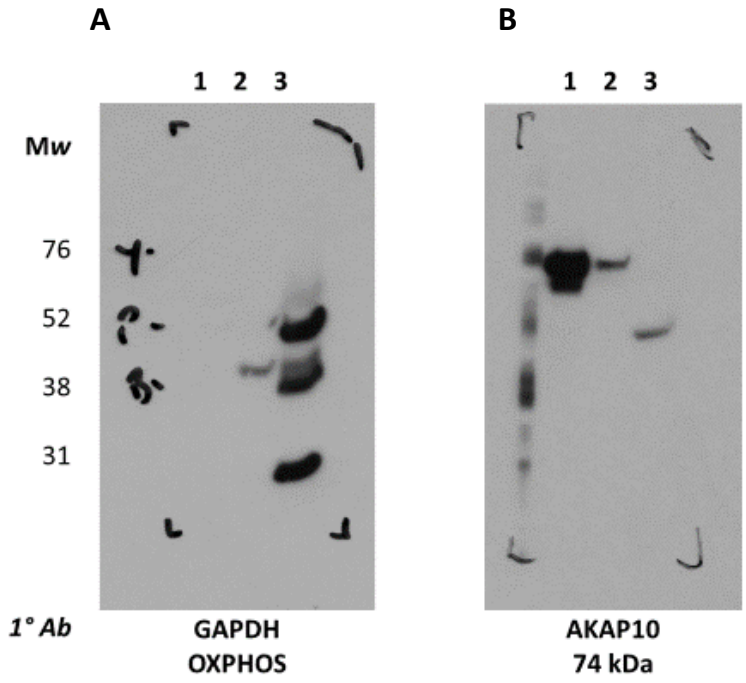


Figure 5.13 Immunoblot for AKAP10 in subcellular fractions of HeLa cells. Cytosolic and mitochondrial fractions shown by separation of GAPDH (cytosol – Lane 2) and OXPHOS (mitochondria) bands (Lane 3). Lane 1 is a positive control for AKAP10 formed from a whole cell lysate in which AKAP10 had been over-expressed.

5.3.6 Effects of Insulin, VEGF and Gkt137831 on PKA RI disulphide bond formation in adult cardiomyocytes from wild-type mice

Adult mouse cardiomyocytes were chosen as model for the subsequent series of experiments as the overall aim was to examine physiologically relevant stimuli that could drive endogenous oxidation of PKA RIα in primary cells rather than a secondary cell line. Moreover, the availability of the transgenic 'Redox-Dead' mouse with a C17S mutation in the D/D of PKA RIα, which is unable to form disulphide bonds between RIα subunits would allow further valuable examination of putative downstream pathways by providing a robust negative control. As used in previous studies[77], the ratio of dimeric (oxidised) and monomeric (reduced) bands of PKA RIα as identified by immunoblot analysis is a measure of relative PKA RIα oxidation (Figure 5.3).

A pellet of freshly isolated adult mouse cardiomyocytes from a wild-type C57/BL6 mouse was divided into six treatment groups as shown in Figure 5.14. This experimental design allowed the comparison of the effects of VEGF, insulin and the Nox4 inhibitor, Gkt137831, on endogenous PKA RIα oxidation.

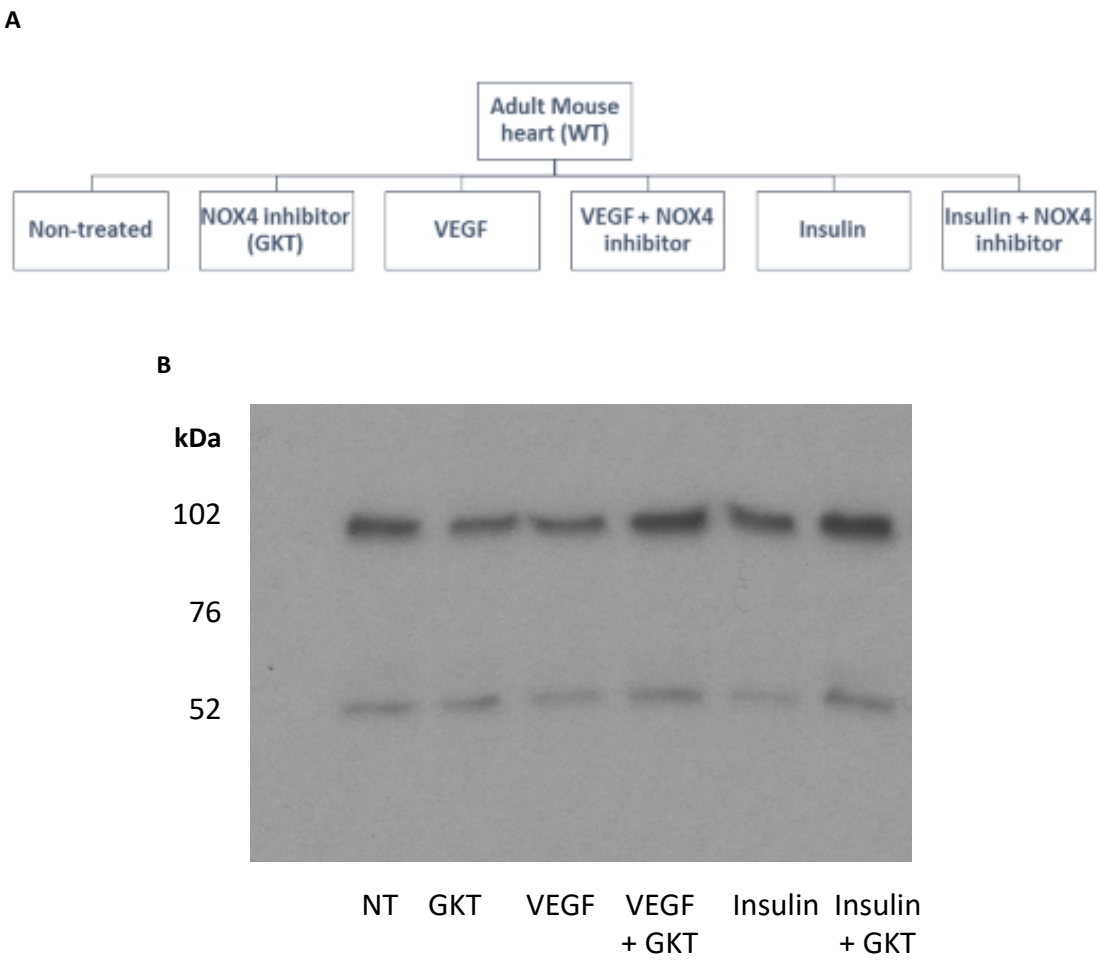


Figure 5.14 Experimental design (A) with example blot (B) of conditions tested to investigate the effects of VEGF and insulin and Nox4 inhibition on endogenous oxidation of PKA RIα. The proportion (%) of dimer (oxidised cysteine with disulphide bonds) of total dimer plus monomer (reduced with no disulphide bond) was calculated for each condition.

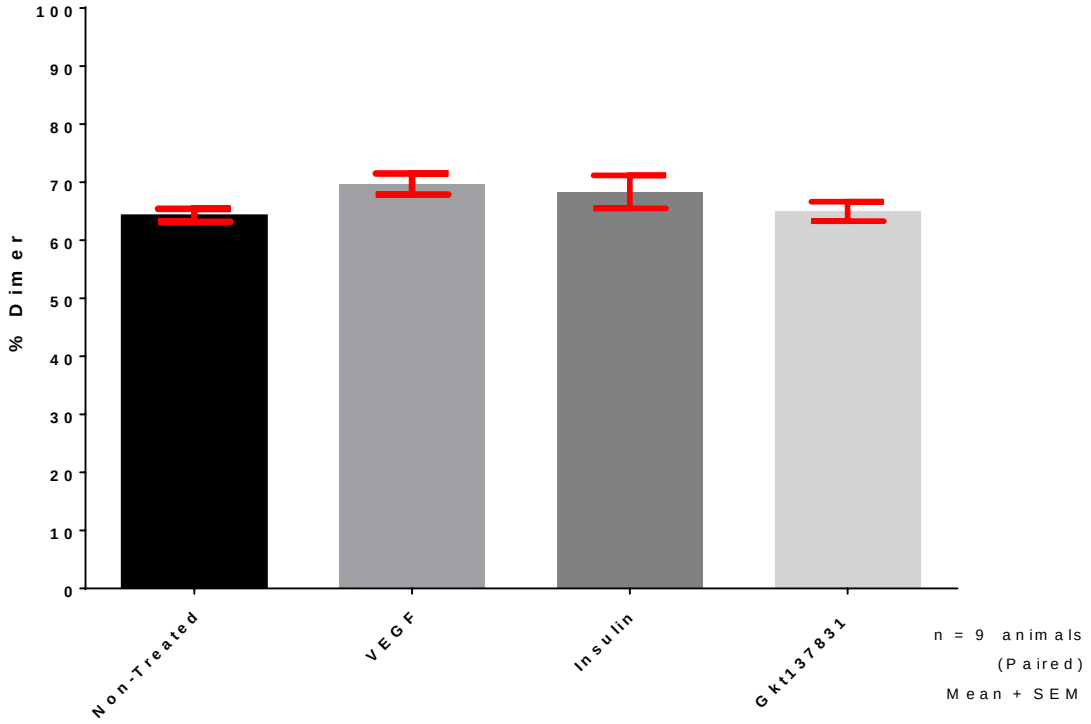


Figure 5.15 Effects of VEGF, Insulin and Gkt137831 on the formation of PKA RI disulphide bonds compared to total (expressed as a percentage of dimer of total PKA RI bands). *n* = 9 animals. The red lines represent the mean + SEM.

The data presented in Figure 5.15 do not show a statistically significant increase in oxidation of endogenous PKA RIα in cells treated with VEGF or insulin for 30 minutes compared to controls. Moreover, incubation for 30 mins with the Nox inhibitor Gkt137831, does not diminish the proportion of oxidised PKA RI compared to control. The data were analysed using a one-way Analysis of Variance (ANOVA).

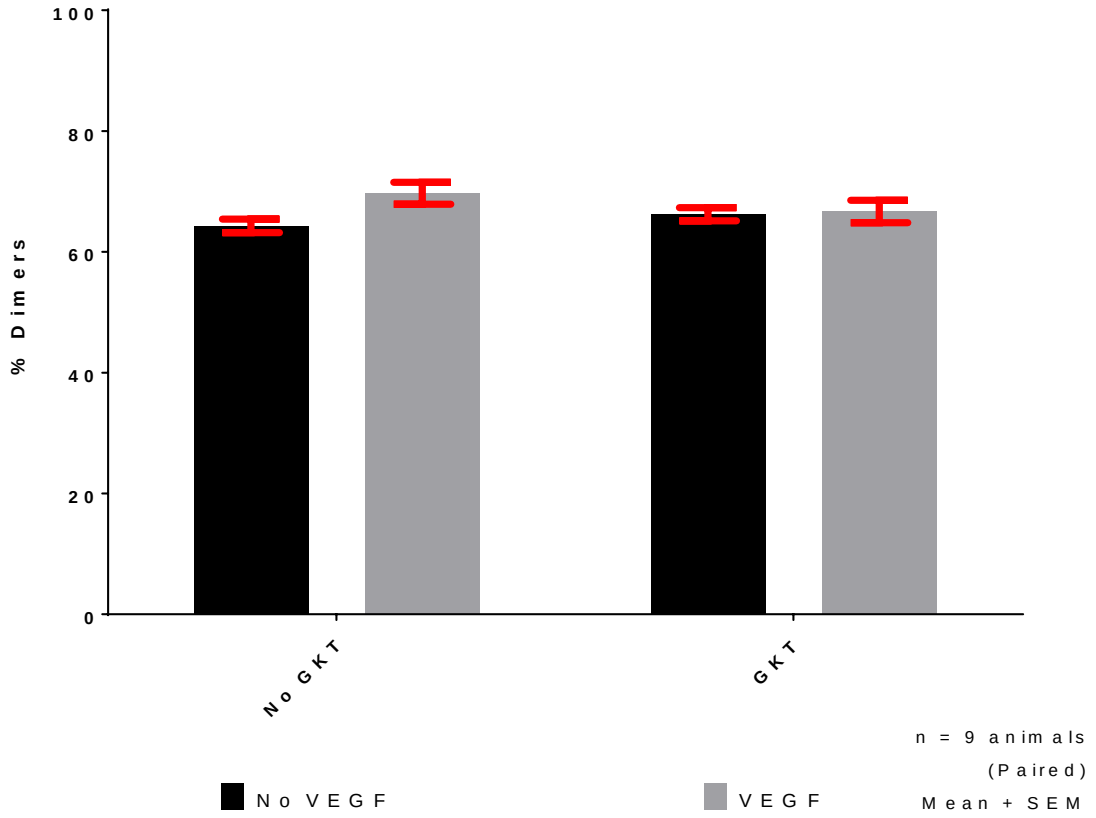


Figure 5.16 Effects of VEGF with and without Gkt137831 on PKA RIα disulphide bond formation (% total PKA as dimer) compared to control. *n* = 9 animals. The red lines represent the mean + SEM.

The data in Figure 5.16 show the mean proportion of oxidised PKA RIα with and without VEGF and the Gkt137831 Nox inhibitor. This allowed a 2x2 factorial experimental design to observe for the effects of each intervention and any possible interaction after analysis with two-way ANOVA. The data do not support an increase in PKA RIα oxidation in response to VEGF and no interaction with Gkt137831.

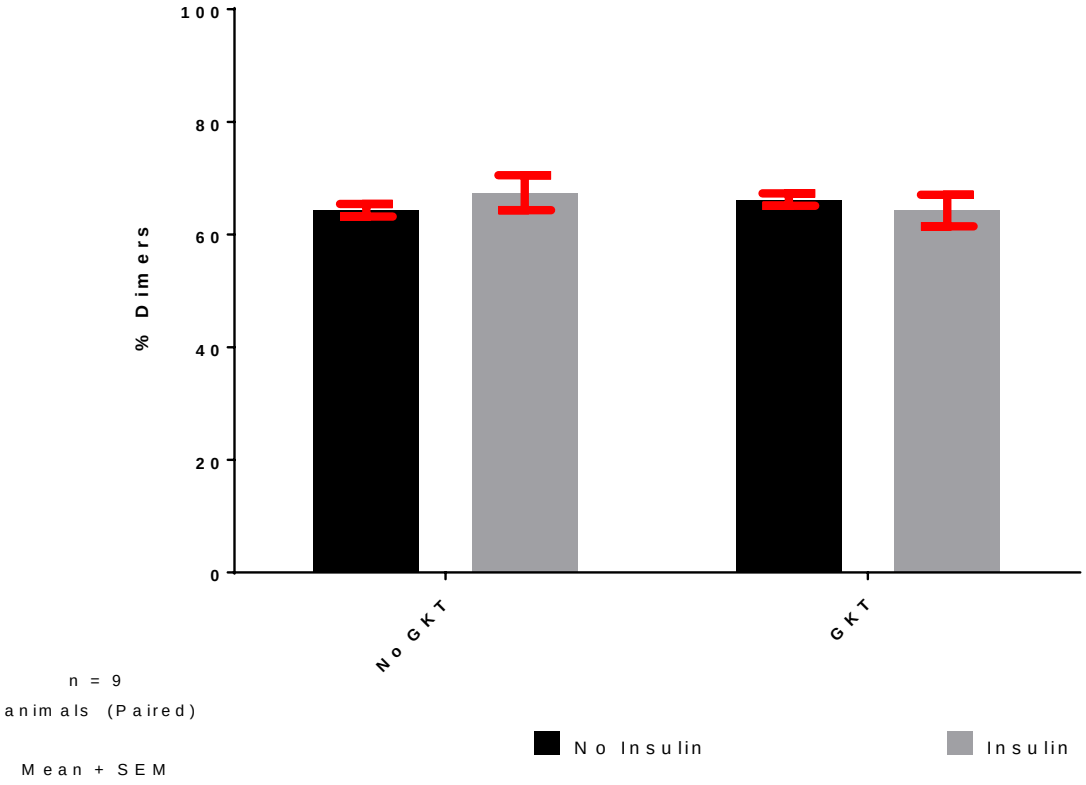


Figure 5.17 Effects of Insulin with and without Gkt137831 on PKA RI disulphide bond formation (% total PKA as dimer) compared to control. *n* = 9 animals. The red lines represent the mean + SEM.

The data in Figure 5.17 show the mean proportion of dimeric, oxidised PKA RIα with and without insulin and the Gkt137831 Nox4 inhibitor. This allowed a factorial experimental design to observe for the effects of each intervention and any possible interaction after analysis with Two-way ANOVA. The data do not support an increase in PKA RIα oxidation in response to insulin and no interaction with Gkt137831. Overall the data in Figures 5.15-5.17 do not support a role for VEGF, insulin and by extension Nox4 in signalling via PKA RIα oxidation in adult mouse cardiomyocytes.

5.4 Discussion

5.4.1 Mobility of GFP-tagged PKA RIα compared to mutants in the RI domain

The data presented in Figures 5.4 – 5.7 support the hypothesis that mutations in the dimerization and docking domain (D/D) of the RIα subunit of PKA affect the mobility of the protein within the cell, consistent with altered affinity to a binding protein such as AKAP10. The experimental approach allows an unbiased assessment of how easily the RIα-GFP subunits diffuse and whether the presence of certain mutations affects this. The first experiment (Figure 5.4) showed that in the presence of two mutations in the RIα D/D, a change in the rate constant consistent with more rapid diffusion of the GFP-tagged protein. These data can be interpreted in the context of the biochemical observations made by Sarma *et al*[49] that such mutations decrease the affinity of PKA RIα-GFP for an AKAP such as AKAP10. However, FRAP presents an unbiased measure of net diffusibility, therefore if a mutation decreased binding for one AKAP with a concomitant increase in binding for another, the net change in diffusibility may be zero – this may also explain why the changes in diffusibility are small compared to the 3-4 fold decrease in affinity observed in the biochemical analysis[49]. The original observation that PKA RIα cysteine residues modulate binding to AKAP10[49] do not refer to other RI-specific AKAPs such as AKAP149 (AKAP1 or D-AKAP1). Therefore, other anchors of Type I PKA that are modulated by disulphide bond formation between RIα subunits may be as yet undiscovered.

In order to examine whether the addition of an oxidant, to induce disulphide bond formation between PKA RIα subunits, as shown in Figure 5.3, can alter the diffusibility of PKA RI-GFP, cells expressing RI-GFP were incubated for five minutes with 250μM H_2O_2 prior to FRAP image acquisition. The data presented in Figure 5.5, when analysed

by Two-way ANOVA, reveal a genotype effect due to C17S mutation consistent with improved diffusibility, which is consistent with diminished AKAP anchoring. The ANOVA analysis in effect makes use of twice the sample size compared to that used in Figure 5.4, which allows the small effect of the single mutation of C17S has on RIα-GFP diffusibility to be identified. No effect of the application of H_2O_2 was identified. Such an effect may be too small to determine even with a large sample size, especially as Figure 5.3 shows only a comparatively small increase in disulphide bond formation from cells in culture compared to those incubated with 250μM H_2O_2 prior to protein extraction.

The expression of RIα-GFP is induced via a plasmid construct, which leads to excess production of the transfected protein. Therefore, PKA RIα-GFP diffusion may be under-estimated due to a saturation of endogenous binding proteins such as RI-binding AKAPs. Therefore, co-expression of RIα-GFP with the AKAP implicated in C17-dependent binding[49], AKAP10, was performed. It may be argued that the effect of co-expressing two plasmids rather than one may be the cause of the slower rate of diffusion. A further experiment may be to compare co-expression with a plasmid-encoded protein, that does not bind PKA RIα, rather than cells without co-expression.

Two-way ANOVA of the data presented in Figure 5.6 shows that there is a reduction in PKA RIα-GFP diffusibility in the presence of AKAP10, consistent with there being a greater binding capacity for RIα in the cell. There was no discernible effect on the C17S mutation and hence no interactive effect. An improved control, over the use of cells transfected with PKA RIα-GFP only, would have been to co-transfect the cells with a scrambled version of AKAP10. This would have controlled for the effect of co-transfection of two plasmids rather than one.

Finally, a combination of the two approaches described above was carried out such that co-expression of wild-type and C17S variants of PKA RIα-GFP with AKAP10 was performed in the presence and absence of 250μM H_2O_2 (Figure 5.7). The aim of this approach was to accentuate any difference in binding due to cysteine disulphide bond formation in the presence of adequate AKAP binding capacity. A limitation of this approach is that exogenous hydrogen peroxide may have numerous effects on the cell. Ideally, a mutation that generates constitutive cysteine disulphide bond formation, as a positive control, would have helped to resolve such confounders but this is not feasible. The data in Figure 5.7 not only show that the C17S mutation is associated with increased diffusibility, consistent with the observations made in cells without supplemental AKAP10, but also an interaction between the genotype and presence of hydrogen peroxide. This interaction may provide evidence that PKA RIα C17 oxidation status, rather than the amino acid residue *per se*, is important for PKA RIα diffusibility. These data extend the observations made by Sarma *et al*[49] not only by making supportive observations in cells, rather than just *in vitro* biochemical observations, but also by suggesting that the redox state of cysteine affects PKA RIα anchoring rather than just the structural properties of the cysteine in the tertiary and quaternary structure of the PKA RIα holoenzyme.

The initial rate of recovery, or rate constant, as measured is the most important, accurate and informative measurement of fluorescence recovery because it is concentration-independent. Therefore, it measures how quickly the unbleached fluorescent molecules moves into the bleached region of the cell. Another measurement is the ‘immobile fraction’, which describes the pool of protein that does not undergo

exchange within the bleached region of the cell. The immobile fraction may be determined by subtracting the post-bleached fluorescent intensity from the pre-bleached intensity (Figure 5.1). This measurement helps to identify what proportion of the PKA RIα-GFP is bound to relatively fixed structures such as subcellular membranes or organelles. Calculation of the immobile fractions as shown in Figures 5.8-5.11 suggest no change in the proportion of PKA RIα-GFP in fixed subcellular locations, whether through mutations in the D/D of RI, the presence of oxidising stimuli which may be expected to increase binding to AKAPs or the presence of increased quantities of AKAP10. AKAP10 has previously been described as being involved in localisation of PKA to the mitochondria[56, 122]. However, the data presented here show that in HeLa cells, AKAP10 is expressed exclusively in the cytosol (Figure 5.13). Closer examination of the original data describing the mitochondrial localisation of AKAP10[56] shows that the bands on Western blots attributed to AKAP10 are found at >100kDa compared to the expected mass of ≈70kDa – a value confirmed by the presence of a positive control generated from the AKAP10 plasmid (Figure 5.13). Therefore, the observations made from the immobile fraction of the FRAP data support the biochemical observations that AKAP10 is not bound to a membrane.

5.4.2 Relative immunoprecipitation of AKAP10 by PKA RI-GFP compared to mutations in the dimerization and docking domain of the R subunit

To test the hypothesis that the cysteine residue at position 17 (C17) in the D/D of PKA RIα is important for the binding to AKAPs such as AKAP10, immunoblot experiments were performed to see if differing amounts of AKAP10 co-immunoprecipitated with RIα-GFP that had been pulled down by agarose breads coated with an anti-GFP antibody.

The data shown in Figure 5.12 show that endogenous AKAP10 is readily bound to RIα-GFP but the effect of the mutations C17s, H24A and their combination does not show a significant difference in co-immunoprecipitation and hence binding affinity. These observations may still support the observations seen with FRAP analysis as a large number of experiments were required to observe subtle differences between the mutations with respect to diffusibility. An alternative explanation may be that the difference in diffusibility is not due to binding to AKAP10 but to another, unidentified AKAP that binds PKA RI (Table 1.1).

5.4.3 PKA RIα dimerization driven by an endogenous source of hydrogen peroxide

It has recently been described that endogenous disulphide bond formation between PKA RIα subunits could be driven by growth hormones such as VEGF and insulin acting via Nox4[103]. Such growth hormones have a multitude of actions on cells such as cardiomyocytes[178, 192], one of which is to increase the activity of Nox4[24, 28]. The link between Nox4 activity and disulphide bond formation in PKA RI homodimers has been implied by the absence of this post-translational modification in Nox4 deficient mice[103].

However, the use of a Nox4 inhibitor to suppress disulphide bond formation and conversely Nox4 over-expression to drive PKA dimerization have not been tested. The experimental design in this chapter sought to identify :

a) whether insulin and VEGF could drive disulphide bond formation in isolated adult mouse cardiomyocytes;

b) if this effect were diminished by the co-incubation with a pharmacological inhibitor of Nox4; and

c) whether basal levels of PKA RIα disulphide bond formation could be diminished in the presence of the Nox4 inhibitor.

Pilot data were used to identify an adequate sample size of nine paired animals based on the variability of the data. A factorial design permitted identification of any possible interaction between the effects of the growth hormone and the Nox4 inhibitor (Gkt137831) on the formation of disulphide bonds, as measured by immunoblots conducted in non-reducing conditions.

The data presented in Figures 5.15 reveal a trend towards increased disulphide bond formation in response to incubation with VEGF and insulin, however it is not statistically significant in a study with an adequate number of paired repeats. Further investigation of the peptide hormones in combination with the inhibitor of Nox4 (Gkt137831) did not show any effect of the hormones alone or in combination with the inhibitor. Equally, Gkt137831 did not have any effect on PKA RIα disulphide bond formation at baseline (Figure 5.15).

These data may be interpreted in a number of ways. Firstly, the effects of the growth hormones may be tissue-specific. In this chapter, adult mouse cardiomyocytes were used rather than the endothelial cells as used in the published article[103]. The conserved cysteine residue at position 17 of the D/D domain of the RI subunit (C17) is constitutively present throughout all cells. However, despite its ubiquity, it may only have a relevance in certain types of cell. For example, the original observation of an endogenous driver of PKA RIα disulphide bond formation is in endothelial cells and appears to relate to their ability to replicate in response to injury, a process which is extremely limited in terminally differentiated adult mammalian cardiomyocytes[193]. Indeed, the level of baseline dimer formation in cardiomyocytes seems to be significantly higher (Figure 4.1) compared to the published data in murine vascular endothelial cells, where dimers are all but absent at baseline[103]. Furthermore, AKAP10 has been implicated in cell growth and survival in the context of cancer, which may support the notion that PKA RI-AKAP10 binding may be of relevant to cells that can undergo division readily[164, 165, 180], rather than terminally differentiated adult cardiomyocytes.

Another interpretation of the data may be that, in the absence of a positive control, Gkt137831, (Nox4/1 inhibitor) was not efficacious in the experimental conditions used. The inhibitor has been validated both acutely *in vitro* as an assessment of Nox isoform selectivity[185]and over a number of hours in cultures of primary mammalian cells, such as pulmonary vascular cells and liver fibroblasts[189, 191]. However, the experimental design in the previously published experiments was to observe the effects of the inhibitor over a number of hours, rather than 30 minutes as in the protocol used in this study. Prolonged periods of incubation with the inhibitor were not possible as adult

mouse cardiomyocytes have a very short survival time in culture such that 50% of myocytes may not survive a few hours, which could give rise to a misleading biochemical analysis.

In summary, the experiments did not provide any evidence to support the hypothesis that insulin or VEGF could act as an endogenous driver of disulphide bond formation between PKA RI subunits in adult mouse cardiomyocytes. Equally, disulphide bond formation at baseline was not affected by the presence of the inhibitor of Nox4 activity. These data do not support the hypothesis that Nox4 can drive oxidation of cysteine residues in endogenous PKA RIα.

5.4.5 Summary

The data presented in this chapter support the hypothesis that the redox state of the cysteine residue (C17) in the D/D of PKA RIα influences the mobility of PKA RI in cells. The initial observation from FRAP imaging studies was that the C17S mutation in PKA RIα was associated with an increase in the rate constant of diffusion, which is consistent with increased mobility within the cell. Importantly, this observation was extended through the observation of an interaction between the presence of an oxidant and the mutation, which supported the view that the redox state of the cysteine residue rather than just the cysteine residue itself was important for mobility and by inference anchoring in the cell.

Mutations in the D/D of the RIα-subunit of PKA affect the diffusibility of RI in the cytosol, where, as it transpires, a binding protein, AKAP10, is found that is sensitive to RIα oxidation. This unexpected observation of AKAP10 being in the cytosol is

supported by the lack of change in immobile fraction on co-expression of AKAP10, thereby suggesting that AKAP10 itself is not firmly anchored to a membrane.

Co-immunoprecipitation of PKA RIα-GFP with AKAP10 occurs in HeLa cells but does not reveal a significant difference in affinity according to RIα-subunit D/D mutation. Such an observation may not be entirely surprising given the small differences observed with the FRAP data and as such immunoblot analysis may lack the sensitivity for such an observation.

The attempt to identify Nox4 as driver of RIα oxidation did not reveal a significant acute effect on the formation of cysteine-based disulphide bonds, either by putative drivers of Nox4 activity or conversely with a pharmacological inhibitor of Nox4. A trend consistent with previously observed data was found but the effect did not reach significance based on an apparently adequate sample size.

In summary, the role of the conserved cysteine residues in the D/D domain of the RIα subunit of PKA appears to be related to anchoring within the cells. However, endogenous drivers of PKA dimerization in adult mouse cardiomyocytes which may provide insight into the physiological relevance of this biochemical phenomenon remain unclear.

Chapter 6

Conclusions

Summary of Conclusions

The data presented constitute a thorough investigation of the effects of redox state on PKA RIα signalling; not only intrinsic catalytic potential of the enzyme but also how functional localisation within cells may be modulated by the redox state. The first main hypothesis was that oxidation of PKA RIα would lead to increased substrate phosphorylation. This hypothesis could not be supported by *in vitro* or live cell FRET experimental data in a novel use of FRET biosensors in adult mouse cardiomyocytes.

The subsequent hypothesis was that the redox state of the enzyme may influence the localisation of PKA RIα in the cell. Subtle changes in diffusibility of PKA RIα influenced by mutations were consistent with the hypothesis that the cysteine residue in question was involved in binding to cytosolic AKAPs. Furthermore, an interaction between the C17S mutation and the presence of an oxidising agent applied to the cells, suggested that the mobility, and by inference anchoring, of the RIα subunit is influenced by the redox state of the residue, rather than simply by the protein structure determined by the cysteine residue at that position. Immunoprecipitation of the GFP-tagged mutants and blotting for AKAP10 did not reveal a consistent change in degree of co-precipitation of AKAP. The finding that AKAP10 was easily pulled-down was consistent with the previous observations in the literature that this binding protein is an important RI-binding protein but that the technique of co-immunoprecipitation may not have been sufficiently sensitive to identify subtle changes in binding between mutants and AKAPs as suggested by the FRAP data.

In summary, the data presented in this thesis do not support the notion that PKA RIα can be activated directly through its oxidation that is by reducing the affinity for the

oxidised RIα subunits for the catalytic subunits. However, modulation of classical cAMP-PKA signalling by redox state of the cell may be brought about by subtle changes in the functional localisation of PKA RIα with respect to its anchoring to AKAPs, such as AKAP10, within complexes that modulate PKA signalling.

Appendices

Timing and Venue of Research

The research presented in this thesis was performed from January 2013 to January 2016 in the Departments of Physiology, Anatomy and Genetics (DPAG) and Cardiovascular Medicine (CVMED) in the University of Oxford, United Kingdom. The supervisors of the research were Professors Manuela Zaccolo (DPAG) and Barbara Casadei (CVMED).

Research Funding

The DPhil project was funded primarily by the Wellcome Trust PhD Programme in Basic Science for Clinicians. The laboratories of the supervisors were supported in the most part by the British Heart Foundation (MZ and BC) and a grant from the Garfield Weston Foundation (BC).

Publications arising out of this work

Lomas O, Brescia M, Carnicer R, Monterisi S, Surdo NC, Zaccolo M. Adenoviral transduction of FRET-based biosensors for cAMP in primary adult mouse cardiomyocytes. Methods Mol Biol. 2015;1294:103-15.

doi: 10.1007/978-1-4939-2537-7_8.

Lomas O, Zaccolo M. Phosphodiesterases maintain signaling fidelity via compartmentalization of cyclic nucleotides. Physiology (Bethesda). 2014 Mar;29(2):141-9. doi: 10.1152/physiol.00040.2013. Review.

Presentation of Work at Scientific Meetings

An improved method for the FRET-based detection of cyclic nucleotide signalling in primary adult mouse cardiomyocytes. Lomas O, Brescia M, Zaccolo M.

Cyclic Nucleotide Phosphodiesterases, Gordon Research Conference, Mount Holyoke College, Massachusetts USA, 1 - 6 June 2014

References

1. Gerschman, R., et al., *Oxygen poisoning and x-irradiation: a mechanism in common.* Science, 1954. **119**(3097): p. 623-6.

2. Sies, H., *1 - Oxidative Stress: Introductory Remarks*, in *Oxidative Stress*, H. Sies, Editor. 1985, Academic Press: London. p. 1-8.

3. Watson, J.D., *Type 2 diabetes as a redox disease.* Lancet, 2014. **383**(9919): p. 841-3.

4. Ungvari, Z., et al., *Role of oxidative-nitrosative stress and downstream pathways in various forms of cardiomyopathy and heart failure.* Curr Vasc Pharmacol, 2005. **3**(3): p. 221-9.

5. Manda, G., et al., *The redox biology network in cancer pathophysiology and therapeutics.* Redox Biol, 2015. **5**: p. 347-357.

6. Donato, A.J., et al., *Direct evidence of endothelial oxidative stress with aging in humans: relation to impaired endothelium-dependent dilation and upregulation of nuclear factor-kappaB.* Circ Res, 2007. **100**(11): p. 1659-66.

7. Schippers, J.H., et al., *ROS homeostasis during development: an evolutionary conserved strategy.* Cell Mol Life Sci, 2012. **69**(19): p. 3245-57.

8. Brooks, D.J., et al., *Evolution of amino acid frequencies in proteins over deep time: inferred order of introduction of amino acids into the genetic code.* Mol Biol Evol, 2002. **19**(10): p. 1645-55.

9. Marino, S.M. and V.N. Gladyshev, *Cysteine function governs its conservation and degeneration and restricts its utilization on protein surfaces.* J Mol Biol, 2010. **404**(5): p. 902-16.

10. Wong, J.W., S.Y. Ho, and P.J. Hogg, *Disulfide bond acquisition through eukaryotic protein evolution.* Mol Biol Evol, 2011. **28**(1): p. 327-34.

11. Holmgren, A., et al., *Thiol redox control via thioredoxin and glutaredoxin systems.* Biochem Soc Trans, 2005. **33**(Pt 6): p. 1375-7.

12. Bardwell, J.C., K. McGovern, and J. Beckwith, *Identification of a protein required for disulfide bond formation in vivo.* Cell, 1991. **67**(3): p. 581-9.

13. Zheng, M., F. Aslund, and G. Storz, *Activation of the OxyR transcription factor by reversible disulfide bond formation.* Science, 1998. **279**(5357): p. 1718-21.

14. Rolfe, D.F. and G.C. Brown, *Cellular energy utilization and molecular origin of standard metabolic rate in mammals.* Physiol Rev, 1997. **77**(3): p. 731-58.

15. Boveris, A. and B. Chance, *The mitochondrial generation of hydrogen peroxide. General properties and effect of hyperbaric oxygen.* Biochem J, 1973. **134**(3): p. 707-16.

16. Ide, T., et al., *Mitochondrial electron transport complex I is a potential source of oxygen free radicals in the failing myocardium.* Circulation Research, 1999. **85**(4): p. 357-363.

17. Ishii, H., et al., *Dopamine metabolism and free-radical related mitochondrial injury during transient brain ischemia in gerbils.* Neurochem Res, 1993. **18**(11): p. 1193-201.

18. Starkov, A.A., et al., *Mitochondrial alpha-ketoglutarate dehydrogenase complex generates reactive oxygen species.* J Neurosci, 2004. **24**(36): p. 7779-88.

19. Bendall, J.K., et al., *Pivotal role of a gp91(phox)-containing NADPH oxidase in angiotensin II-induced cardiac hypertrophy in mice.* Circulation, 2002. **105**(3): p. 293-6.

20. Kuroda, J., et al., *NADPH oxidase 4 (Nox4) is a major source of oxidative stress in the failing heart.* Proc Natl Acad Sci U S A, 2010. **107**(35): p. 15565-70.

21. Ago, T., et al., *Upregulation of Nox4 by hypertrophic stimuli promotes apoptosis and mitochondrial dysfunction in cardiac myocytes.* Circ Res, 2010. **106**(7): p. 1253-64.

22. Ushio-Fukai, M., *VEGF signaling through NADPH oxidase-derived ROS.* Antioxid Redox Signal, 2007. **9**(6): p. 731-9.

23. Yeh, Y.H., et al., *Transforming growth factor-beta and oxidative stress mediate tachycardia-induced cellular remodelling in cultured atrial-derived myocytes.* Cardiovasc Res, 2011. **91**(1): p. 62-70.

24. Mahadev, K., et al., *The NAD(P)H oxidase homolog Nox4 modulates insulin-stimulated generation of H2O2 and plays an integral role in insulin signal transduction.* Mol Cell Biol, 2004. **24**(5): p. 1844-54.

25. Shiose, A., et al., *A novel superoxide-producing NAD(P)H oxidase in kidney.* J Biol Chem, 2001. **276**(2): p. 1417-23.

26. Zhao, Q.D., et al., *NADPH oxidase 4 induces cardiac fibrosis and hypertrophy through activating Akt/mTOR and NFkappaB signaling pathways.* Circulation, 2015. **131**(7): p. 643-55.

27. Dikalov, S.I., et al., *Distinct roles of Nox1 and Nox4 in basal and angiotensin II-stimulated superoxide and hydrogen peroxide production.* Free Radic Biol Med, 2008. **45**(9): p. 1340-51.

28. Anilkumar, N., et al., *Nox4 and nox2 NADPH oxidases mediate distinct cellular redox signaling responses to agonist stimulation.* Arterioscler Thromb Vasc Biol, 2008. **28**(7): p. 1347-54.

29. Kosower, N.S., et al., *Diamide, a new reagent for the intracellular oxidation of glutathione to the disulfide.* Biochemical and Biophysical Research Communications, 1969. **37**(4): p. 593-596.

30. Tsien, R.W., *Cyclic AMP and contractile activity in heart.* Adv Cyclic Nucleotide Res, 1977. **8**: p. 363-420.

31. Miki, N., et al., *Purification and properties of the light-activated cyclic nucleotide phosphodiesterase of rod outer segments.* J Biol Chem, 1975. **250**(16): p. 6320-7.

32. Northrop, G. and R.E. Parks, Jr., *3', 5'-Amp-Induced Hyperglycemia in Intact Rats and in the Isolated Perfused Rat Liver.* Biochem Pharmacol, 1964. **13**: p. 120-3.

33. Knighton, D.R., et al., *Crystal structure of the catalytic subunit of cyclic adenosine monophosphate-dependent protein kinase.* Science, 1991. **253**(5018): p. 407-414.

34. Keshwani, M.M., et al., *Cotranslational cis-phosphorylation of the COOH-terminal tail is a key priming step in the maturation of cAMP-dependent protein kinase.* Proc Natl Acad Sci U S A, 2012. **109**(20): p. E1221-9.

35. Taylor, S.S., J.A. Buechler, and W. Yonemoto, *cAMP-dependent protein kinase: framework for a diverse family of regulatory enzymes.* Annu Rev Biochem, 1990. **59**: p. 971-1005.

36. Ashby, C.D. and D.A. Walsh, *Characterization of the interaction of a protein inhibitor with adenosine 3',5'-monophosphate-dependent protein kinases. I. Interaction with the catalytic subunit of the protein kinase.* J Biol Chem, 1972. **247**(20): p. 6637-42.

37. Ashby, C.D. and D.A. Walsh, *Characterization of the interaction of a protein inhibitor with adenosine 3',5'-monophosphate-dependent protein kinases. II. Mechanism of action with the holoenzyme.* J Biol Chem, 1973. **248**(4): p. 1255-61.

38. Ingebritsen, T.S. and P. Cohen, *Protein phosphatases: properties and role in cellular regulation.* Science, 1983. **221**(4608): p. 331-8.

39. Francis, S.H. and J.D. Corbin, *Structure and function of cyclic nucleotide-dependent protein kinases.* Annu Rev Physiol, 1994. **56**: p. 237-72.

40. Taylor, S.S., et al., *PKA: lessons learned after twenty years.* Biochim Biophys Acta, 2013. **1834**(7): p. 1271-8.

41. Brunton, L.L., J.S. Hayes, and S.E. Mayer, *Functional compartmentation of cyclic AMP and protein kinase in heart.* Adv Cyclic Nucleotide Res, 1981. **14**: p. 391-7.

42. Brunton, L.L., J.S. Hayes, and S.E. Mayer, *Hormonally specific phosphorylation of cardiac troponin I and activation of glycogen phosphorylase.* Nature, 1979. **280**(5717): p. 78-80.

43. Imaizumi-Scherrer, T., et al., *Type I protein kinase a is localized to interphase microtubules and strongly associated with the mitotic spindle.* Exp Cell Res, 2001. **264**(2): p. 250-65.

44. Imaizumi-Scherrer, T., et al., *Accumulation in fetal muscle and localization to the neuromuscular junction of cAMP-dependent protein kinase A regulatory and catalytic subunits RI alpha and C alpha.* The Journal of cell biology, 1996. **134**(5): p. 1241-1254.

45. Skalhegg, B.S., et al., *Location of cAMP-dependent protein kinase type I with the TCR-CD3 complex.* Science, 1994. **263**(5143): p. 84-7.

46. Pidoux, G. and K. Tasken, *Specificity and spatial dynamics of protein kinase A signaling organized by A-kinase-anchoring proteins.* J Mol Endocrinol, 2010. **44**(5): p. 271-84.

47. Klauck, T.M., et al., *Coordination of three signaling enzymes by AKAP79, a mammalian scaffold protein.* Science, 1996. **271**(5255): p. 1589-92.

48. Lomas, O. and M. Zaccolo, *Phosphodiesterases Maintain Signaling Fidelity via Compartmentalization of Cyclic Nucleotides.* Physiology (Bethesda), 2014. **29**(2): p. 141-9.

49. Sarma, G.N., et al., *Structure of D-AKAP2:PKA RI complex: insights into AKAP specificity and selectivity.* Structure (London, England : 1993), 2010. **18**(2): p. 155-166.

50. Huang, L.J., et al., *Identification of a novel protein kinase A anchoring protein that binds both type I and type II regulatory subunits.* The Journal of biological chemistry, 1997. **272**(12): p. 8057-8064.

51. Huang, L.J., et al., *D-AKAP2, a novel protein kinase A anchoring protein with a putative RGS domain.* Proc Natl Acad Sci U S A, 1997. **94**(21): p. 11184-9.

52. Means, C.K., et al., *An entirely specific type I A-kinase anchoring protein that can sequester two molecules of protein kinase A at mitochondria.* Proc Natl Acad Sci U S A, 2011. **108**(48): p. E1227-35.

53. Kovanich, D., et al., *Sphingosine kinase interacting protein is an A-kinase anchoring protein specific for type I cAMP-dependent protein kinase.* Chembiochem, 2010. **11**(7): p. 963-71.

54. Burgers, P.P., et al., *A small novel A-kinase anchoring protein (AKAP) that localizes specifically protein kinase A-regulatory subunit I (PKA-RI) to the plasma membrane.* J Biol Chem, 2012. **287**(52): p. 43789-97.

55. Brown, R.L., et al., *AKAP7γ is a nuclear RI-binding AKAP.* Biochemical and Biophysical Research Communications, 2003. **306**(2): p. 394-401.

56. Wang, L., et al., *Cloning and mitochondrial localization of full-length D-AKAP2, a protein kinase A anchoring protein.* Proc Natl Acad Sci U S A, 2001. **98**(6): p. 3220-5.

57. Reinton, N., et al., *Localization of a novel human A-kinase-anchoring protein, hAKAP220, during spermatogenesis.* Dev Biol, 2000. **223**(1): p. 194-204.

58. Deming, P.B., et al., *Anchoring of protein kinase A by ERM (ezrin-radixin-moesin) proteins is required for proper netrin signaling through DCC (deleted in colorectal cancer).* J Biol Chem, 2015. **290**(9): p. 5783-96.

59. Aye, T.T., et al., *Selectivity in enrichment of cAMP-dependent protein kinase regulatory subunits type I and type II and their interactors using modified cAMP affinity resins.* Mol Cell Proteomics, 2009. **8**(5): p. 1016-28.

60. Amieux, P.S., et al., *Compensatory regulation of RIalpha protein levels in protein kinase A mutant mice.* J Biol Chem, 1997. **272**(7): p. 3993-8.

61. Veugelers, M., et al., *Comparative PRKAR1A genotype-phenotype analyses in humans with Carney complex and prkar1a haploinsufficient mice.* Proc Natl Acad Sci U S A, 2004. **101**(39): p. 14222-7.

62. Correa, R., P. Salpea, and C.A. Stratakis, *Carney complex: an update.* European Journal of Endocrinology, 2015. **173**(4): p. M85-M97.

63. Mantovani, G., et al., *Different expression of protein kinase A (PKA) regulatory subunits in cortisol-secreting adrenocortical tumors: relationship with cell proliferation.* Exp Cell Res, 2008. **314**(1): p. 123-30.

64. Miller, W.R., *Regulatory subunits of PKA and breast cancer.* Ann N Y Acad Sci, 2002. **968**: p. 37-48.

65. Bradbury, A.W., et al., *Protein kinase A (PK-A) regulatory subunit expression in colorectal cancer and related mucosa.* Br J Cancer, 1994. **69**(4): p. 738-42.

66. Mantovani, G., et al., *High expression of PKA regulatory subunit 1A protein is related to proliferation of human melanoma cells.* Oncogene, 2008. **27**(13): p. 1834-43.

67. Tortora, G., et al., *Differential effects of protein kinase A sub-units on Chinese-hamster-ovary cell cycle and proliferation.* Int J Cancer, 1994. **59**(5): p. 712-6.

68. Bubis, J., T.S. Vedvick, and S.S. Taylor, *Antiparallel alignment of the two protomers of the regulatory subunit dimer of cAMP-dependent protein kinase I.* J Biol Chem, 1987. **262**(31): p. 14961-6.

69. Titani, K., et al., *Amino acid sequence of the regulatory subunit of bovine type I adenosine cyclic 3',5'-phosphate dependent protein kinase.* Biochemistry, 1984. **23**(18): p. 4193-4199.

70. León, D.A., et al., *A stable alpha-helical domain at the N terminus of the RIalpha subunits of cAMP-dependent protein kinase is a novel*

dimerization/docking motif. The Journal of biological chemistry, 1997. **272**(45): p. 28431-28437.

71. Giorgi, C., et al., *Redox control of protein kinase C: cell- and disease-specific aspects.* Antioxid Redox Signal, 2010. **13**(7): p. 1051-85.

72. Burgoyne, J.R., et al., *Cysteine redox sensor in PKGIa enables oxidant-induced activation.* Science, 2007. **317**(5843): p. 1393-7.

73. Zhong, H., et al., *The transcriptional activity of NF-kappaB is regulated by the IkappaB-associated PKAc subunit through a cyclic AMP-independent mechanism.* Cell, 1997. **89**(3): p. 413-424.

74. Dulin, N.O., et al., *Cyclic AMP-independent Activation of Protein Kinase A by Vasoactive Peptides.* Journal of Biological Chemistry, 2001. **276**(24): p. 20827-20830.

75. Shell, J.R. and D.S. Lawrence, *Proteolytic regulation of the mitochondrial cAMP-dependent protein kinase.* Biochemistry, 2012. **51**(11): p. 2258-2264.

76. Brennan, J.P., et al., *Detection and mapping of widespread intermolecular protein disulfide formation during cardiac oxidative stress using proteomics with diagonal electrophoresis.* J Biol Chem, 2004. **279**(40): p. 41352-60.

77. Brennan, J.P., et al., *Oxidant-induced activation of type I protein kinase A is mediated by RI subunit interprotein disulfide bond formation.* J Biol Chem, 2006. **281**(31): p. 21827-36.

78. de Piña, M.Z., et al., *Signaling the signal, cyclic AMP-dependent protein kinase inhibition by insulin-formed H2O2 and reactivation by thioredoxin.* The Journal of biological chemistry, 2008. **283**(18): p. 12373-12386.

79. Rao, R.K. and L.W. Clayton, *Regulation of protein phosphatase 2A by hydrogen peroxide and glutathionylation.* Biochemical and biophysical research communications, 2002. **293**(1): p. 610-616.

80. Humphries, K.M., J.K. Pennypacker, and S.S. Taylor, *Redox regulation of cAMP-dependent protein kinase signaling: kinase versus phosphatase inactivation.* J Biol Chem, 2007. **282**(30): p. 22072-9.

81. Persad, S., et al., *Biphasic alterations in cardiac beta-adrenoceptor signal transduction mechanism due to oxyradicals.* Journal of Pharmacology and Experimental Therapeutics, 1997. **282**(3): p. 1623-1631.

82. Jones, D.P., *Redefining oxidative stress.* Antioxid Redox Signal, 2006. **8**(9-10): p. 1865-79.

83. Fischer, E.H. and E.G. Krebs, *Conversion of phosphorylase b to phosphorylase a in muscle extracts.* J Biol Chem, 1955. **216**(1): p. 121-32.

84. Lee, S.R., et al., *Reversible inactivation of protein-tyrosine phosphatase 1B in A431 cells stimulated with epidermal growth factor.* J Biol Chem, 1998. **273**(25): p. 15366-72.

85. Finkel, T., *Signal transduction by reactive oxygen species.* J Cell Biol, 2011. **194**(1): p. 7-15.

86. Weerapana, E., et al., *Quantitative reactivity profiling predicts functional cysteines in proteomes.* Nature, 2010. **468**(7325): p. 790-5.

87. Go, Y.M. and D.P. Jones, *Redox control systems in the nucleus: mechanisms and functions.* Antioxid Redox Signal, 2010. **13**(4): p. 489-509.

88. Bak, D.W. and E. Weerapana, *Cysteine-mediated redox signalling in the mitochondria.* Molecular BioSystems, 2014. **11**(3): p. 678-697.

89. Nemoto, S., et al., *Role for Mitochondrial Oxidants as Regulators of Cellular Metabolism.* Molecular and Cellular Biology, 2000. **20**(19): p. 7311-7318.

90. Williams, D.A., et al., *Calcium gradients in single smooth muscle cells revealed by the digital imaging microscope using Fura-2.* Nature, 1985. **318**(6046): p. 558-61.

91. Buckler, K.J. and R.D. Vaughan-Jones, *Application of a new pH-sensitive fluoroprobe (carboxy-SNARF-1) for intracellular pH measurement in small, isolated cells.* Pflugers Arch, 1990. **417**(2): p. 234-9.

92. Nikolaev, V.O., et al., *Novel single chain cAMP sensors for receptor-induced signal propagation.* J Biol Chem, 2004. **279**(36): p. 37215-8.

93. Allen, M.D. and J. Zhang, *Subcellular dynamics of protein kinase A activity visualized by FRET-based reporters.* Biochem Biophys Res Commun, 2006. **348**(2): p. 716-21.

94. Adams, S.R., et al., *Fluorescence ratio imaging of cyclic AMP in single cells.* Nature, 1991. **349**(6311): p. 694-7.

95. Zaccolo, M., et al., *A genetically encoded, fluorescent indicator for cyclic AMP in living cells.* Nat Cell Biol, 2000. **2**(1): p. 25-9.

96. Zhang, J., et al., *Genetically encoded reporters of protein kinase A activity reveal impact of substrate tethering.* Proc Natl Acad Sci U S A, 2001. **98**(26): p. 14997-5002.

97. Zhang, J., et al., *Insulin disrupts beta-adrenergic signalling to protein kinase A in adipocytes.* Nature, 2005. **437**(7058): p. 569-73.

98. Komatsu, N., et al., *Development of an optimized backbone of FRET biosensors for kinases and GTPases.* Molecular Biology of the Cell, 2011. **22**(23): p. 4647-4656.

99. Depry, C., M.D. Allen, and J. Zhang, *Visualization of PKA activity in plasma membrane microdomains.* Mol Biosyst, 2011. **7**(1): p. 52-8.

100. Ponsioen, B., et al., *Detecting cAMP-induced Epac activation by fluorescence resonance energy transfer: Epac as a novel cAMP indicator.* EMBO Rep, 2004. **5**(12): p. 1176-80.

101. Klarenbeek, J., et al., *Fourth-generation epac-based FRET sensors for cAMP feature exceptional brightness, photostability and dynamic range: characterization of dedicated sensors for FLIM, for ratiometry and with high affinity.* PLoS One, 2015. **10**(4): p. e0122513.

102. Goedhart, J., et al., *Structure-guided evolution of cyan fluorescent proteins towards a quantum yield of 93%.* Nat Commun, 2012. **3**: p. 751.

103. Burgoyne, J.R., et al., *Deficient angiogenesis in redox-dead Cys17Ser PKARIα knock-in mice.* Nat Commun, 2015. **6**: p. 7920.

104. Claycomb, W.C. and M.C. Palazzo, *Culture of the terminally differentiated adult cardiac muscle cell: a light and scanning electron microscope study.* Dev Biol, 1980. **80**(2): p. 466-82.

105. Dow, J.W., N.G. Harding, and T. Powell, *Isolated cardiac myocytes. I. Preparation of adult myocytes and their homology with the intact tissue.* Cardiovasc Res, 1981. **15**(9): p. 483-514.

106. Cruz, C., et al., *Protective effects of bepridil on calcium injury of anoxic myocytes isolated from adult rat heart ventricular muscle.* J Pharmacol Exp Ther, 1987. **242**(3): p. 1126-32.

107. Zaccolo, M., *cAMP signal transduction in the heart: understanding spatial control for the development of novel therapeutic strategies.* Br J Pharmacol, 2009. **158**(1): p. 50-60.

108. Pavlovic, D., L.M. McLatchie, and M.J. Shattock, *The rate of loss of T-tubules in cultured adult ventricular myocytes is species dependent.* Exp Physiol, 2010. **95**(4): p. 518-27.

109. Li, Z., et al., *Adenovirus-mediated gene transfer to adult mouse cardiomyocytes is selectively influenced by culture medium.* J Gene Med, 2003. **5**(9): p. 765-72.

110. Crespo, F.L., et al., *Mitochondrial reactive oxygen species mediate cardiomyocyte formation from embryonic stem cells in high glucose.* Stem Cells, 2010. **28**(7): p. 1132-42.

111. Louch, W.E., K.A. Sheehan, and B.M. Wolska, *Methods in cardiomyocyte isolation, culture, and gene transfer.* J Mol Cell Cardiol, 2011. **51**(3): p. 288-98.

112. Masters, J.R., *HeLa cells 50 years on: the good, the bad and the ugly.* Nat Rev Cancer, 2002. **2**(4): p. 315-9.

113. Thomas, P. and T.G. Smart, *HEK293 cell line: a vehicle for the expression of recombinant proteins.* J Pharmacol Toxicol Methods, 2005. **51**(3): p. 187-200.

114. Zhong, H., et al., *Subcellular dynamics of type II PKA in neurons.* Neuron, 2009. **62**(3): p. 363-74.

115. Zheng, L., U. Baumann, and J.L. Reymond, *An efficient one-step site-directed and site-saturation mutagenesis protocol.* Nucleic Acids Res, 2004. **32**(14): p. e115.

116. Winship, P.R., *An improved method for directly sequencing PCR amplified material using dimethyl sulphoxide.* Nucleic Acids Res, 1989. **17**(3): p. 1266.

117. Matsuyama, A., et al., *pDUAL, a multipurpose, multicopy vector capable of chromosomal integration in fission yeast.* Yeast, 2004. **21**(15): p. 1289-305.

118. Laemmli, U.K., *Cleavage of structural proteins during the assembly of the head of bacteriophage T4.* Nature, 1970. **227**(5259): p. 680-5.

119. Chiari, M., et al., *Kinetics of cysteine oxidation in immobilized pH gradient gels.* Journal of Chromatography A, 1990. **499**: p. 699-711.

120. Crow, M.K., N. Karasavvas, and A.H. Sarris, *Protein aggregation mediated by cysteine oxidation during the stacking phase of discontinuous buffer SDS-PAGE.* Biotechniques, 2001. **30**(2): p. 311-6.

121. Yamaji, R., et al., *Hypoxia up-regulates glyceraldehyde-3-phosphate dehydrogenase in mouse brain capillary endothelial cells: involvement of Na+/Ca2+ exchanger.* Biochim Biophys Acta, 2003. **1593**(2-3): p. 269-76.

122. Lefkimmiatis, K., *cAMP signalling meets mitochondrial compartments.* Biochem Soc Trans, 2014. **42**(2): p. 265-9.

123. Hansen, J.M., Y.M. Go, and D.P. Jones, *Nuclear and mitochondrial compartmentation of oxidative stress and redox signaling.* Annu Rev Pharmacol Toxicol, 2006. **46**(1): p. 215-34.

124. Malinouski, M., et al., *Hydrogen peroxide probes directed to different cellular compartments.* PLoS One, 2011. **6**(1): p. e14564.

125. Payne, M.C., et al., *Dynamic changes in expression of myosin phosphatase in a model of portal hypertension.* Am J Physiol Heart Circ Physiol, 2004. **286**(5): p. H1801-10.

126. Murray, J., et al., *Monitoring oxidative and nitrative modification of cellular proteins; a paradigm for identifying key disease related markers of oxidative stress.* Adv Drug Deliv Rev, 2008. **60**(13-14): p. 1497-503.

127. Satoh, K., et al., *Highly cooperative dependence of sarco/endoplasmic reticulum calcium ATPase SERCA2a pump activity on cytosolic calcium in living cells.* J Biol Chem, 2011. **286**(23): p. 20591-9.

128. Burke, B., J. Tooze, and G. Warren, *A monoclonal antibody which recognises each of the nuclear lamin polypeptides in mammalian cells.* EMBO J, 1983. **2**(3): p. 361-7.

129. Skalhegg, B.S., et al., *Identification, purification, and characterization of subunits of cAMP-dependent protein kinase in human testis. Reverse mobilities of human RII alpha and RII beta on sodium dodecyl sulfate-polyacrylamide gel electrophoresis compared with rat and bovine RIIs.* J Biol Chem, 1992. **267**(8): p. 5374-9.

130. DeManno, D.A., et al., *Characterization of recombinant RI beta and evaluation of the presence of RI beta protein in rat brain and testicular extracts.* Biochimica et biophysica acta, 1994. **1222**(3): p. 501-510.

131. Ilouz, R., et al., *Localization and quaternary structure of the PKA RIβ holoenzyme.* Proc Natl Acad Sci U S A, 2012. **109**(31): p. 12443-8.

132. Solberg, R., et al., *Molecular cloning, cDNA structure and tissue-specific expression of the human regulatory subunit RI beta of cAMP-dependent protein kinases.* Biochem Biophys Res Commun, 1991. **176**(1): p. 166-72.

133. Clegg, C.H., G.G. Cadd, and G.S. McKnight, *Genetic characterization of a brain-specific form of the type I regulatory subunit of cAMP-dependent protein kinase.* Proc Natl Acad Sci U S A, 1988. **85**(11): p. 3703-7.

134. Skalhegg, B.S. and K. Tasken, *Specificity in the cAMP/PKA signaling pathway. differential expression, regulation, and subcellular localization of subunits of PKA.* Front Biosci, 1997. **2**: p. d331-42.

135. Zaccolo, M. and T. Pozzan, *Discrete microdomains with high concentration of cAMP in stimulated rat neonatal cardiac myocytes.* Science, 2002. **295**(5560): p. 1711-5.

136. Eng, J., R.M. Lynch, and R.S. Balaban, *Nicotinamide adenine dinucleotide fluorescence spectroscopy and imaging of isolated cardiac myocytes.* Biophys J, 1989. **55**(4): p. 621-30.

137. Nagai, T., et al., *A variant of yellow fluorescent protein with fast and efficient maturation for cell-biological applications.* Nat Biotechnol, 2002. **20**(1): p. 87-90.

138. Tam, J.P., et al., *Disulfide Bond Formation in Peptides by Dimethyl-Sulfoxide - Scope and Applications.* Journal of the American Chemical Society, 1991. **113**(17): p. 6657-6662.

139. Francis, S.H., I.V. Turko, and J.D. Corbin, *Cyclic nucleotide phosphodiesterases: relating structure and function.* Prog Nucleic Acid Res Mol Biol, 2001. **65**: p. 1-52.

140. Hidaka, H., M. Hagiwara, and T. Chijiwa, *Molecular pharmacology of protein kinases.* Neurochem Res, 1990. **15**(4): p. 431-4.

141. Murray, A.J., *Pharmacological PKA inhibition: all may not be what it seems.* Sci Signal, 2008. **1**(22): p. re4.

142. Davies, S.P., et al., *Specificity and mechanism of action of some commonly used protein kinase inhibitors.* Biochem J, 2000. **351**(Pt 1): p. 95-105.

143. Lum, H., et al., *Expression of PKA inhibitor (PKI) gene abolishes cAMPmediated protection to endothelial barrier dysfunction.* American Journal of Physiology-Cell Physiology, 1999. **277**(3).

144. Bienert, G.P., et al., *Specific aquaporins facilitate the diffusion of hydrogen peroxide across membranes.* J Biol Chem, 2007. **282**(2): p. 1183-92.

145. Komatsu, N., et al., *Development of an optimized backbone of FRET biosensors for kinases and GTPases.* Mol Biol Cell, 2011. **22**(23): p. 4647-56.

146. Di Benedetto, G., et al., *Protein kinase A type I and type II define distinct intracellular signaling compartments.* Circ Res, 2008. **103**(8): p. 836-44.

147. Nikolaev, V.O., et al., *Cyclic AMP imaging in adult cardiac myocytes reveals far-reaching beta1-adrenergic but locally confined beta2-adrenergic receptor-mediated signaling.* Circ Res, 2006. **99**(10): p. 1084-91.

148. Depry, C. and J. Zhang, *Using FRET-based reporters to visualize subcellular dynamics of protein kinase A activity.* Methods Mol Biol, 2011. **756**: p. 285-94.

149. Mongillo, M., et al., *Fluorescence resonance energy transfer-based analysis of cAMP dynamics in live neonatal rat cardiac myocytes reveals distinct functions of compartmentalized phosphodiesterases.* Circ Res, 2004. **95**(1): p. 67-75.

150. Tian, Q., et al., *Functional and morphological preservation of adult ventricular myocytes in culture by sub-micromolar cytochalasin D supplement.* J Mol Cell Cardiol, 2012. **52**(1): p. 113-24.

151. Lomas, O., et al., *Adenoviral Transduction of FRET-Based Biosensors for cAMP in Primary Adult Mouse Cardiomyocytes*, in *cAMP Signaling*, M. Zaccolo, Editor. 2015, Springer New York. p. 103-115.

152. Wright, W.E. and J.W. Shay, *Historical claims and current interpretations of replicative aging.* Nat Biotechnol, 2002. **20**(7): p. 682-8.

153. Banky, P., L.J. Huang, and S.S. Taylor, *Dimerization/docking domain of the type Ialpha regulatory subunit of cAMP-dependent protein kinase. Requirements for dimerization and docking are distinct but overlapping.* J Biol Chem, 1998. **273**(52): p. 35048-55.

154. Buxton, I.L. and L.L. Brunton, *Compartments of cyclic AMP and protein kinase in mammalian cardiomyocytes.* J Biol Chem, 1983. **258**(17): p. 10233-9.

155. Cardinale, D., et al., *Increased perioperative N-terminal pro-B-type natriuretic peptide levels predict atrial fibrillation after thoracic surgery for lung cancer.* Circulation, 2007. **115**(11): p. 1339-44.

156. Reiners, J.J., Jr., et al., *Depletion of cellular glutathione by conditions used for the passaging of adherent cultured cells.* Toxicol Lett, 2000. **115**(2): p. 153-63.

157. Bishop, C.T., et al., *Free radical damage to cultured porcine aortic endothelial cells and lung fibroblasts: modulation by culture conditions.* In Vitro Cell Dev Biol, 1985. **21**(4): p. 229-36.

158. Turrens, J.F., B.A. Freeman, and J.D. Crapo, *Hyperoxia increases H2O2 release by lung mitochondria and microsomes.* Arch Biochem Biophys, 1982. **217**(2): p. 411-21.

159. Seitz, H., et al., *Differential binding studies applying functional protein microarrays and surface plasmon resonance.* Proteomics, 2006. **6**(19): p. 5132-9.

160. Ang, S.K., et al., *Mitochondrial thiol oxidase Erv1: both shuttle cysteine residues are required for its function with distinct roles.* Biochem J, 2014. **460**(2): p. 199-210.

161. Dusanka, M., et al., *Biogenesis of the essential Tim9-Tim10 chaperone complex of mitochondria: site-specific recognition of cysteine residues by the intermembrane space receptor Mia40.* The Journal of biological chemistry, 2007. **282**(31): p. 22472-22480.

162. Chen, Q., R.Y. Lin, and C.S. Rubin, *Organelle-specific targeting of protein kinase AII (PKAII). Molecular and in situ characterization of murine A kinase anchor proteins that recruit regulatory subunits of PKAII to the cytoplasmic surface of mitochondria.* The Journal of biological chemistry, 1997. **272**(24): p. 15247-15257.

163. Wong, W. and J.D. Scott, *AKAP signalling complexes: focal points in space and time.* Nature reviews Molecular cell biology, 2004.

164. Wang, M.-J.J., et al., *The Ile646Val (2073A>G) polymorphism in the kinase-binding domain of A-kinase anchoring protein 10 and the risk of colorectal cancer.* Oncology, 2009. **76**(3): p. 199-204.

165. Wirtenberger, M., et al., *The functional genetic variant Ile646Val located in the kinase binding domain of the A-kinase anchoring protein 10 is associated with familial breast cancer.* Carcinogenesis, 2007. **28**(2): p. 423-426.

166. Kammerer, S., et al., *Amino acid variant in the kinase binding domain of dual-specific A kinase-anchoring protein 2: a disease susceptibility polymorphism.* Proc Natl Acad Sci U S A, 2003. **100**(7): p. 4066-71.

167. Bossis, G. and F. Melchior, *Regulation of SUMOylation by reversible oxidation of SUMO conjugating enzymes.* Mol Cell, 2006. **21**(3): p. 349-57.

168. Woo, H.A., et al., *Inactivation of peroxiredoxin I by phosphorylation allows localized H(2)O(2) accumulation for cell signaling.* Cell, 2010. **140**(4): p. 517-28.

169. Nisimoto, Y., et al., *Nox4: a hydrogen peroxide-generating oxygen sensor.* Biochemistry, 2014. **53**(31): p. 5111-20.

170. Zhang, J., et al., *NOX4-Dependent Hydrogen Peroxide Overproduction in Human Atrial Fibrillation and HL-1 Atrial Cells: Relationship to Hypertension.* Front Physiol, 2012. **3**: p. 140.

171. Anderson, E.J., et al., *Monoamine oxidase is a major determinant of redox balance in human atrial myocardium and is associated with postoperative atrial fibrillation.* J Am Heart Assoc, 2014. **3**(1): p. e000713.

172. Takimoto, E. and D.A. Kass, *Role of oxidative stress in cardiac hypertrophy and remodeling.* Hypertension, 2007. **49**(2): p. 241-8.

173. Margulis, L. and D. Bermudes, *Symbiosis as a mechanism of evolution: status of cell symbiosis theory.* Symbiosis, 1985. **1**: p. 101-24.

174. Trendelenburg, G., et al., *Molecular characterization of AKAP149, a novel A kinase anchor protein with a KH domain.* Biochem Biophys Res Commun, 1996. **225**(1): p. 313-9.

175. Acin-Perez, R., et al., *Cyclic AMP produced inside mitochondria regulates oxidative phosphorylation.* Cell Metab, 2009. **9**(3): p. 265-76.

176. Gu, H., et al., *Mitochondrial E3 ligase March5 maintains stemness of mouse ES cells via suppression of ERK signalling.* Nature communications, 2015. **6**: p. 7112.

177. Yonashiro, R., et al., *Mitochondrial ubiquitin ligase MITOL ubiquitinates mutant SOD1 and attenuates mutant SOD1-induced reactive oxygen species generation.* Molecular biology of the cell, 2009. **20**(21): p. 4524-4530.

178. Zentilin, L., et al., *Cardiomyocyte VEGFR-1 activation by VEGF-B induces compensatory hypertrophy and preserves cardiac function after myocardial infarction.* FASEB J, 2010. **24**(5): p. 1467-78.

179. Aikawa, R., et al., *Oxidative stress activates extracellular signal-regulated kinases through Src and Ras in cultured cardiac myocytes of neonatal rats.* J Clin Invest, 1997. **100**(7): p. 1813-1821.

180. Wang, M., et al., *The PKA RIalpha/A-kinase anchoring proteins 10 signaling pathway and the prognosis of colorectal cancer.* J Gastroenterol Hepatol, 2015. **30**(3): p. 496-503.

181. Giordano, F.J., et al., *A cardiac myocyte vascular endothelial growth factor paracrine pathway is required to maintain cardiac function.* Proc Natl Acad Sci U S A, 2001. **98**(10): p. 5780-5.

182. Levy, A.P., et al., *Regulation of vascular endothelial growth factor in cardiac myocytes.* Circ Res, 1995. **76**(5): p. 758-66.

183. Seko, Y., et al., *Vascular endothelial growth factor (VEGF) activates Raf-1, mitogen-activated protein (MAP) kinases, and S6 kinase (p90rsk) in cultured rat cardiac myocytes.* Journal of Cellular Physiology, 1998. **175**(3): p. 239-246.

184. Mukherjee, S.P., R.H. Lane, and W.S. Lynn, *Endogenous hydrogen peroxide and peroxidative metabolism in adipocytes in response to insulin and sulfhydryl reagents.* Biochem Pharmacol, 1978. **27**(22): p. 2589-94.

185. Krieger-Brauer, H.I., P.K. Medda, and H. Kather, *Insulin-induced activation of NADPH-dependent H2O2 generation in human adipocyte plasma membranes is mediated by Galphai2.* J Biol Chem, 1997. **272**(15): p. 10135-43.

186. Hayes, G.R. and D.H. Lockwood, *Role of insulin receptor phosphorylation in the insulinomimetic effects of hydrogen peroxide.* Proc Natl Acad Sci U S A, 1987. **84**(22): p. 8115-9.

187. Heineke, J. and J.D. Molkentin, *Regulation of cardiac hypertrophy by intracellular signalling pathways.* Nat Rev Mol Cell Biol, 2006. **7**(8): p. 589-600.

188. Aikawa, R., et al., *Insulin prevents cardiomyocytes from oxidative stress-induced apoptosis through activation of PI3 kinase/Akt.* Circulation, 2000. **102**(23): p. 2873-2879.

189. Green, D.E., et al., *The Nox4 inhibitor GKT137831 attenuates hypoxia-induced pulmonary vascular cell proliferation.* Am J Respir Cell Mol Biol, 2012. **47**(5): p. 718-26.

190. Aoyama, T., et al., *Nicotinamide adenine dinucleotide phosphate oxidase in experimental liver fibrosis: GKT137831 as a novel potential therapeutic agent.* Hepatology, 2012. **56**(6): p. 2316-27.

191. Jiang, J.X., et al., *Liver fibrosis and hepatocyte apoptosis are attenuated by GKT137831, a novel NOX4/NOX1 inhibitor in vivo.* Free Radic Biol Med, 2012. **53**(2): p. 289-96.

192. Muniyappa, R., et al., *Cardiovascular actions of insulin.* Endocr Rev, 2007. **28**(5): p. 463-91.

193. Senyo, S.E., et al., *Mammalian heart renewal by pre-existing cardiomyocytes.* Nature, 2013. **493**(7432): p. 433-6.